

Generalizing deep learning models for medical image classification

Sarah Matta^{a,b,*}, Mathieu Lamard^{a,b}, Philippe Zhang^{c,b,a}, Alexandre Le Guilcher^c, Laurent Borderie^c, Béatrice Cochener^{a,b,d} and Gwennolé Quéllec^b

^aUniversité de Bretagne Occidentale, Brest, Bretagne, 29200, France

^bInserm, UMR 1101, Brest, F-29200, France

^cEvolucare Technologies, Villers-Bretonneux, F-80800, France

^dService d'Ophthalmologie, CHRU Brest, Brest, F-29200, France

ARTICLE INFO

Keywords:

Domain generalization
Medical image analysis
Covariate shift
Concept shift
Domain shift
Noisy labels

ABSTRACT

Numerous Deep Learning (DL) models have been developed for a large spectrum of medical image analysis applications, which promises to reshape various facets of medical practice. Despite early advances in DL model validation and implementation, which encourage healthcare institutions to adopt them, some fundamental questions remain: are the DL models capable of generalizing? What causes a drop in DL model performances? How to overcome the DL model performance drop? Medical data are dynamic and prone to domain shift, due to multiple factors such as updates to medical equipment, new imaging workflow, and shifts in patient demographics or populations can induce this drift over time. In this paper, we review recent developments in generalization methods for DL-based classification models. We also discuss future challenges, including the need for improved evaluation protocols and benchmarks, and envisioned future developments to achieve robust, generalized models for medical image classification.

1. Introduction

Deep Learning (DL) models are the current state-of-art method for medical image classification. The availability of high quality labeled data, typically through multi-site collaboration projects, has paved the way to employ these data driven-based approaches in supervised medical image analysis. Nowadays, DL models have achieved human level performances in different medical domains such as dermatology [55], oncology [127], histopathology [77] and ophthalmology [45].

Current large-scale clinical DL models are often trained using a single large dataset collected from a specific population, typically through a partnership with one healthcare institution. Once the models have been approved by regulatory authorities, they should be deployed to different populations, image acquisition protocols or devices. In such cases, it is important to ensure that the performance drop is minimal. However, recent prospective validation studies have shown significant decreases in model performance when confronted to domain shifts across different institutions, notably in the contexts of chest X-rays [42, 147, 227], MRIs [1, 129], pathology [184, 183, 191] and fundus photography [131]. This is mainly because the assumption that training and testing data are drawn from the same distribution (Independent and Identically Distributed (IID) assumption) for which most of the DL models rely on, may be not hold in real-world scenarios.


More generally, the differences between the training and testing data are defined as shifts between the respective data distributions. These data distributions can be expressed as

the product of the probability of the input data $p(x)$ and the conditional probability of the output labels given the input data $p(y|x)$, resulting in the joint distribution $p(x, y)$. The IID setup, also known as within-distribution generalization, corresponds to the traditional evaluation form where there is no shift in data distributions, $p(x_{testing}) = p(x_{training})$ and $p(y_{testing}|x_{testing}) = p(y_{training}|x_{training})$. This type of evaluation is the simplest form of generalization. The more challenging setup, the non-IID setup, corresponds to the other cases where shift occur between train and test data distribution. These cases are commonly referred to as out-of-distribution (OOD) shifts [84].

While characterization of this OOD shift is still an open problem, recent work Cohen et al. [42], Shen et al. [172] have identified two main data shift types: *the covariate shift* and *the concept shift*. The *covariate shift*, the most commonly considered data distribution shift in OOD, occurs when the distribution of the data changes $p(x_{testing}) \neq p(x_{training})$, while keeping the conditional probability of the labels given the input $p(y_{testing}|x_{testing}) = p(y_{training}|x_{training})$ (which describes the task). On the other hand, the *concept shift* corresponds to the case where the relationship between the input and class variables changes [136]. In other terms, $p(y_{testing}|x_{testing}) \neq p(y_{training}|x_{training})$.

In practice, in the medical field, covariate shift can occur due to the data heterogeneity caused by using different acquisition protocols across medical centers (difference in staining procedure, multi-vendor scanners/cameras, variable acquisition parameters) which might lead to variability in terms of illumination, color or optical artifacts. Moreover, obtaining high quality image is not always guaranteed, and images may be low quality due to using low-cost imaging systems or due to tissue preparation or preservation artifacts.

*Corresponding author

 sarah.m.matta@gmail.com (S. Matta)

ORCID(s): 0000-0001-6052-4752 (S. Matta); 0000-0003-1669-7140 (G. Quéllec)

In some cases, it can also be prone to the operator subjectivity such as in ultrasound or endoscopy imaging, where the operator moves the device.

On the other hand, concept shift is mainly caused by label noise. In fact, the challenge reside in collecting accurate labeled medical image dataset. Manual annotations are error-prone, tedious, and time-consuming. In addition, as labels are provided by experts, certain level of subjectivity is expected. In fact, different classification systems for disease may be adopted. For instance, for Diabetic Retinopathy (DR) screening grading and management, different disease severity scales exist, such as the International Classification for Diabetic Retinopathy (ICDR), the English DR NHS, the Scottish DR grading scheme, the Canadian Tele-Screening Grading [25], and the French DR grading which follows the International Grading System [208].

Generalizing DL models is considered to be one of the biggest challenges facing a wider adoption and successful deployment of DL models in medical applications. To cope with this serious problem, recent effort has focused on improving DL model generalizability and developing robust DL models in non-IID settings. A straightforward solution to mitigate data heterogeneity and this distribution shift problem in medical imaging is to adapt DL models to the target domain using *Domain Adaptation (DA)* methods. DA methods can be categorized into *Supervised Domain Adaptation (SDA)* and *Unsupervised Domain Adaptation (UDA)* techniques based on the availability of labels in the target domain. In SDA, a limited amount of labeled data from the test domain is available for training the DL models. Typically, this involves *transfer learning*, where a pre-trained DL model on a large dataset from the source domain is fine-tuned on the targeted dataset using supervised learning. In contrast, UDA methods focus on scenarios where labeled data in the target domain is not available and only unlabeled target data are available for training. It aims to transfer the knowledge from a label-rich training (e.g source) domain to a test (target) domain, without the need of a labeled target domain.

However, UDA methods are limited in practice, as they still require access to a part of the test-domain data during the training procedure. To overcome this limitation, *Domain Generalization (DG)* methods have emerged as a more promising solution. In DG, the goal is to develop a DL model that is able to generalize to one unseen target domain via learning from a single or multiple source domains, without having access to the testing data from the target domain. However, training DG methods using *multi-source data* (multi-DG) has been considered as costly since collecting medical from multiple sources is challenging, and medical data are subject to privacy regulations. To address this problem, recent work focused on an additional research line, called *single domain generalization* (single-DG), in which the goal is to develop a DL model that is able to generalize to multiple target domains via learning from a single source domain [115]. Alternatively, *semi-supervised domain generalization* [231] combines the single-DG and

multi-DG by using one labeled sources domain and several unlabeled source domain to boost the performances.

2. Aims and scope of this paper

DG in computer vision dataset is becoming an emerging field: numerous surveys have been proposed [235, 204]. In the medical field, research has focused on domain adaptation [67] or unsupervised domain adaptation [101]. Other medical research has reviewed the problem of learning with noisy labels [93, 238, 153]. However, to the best of our knowledge, no medical review has studied the problem of generalization of DL models in the medical field with a focus on both domain shift problems: covariate shift and concept shift. This paper presents the first systematic review of generalization research in medical image classification.

For the literature review, we used the following query on Scopus: “*domain generalization*” OR “*noisy labels*” OR “*covariate shift*” OR “*concept shift*”. We included papers published from 1 January 2020 to 10 April 2023 (included). A total of 2086 papers were found. First, the search results were reviewed and duplicated records were removed. This resulted in 2027 papers. Abstracts and titles were manually reviewed and papers which are in the medical field were retained. A total of 372 papers were selected. Then, we selected the papers dealing with medical image classification and deep learning methods. Thus, 144 papers were selected. Out of these papers, 3 papers were excluded because they were not in English, and 3 other papers were excluded because they were reviews (these reviews [238, 93, 153] were previously introduced in this section). Furthermore, one paper was excluded as it presented the results of a challenge. Therefore, 137 articles were retained. For the purpose of assessing DL generalizability, using more than one dataset is desirable. We considered papers including more than one dataset, or including a multi-center dataset. While the main focus was on DG, we did not restrict our query to DG methods (or a type of DG, i.e., multi-DG) as UDA methods can also be extended to DG. This corresponds to 82 articles. Among these papers, 4 papers [125, 162, 197, 99] did not propose a new method for tackling concept shift or covariate shift, so they were discarded. Thus, the total number of papers considered in this study was 78 papers.

The organization of this paper is as follows. In Section 3, we briefly describe the problem of domain generalization. In Section 4, we present public medical datasets used for generalization research. Section 5 summarizes previous findings in clinical domain generalization benchmarks. In Section 6, we present our taxonomy, in which we review DL methods that have dealt with covariate shift in the medical domain (Section 6.1) and DL methods aiming to overcome the problem of concept shift and noisy labels (Section 6.2). Section 7 discusses the benefit of current DG methods based on the results of challenge data. Furthermore, it presents trends in DG development, related research to DG, implementation details, and future directions. Finally, Section 8 concludes this work.

3. Domain generalization problem formulation

Consider $\mathcal{X} \times \mathcal{Y}$ as the combined space of images (\mathcal{X}) and their respective class labels (\mathcal{Y}). Let \mathcal{S} denote the source domain, composed of data sampled from a distribution, $\mathcal{S} = \{(x_j, y_j)\}_{j=1}^n \sim p(\mathcal{X}, \mathcal{Y})$, where $x_i \in \mathcal{X} \in \mathbb{R}^d$ denotes the sample in the input space, $y_i \in \mathcal{Y} \in \mathbb{R}$ designates the label belonging to the output space, n is the data size of source domain, $p(\mathcal{X}, \mathcal{Y})$ is the joint space of images \mathcal{X} and their respective class labels \mathcal{Y} . In domain generalization, M source domains $\mathcal{S}^i = \{(x_j^i, y_j^i)\}_{j=1}^{n_i}$ (where \mathcal{S}^i denotes the i -th domain, and n_i is the data size of source domain i) are provided for training: $\mathcal{S}_{train} = \{\mathcal{S}^i \mid i = 1, \dots, M\}$.

DG approaches aim to learn a robust and generalizable predictive function $f : \mathcal{X} \rightarrow \mathcal{Y}$ using the M training source domains and optimizing it to achieve a minimum prediction error on an unseen target domain $\mathcal{T} \sim q(\mathcal{X}, \mathcal{Y})$. In contrast to domain adaptation approaches, the target domain is inaccessible during training and is sampled from an unknown and different distribution than the M source domains, that is $p(\mathcal{X}, \mathcal{Y})^i \neq q(\mathcal{X}, \mathcal{Y})$ for $i \in \{1, \dots, M\}$ [204]. Therefore, the DG objective can be formulated as follows:

$$\min_f \mathbb{E}_{(x,y) \in \mathcal{T}} [\mathcal{L}(f(x), y)] \quad (1)$$

where \mathbb{E} is the expectation and $\mathcal{L}(\cdot, \cdot)$ is the classification loss function.

4. Public medical datasets for generalization research

There exist many public datasets which have been adopted for generalization research in the medical field. Some of these datasets were proposed as part of a challenge. Table 1 and Table 2 summarize the public medical datasets which can be used for generalization research. In this section, we will give brief details for public datasets available as part of a challenge and which are the most relevant in DG context.

MIDOG datasets Mitosis Domain Generalization (MIDOG) dataset targets the detection of mitotic figures in histopathology images under domain shift regime.

- MIDOG 2021 dataset [12]: This dataset was part of the MICCAI MIDOG 2021 challenge which aims to evaluate methods that mitigate domain shift and derive scanner-agnostic algorithms. It addresses DG in histopathology. The main task was mitosis detection in breast cancer. The challenge dataset features 300 cases, 6 scanners, and more than 2500 mitosis. The domains are defined by scanner types. Namely, Hamamatsu NanoZoomer XR (C12000-22, Hamamatsu, Hamamatsu City, Japan) (Scanner A), Hamamatsu NanoZoomer S360 (Hamamatsu, Hamamatsu City, Japan) (Scanner B), Aperio Scanscope CS2 (Leica Biosystems, Nussloch, Germany) (Scanner C) and Leica Aperio GT 450 (Leica Biosystems, Nussloch, Germany)(Scanner D), 3DHISTECH Panoramic 1000 (3DHISTECH, Budapest, Hungary) (Scanner

E), Hamamatsu NanoZoomer 2.0RS (C10730-12, Hamamatsu, Hamamatsu City, Japan) (Scanner F).

- MIDOG 2022 dataset: It originates from MIDOG 2022 challenge [11]. It is a multi-tumor, multi-species, multi-laboratory and multi-scanner dataset. The main task was mitosis detection. The goal of this challenge is to develop strategies that lead to machine learning solutions that are invariant to this tissue-related domain-shift. 6 tumor domains were provided for developing the DL models: Human breast carcinoma, retrieved from the University Medical Center Utrecht (Domain A), Canine lung carcinoma, retrieved from the University of Veterinary Medicine Vienna (VMU) (Domain B), Canine lymphosarcoma, retrieved from the VMU (domain C), Canine cutaneous mast cell tumor, retrieved from the DA of FUB (Domain D), Human pancreatic and gastrointestinal neuroendocrine tumor, retrieved from the UMC Utrecht (Domain E). The evaluation was carried out on ten independent tumor domains.
- MIDOG++ dataset [13] is an extension of MIDOG 2021 and 2022 challenge datasets. It consists of 7 tumor types: breast carcinoma, lung carcinoma, lymphosarcoma, cutaneous mast cell tumor, neuroendocrine tumor, soft tissue sarcoma, and melanoma. The domains of the dataset include different tumor types, laboratories, whole slide image scanners, and species.

CAMELYON datasets Cancer Metastases in Lymph nodes challenge (CAMELYON) datasets target the automated detection of cancer metastases in Whole-Slide Images (WSIs) of sentinel lymph nodes.

- CAMELYON16 dataset [20] originates from CAMELYON16, in 2016. The dataset includes 399 WSIs collected from 2 centers.
- PatchCamelyon [196] is a large-scale patch-level dataset derived from Camelyon16 dataset.
- CAMELYON17 dataset [100] originates from the CAMELYON17 challenge which was held in 2017. In comparison to CAMELYON16 which focuses on slide level analysis, CAMELYON17 focus on patient level analysis. The dataset comprises 1000 WSIs collected from 5 centers.

UBC-OCEAN dataset The University of British Columbia - Ovarian Cancer Subtype Classification and Outlier Detection (UBC-OCEAN) competition aims to classify ovarian cancer subtypes from microscopy scans of biopsy samples¹. The UBC-OCEAN dataset consists of an extensive ovarian cancer dataset of histopathology images obtained from more than 20 medical centers. However, the origin of the image is not given in the meta-data. The test set contains images from

¹<https://www.kaggle.com/competitions/UBC-OCEAN/overview>

different source hospitals than the train set. The class other is not present in the training set.

LUNA-16 : The goal of LUNA-16 challenge is the automated detection of pulmonary nodules in thoracic Computed Tomography (CT) scans [169]. This challenge use data from a large public LIDC-IDRI dataset [9]. More precisely, scans with a slice thickness greater than 2.5 mm were excluded. The resulting dataset contains 888 CT scans.

PANDA dataset : The goal of Prostate Cancer Grade Assessment (PANDA) challenge [27] is the diagnosis of prostate cancer in biopsies. It aims to develop AI algorithms for Gleason grading. In total, the PANDA dataset comprises 12,625 WSIs of prostate biopsies retrospectively collected from 6 different sites for algorithm development, tuning and independent validation. Cases for development, tuning and internal validation originated from two European (EU) centers: Radboud University Medical Center, Nijmegen, the Netherlands and Karolinska Institutet, Stockholm, Sweden. The external validation data consisted of a US (741 cases) and an EU set (330 cases).

5. Domain generalization benchmarks

Zhang et al. [228] benchmarked² the performance of eight DG methods on multi-site clinical times series from Intensive Care Units (ICUs) and chest X-ray imaging data from four sites. They compared the performances of these models to a baseline approach which consists of using *Empirical Risk Minimization* (ERM), where a single model is learned on pooled data across all training sources. In contrast to DG methods, this method assumes that the samples are IID. It minimizes the global average risk, defined as $R_{ERM}(\theta) = \frac{1}{n} \sum_{i=1}^n \mathcal{L}(x_i, y_i; \theta)$ where \mathcal{L} is the classification loss, θ is the model's parameters, and n is the number of samples [23].

In line with prior work on general imaging datasets [69], their experiments on real-world medical imaging data revealed that the current DG methods do not consistently achieve significant gains in OOD performance over ERM. In addition, the authors proposed a framework for augmenting clinical datasets via synthetic domain shifts and sampling bias.

6. Taxonomy of generalization research in medical classification domain

Depending on the assumed domain shift (covariate shift or concept shift), a plethora of methods have been proposed. To make it easier for the reader to find the methods suited to their problem, we have therefore chosen to first separate the methods based on this criterion. In this section, we present our categorization of methods based on covariate shift (Figure 1) and concept shift (Figure 2). These methods are detailed in the following sections (Section 6.1 and Section 6.2). Table 3 presents the notations used in this paper.

²<https://github.com/MLforHealth/ClinicalDG>

6.1. Covariate shift in medical imaging

Data heterogeneity is a key challenge for DL model generalizability. Covariate shift, in particular, is considered one of the most prominent shift in medicine. It is difficult to avoid this type of shift in medical imaging. It is mainly caused by the use of different type of acquisition systems and protocols, which may present notable differences among domains (i.e., changes in intensity values and contrast). Another factor to covariate shift is the differences in the characteristics of the lesions or diseases (shape, size, malignancy and location) and biological variations between patients (age, sex). Solutions for tackling the covariate shift can be categorized into: data manipulation (Section 6.1.1), representation (Section 6.1.2) and learning methods (Section 6.2.2).

6.1.1. Data manipulation

Data manipulation methods focus on data-driven approaches to achieve robust model to domain shift, hence improve the generality of DL models. These methods can be categorized into *data homogenization* and *data augmentation*. Data homogenization attempts to normalize the data and reduce the variance which exists between source domains. On the contrary, data augmentation applies augmentation techniques (severe augmentations) to expand the style variance and incorporate more diversity.

6.1.1.1 Data homogenization

Data homogenization aims to pre-process images in a way to eliminate specific signals of each domain.

Almahfouz Nasser et al. [5] proposed a *Pre-processing Homogenizer* strategy for reducing domain shift. Their pre-processing pipeline consists of training an auto-encoder to reconstruct the input images using a mean square loss. The main idea is to learn a uniform domain appearance of input images. To further erase domain specific signals, they incorporated an adversarial loss to the encoder using a domain discriminator. The domain discriminator is a network trained to detect the domain label (i.e., the scanner technology used to acquire images) using features arising from the encoder. In contrast, the autoencoder is trained to maximize the domain label prediction loss and minimize the reconstruction loss simultaneously to obtain domain-invariant features. This solution was applied for the MIDOG 2021 challenge (Table 1). Unfortunately, according to the leaderboard on grand challenge, this method performed very poorly with a F1 score of 0.0030 on the test set.

Yin et al. [224] proposed a novel DG method based on *Adversarial Frequency Alignment (AFA)*. Their DG framework comprises four networks: an encoder-decoder in the *Adaptive Transition Module (ATM)*, a fidelity discriminator, a multi-domain discriminator and a classification network. The goal of the ATM module (autoencoder) is to learn a frequency attention map that can align different domain images in a common frequency domain. It can be considered as a "data homogenizer". Given an input image coming from multiple source domains, it produces a reconstructed image, which eliminates significant domain shifts in the frequency

Generalizing deep learning models for medical image classification

Dataset	Modality (Organs)	Number of cases	Reference
MIDOG 2021 dataset [12]		300 images	https://midog2021.grand-challenge.org/
VGH [19]		5,920 images	https://tma.im/tma_portal/C-Path/supp.html
NKI [19]		8,337 images	
Camelyon16 WILDS dataset [20]	Histopathology (Breast)	399 WSI	https://camelyon16.grand-challenge.org/Data/
PatchCamelyon [196]		327,680 color images	https://patchcamelyon.grand-challenge.org/
Camelyon17 WILDS dataset [100]		1000 WSI	https://camelyon17.grand-challenge.org/Data/
TCGA-BRCA		1,098 cases	https://portal.gdc.cancer.gov/projects/TCGA-BRCA
BACH dataset	Microscopy,Histopathology (Breast)	400 microscopy images 30 WSI	https://iciar2018-challenge.grand-challenge.org/Dataset/
MIDOG 2022 dataset [11]	Histopathology (Multi-organs)	405 images	https://midog2022.grand-challenge.org/
MIDOG++ dataset [13]	Histopathology (Multi-organs)	503 images	https://github.com/DeepMicroscopy/MIDOGpp
UBC-OCEAN	Histopathology (Ovaries)	538 training images	https://www.kaggle.com/competitions/UBC-OCEAN/data
PANDA	Histopathology (Prostate)	12,625 WSIs	https://www.kaggle.com/c/prostate-cancer-grade-assessment
DiagSet-B		4675 scans	https://github.com/michalkoziarski/DiagSet
SICAPv2 [179]		155 biopsies (95 patients)	https://data.mendeley.com/datasets/9xms8dvs3/1
TUPAC-16[22]	Histopathology (Colon)	1076 cases	https://tupac.grand-challenge.org/Dataset/
Kather16 [95]	Histopathology (Colon)	5,000 patches	https://zenodo.org/records/53169
Kather19 [94]		100,000 patches	http://dx.doi.org/10.5281/zenodo.1214456
CRC-TP [89]		196,000 patches	https://warwick.ac.uk/TIAlab/data/crchistolabelednuclieihe/
IHC [120]		1,376 images	http://fimm.webmicroscope.net/supplements/epistroma
CRC-VALHE-7K		7,180 image patches	https://zenodo.org/records/1214456
Stanford-CRC [220]		66,578 image tiles	https://github.com/rikiyay/MSinet
CRC-DX-TRAIN dataset		93,408 image tiles	https://zenodo.org/records/2538835#_XwCKDZKkHY
CRC-DX-TEST dataset		99,904 image tiles	https://zenodo.org/records/2538835#_XwCKDZKkHY
Chaoyang Dataset [241]		6,160 WSI	https://bupt-ai-cz.github.io/HSA-NRL/
DigestPath2019 [113]		690 patients	https://digestpath2019.grand-challenge.org/
TCGA-LGG	Histopathology (Brain)	516 cases	https://portal.gdc.cancer.gov/projects/TCGA-LGG
TCGA-GBM		617 cases	https://portal.gdc.cancer.gov/projects/TCGA-LGG
TCGA-LUAD	Histopathology (Lung)	585 cases	https://portal.gdc.cancer.gov/projects/TCGA-LUAD
TCGA-LUSC		504 cases	https://portal.gdc.cancer.gov/projects/TCGA-LUSC
ADNI-1 [87]	MRIs (Brain)	748 subjects	https://adni.loni.usc.edu/data-samples/access-data/
ADNI-2 [87]		708 subjects	https://adni.loni.usc.edu/data-samples/access-data/
AIBL [54]		549 subjects	https://adni.loni.usc.edu/data-samples/access-data/
ISIC-2017 [40]	Dermoscopic images	2,750 images	https://challenge.isic-archive.com/data/
ISIC-2019[193]		33,569 images	
HAM10000 (HAM)[193]		10,000 images	https://dataverse.harvard.edu/dataset.xhtml?persistentId=doi:10.7910/DVN/DBW86T
Dermofit (DMF)		1,300images	https://homepages.inf.ed.ac.uk/rbf/DERMOFIT/datasets.htm
Derm7pt (D7P) [96]		2,000 images	http://derm.cs.sfu.ca
INbreast [135]	Mammography (Breast)	115 cases	https://www.kaggle.com/datasets/ramanathansp20/inbreast-dataset
OPTIMAM dataset [73]		179,326 cases	https://medphys.royalsurrey.nhs.uk/omid/
BCDR [124]		3,703 digitised film mammograms	https://www.medicmind.tech/cancer-imaging-data
LIDC-IDRI [9]	CT(Lung)	1,018 scans (1,010 subjects)	http://ncia.nci.nih.gov/
LUNA-16		888 scans	https://luna16.grand-challenge.org/Data/
LUNA-DG [224]		887 scans	https://github.com/meisun1207/LUNA-DG
NLST [188, 189]		25,681 patients (77,040 images)	https://cdas.cancer.gov/nlst/
COVID19-Diag		226 CT volumes	https://github.com/MLMIP/COVID19-Diag
ChestX-ray14 (NIH) [207]	X-ray (Chest)	112,120 images (30,805 subjects)	https://nihcc.app.box.com/v/ChestXray-NIHCC
CheXpert (CXP) [85]		224,316 images (65,240 subjects)	https://stanfordmlgroup.github.io/competitions/chexpert/
MIMIC-CXR (MMC) [90]		377,110 images (65,179 subjects)	https://physionet.org/content/mimic-cxr/2.0.0/
PadChest [28]		160,000 images(67,000 subjects)	https://bimcv.cipf.es/bimcv-projects/padchest/
Open-i dataset [46]		8,121 images	http://openi.nlm.nih.gov/
Tawsifur [150, 38]		931 images	https://www.kaggle.com/datasets/tawsifurrahman/covid19-radiography-database
Skytells		1,017 images	https://github.com/skytells-research/COVID-19-XRay-Dataset

Table 1
Public medical datasets used for generalization research

domain. To this end, it is trained using adversarial learning by employing a fidelity discriminator and a multi-domain discriminator in the frequency domain. In contrast, the classification model is trained in the original spacial domain to classify nodules. It is applied after the ATM module. This method was evaluated in the context of lung nodule detection from CT images. The evaluation on both **LUNA-DG** and on an in-house dataset showed that the AFA is an efficient method. They reported a competition performance metric [138] of 0.911 on the target test set of LUNA-DG.

Gunasinghe et al. [70] also investigated data homogenization to enhance the performances of DL models when applied to data with variations stemming from the use of different medical devices. Three different preprocessing methods were considered: median filter, input standardization,

and randomized multi-image histogram matching. The median filter is a non-linear digital preprocessing technique, used to remove noise from an image. Input standardization aims to attenuate illumination variations. In their work, they used a method inspired by Quellec et al. [149], where RGB images are converted to the YCbCr color space and the channel holding the luminance information (Y) is standardized. Following this normalization, the color space is changed back to RGB. Histogram matching is a technique that transforms the histograms of the red, green and blue channels of an image to match those of a specific reference image. In randomized multi-image histogram matching, histogram matching is performed sequentially using multiple reference images selected from the training source domain. The authors studied these preprocessing strategies in combination and individually to evaluate their impact on the

Dataset	Modality (Organs)	Number of cases	Reference
UK Biobank retinal photography dataset [185]		58,700 patients	https://www.ukbiobank.ac.uk/
EyePACs		88,702 images	https://www.kaggle.com/c/diabetic-retinopathy-detection/data
APTOS		3,662 images	https://www.kaggle.com/c/aptos2019-blindness-detection
Messidor		1,200 images	https://www.adcis.net/en/third-party/messidor/
PALM		1,200 images	https://palm.grand-challenge.org/
AV-DRIVE [82]	Fundus photography (Eye)	40 Images	https://drive.grand-challenge.org/
LES-AV		22 images	https://figshare.com/articles/dataset/LES-AV_dataset/11857698
HRF		45 images	https://www5.cs.fau.de/research/data/fundus-images/
REFUGE		1,200 images	https://refuge.grand-challenge.org/
REFUGE2		2,000 images	https://refuge.grand-challenge.org/
STARE		20 images	https://cecas.clemson.edu/~ahoover/stare/probing/index.html
RIGA		750 images	https://academictorrents.com/details/eb9dd9216a1c9a622250ad70a400204e7531196d
DDR		13,673 images	https://drive.google.com/drive/folders/1z6tSFmxW_aNayUqVxx6h6bY4kwGzUJTEC
RIMONEv2 [17]		455 images	https://medimg.webs.uil.es/
FGADR		1,842 images	https://csyizhou.github.io/FGADR/
Endovis Challenge dataset [4]	Endoscopic (Abdominal organs)	8 sequences	https://endovisub2017-roboticinstrumentsegmentation.grand-challenge.org/
Heidelberg colorectal dataset [128]	Laparoscopy (Colorectum)	30 laparoscopic videos	https://robustnisi2019.grand-challenge.org/Data/
CholecSeg8k [79]	Laparoscopy (Abdomen)	17 videos from Cholec80 dataset	http://camma.u-strasbg.fr/datasets
SurgicalActions [164]	Laparoscopy (Gynecologic organs)	160 videos	http://www-itec.aau.at/ftp/datasets/SurgicalActions160
Cataract-101 [165]	Video (Eye)	101 cataract surgeries	http://ftp.itec.aau.at/datasets/ovid/cat-101/
PathVQA [76]	Multiple modalities (multi-organs)	4,998 pathology images (multi-organs)	https://github.com/UCSD-AI4H/PathVQA
VQA-RAD[106]	Radiology (multi-organs)	315 radiology images.	https://osf.io/89kps/
OrganCMNIST	CT (Abdomen)	23,583	https://mednist.com/

Table 2
Public medical datasets used for generalization research

model generalization for glaucoma detection using fundus photographs. To this end, the experiments were conducted on two public datasets, RIMONEv2 and REFUGE which include different fundus camera devices. The results have shown that standardization of images led to greater performances in most scenarios with an average of 0.85 Area Under the Receiver Operator Characteristic Curve (AUC).

Garrucho et al. [59] presented another data homogenization strategy, named intensity scale standardization. Intensity along with texture are considered to be domain-dependent feature. Inspired by Nyúl et al. [140], they proposed to perform intensity scale standardization for attenuating domain shift. It is a two-step technique: 1) it learns a standardized histogram from the training images, extracting the histogram landmarks, and 2) these landmarks are used to linearly map the intensities of input images. The authors applied this technique for mass detection in mammography. They showed that it enhanced the generalization performance. It outperformed MixStyle, Cutout, RandConv and histogram equalization.

Wang et al. [205] introduced a method for harmonizing data from different sources. Inspired by Pawlowski et al. [144], they propose to use normalizing-flow-based method for counterfactual inference within a Structural Causal Model (SCM), to attain harmonization of data. The idea is to explicitly model the causal relationship of known confounders such as site, gender and age, and ROI features (i.e., the imaging measurement) in a SCM which uses normalizing flows to model probability distributions. Counterfactual inference can be performed upon such a model to sample harmonized data by intervening upon these variables. This method has been evaluated for age regression and Alzheimer’s disease classification. It showed better cross-domain generalization compared to state-of-the-art algorithms such as ComBat and IRM, and to models trained on raw data.

6.1.1.2 Data augmentation

While data-augmentation in DL is used to prevent overfitting on the training set and improve in-domain generalizability, when applied in the context of DG, it aims to improve the DL generalizability to unseen target domains. Therefore, the generated samples in DG may be visually different to those in the source domain, in contrast to typical synthesized images [115].

In this context, Li et al. [115] proposed a *Fourier-based method* that generates adversarial data via spontaneous *Amplitude SPECTrum diverSification* (ASPECTS) for single-DG. This method is inspired by a multi-source DG [215] which improves the diversity of training data by combining the frequency components of samples from different source domains. Specifically, the suggested method first applies the Discrete Fourier transform to convert the image into the frequency domain, and then generates diverse samples by modifying the amplitude spectrum using a variety of randomization operations. The premise of the suggested method is that the amplitude spectrum of images after Fourier transformation mostly contains domain-invariant information. Therefore, the authors proposed to generate new adversarial samples by modifying the amplitude spectrum, i.e., randomize the amplitude and position of points in the amplitude spectrum using rescaling and pixel shuffling operations. In contrast to the existing single-DG methods, their proposed method does not require to train an extra network/module for adversarial sample generation. It has been validated on two medical datasets: a public Mitosis Domain Generalization (MIDOG) dataset and a private multicenter colposcopic image datasets. The authors reported an average accuracy over all out-of-domain data of 0.6285 for the MIDOG dataset and of 0.6287 for the multicenter colposcopic image dataset.

Zhang et al. [231] integrated a similar strategy, using *domain randomization* in their framework for enhancing DL generalizability. The end goal was to encourage DL

Notation	Description	Notation	Description
x, y	Instance/clean label	KL	Kullback-Leibler divergence
\mathcal{X}, \mathcal{Y}	Feature/label space	D_{KL}	Symmetrized Kullback-Leibler
Y	Pair labels	s	Soft label distribution
θ	Model parameter	f	Network prediction with input x
$\mathcal{L}(\cdot, \cdot)$	Loss function	c	Number of classes
$L(\cdot)$	Cross-entropy loss	e	Training epoch
E, C	Feature extractor (encoder)/classifier	H	History of predictions
F	Projection layer	z^c	Label prediction
C_D	Domain classifier (domain discriminator)	z^f	Feature representation
C_S	Category classifier	\bar{z}	Temporal ensembling momentum
f	Predictive function	m	Momentum coefficient
\mathbb{E}	Expectation	μ	Mean value
S	Source domain	v, δ, β	Hyperparameters
\mathcal{T}	Target domain	w	Weight
α	Learnable parameter	B	Batch of selected images
M	Number of source domains	\hat{z}^f	Ensemble target of the features after applying EMA to feature representations within previous epochs.
p, q	Distribution	\hat{z}^c	Ensemble target of the labels after applying EMA to label predictions within previous epochs.
n_i	Data size of source domain i	N	Total number of negative samples
n	Data size of total training data	P	Total number of positive samples
R	Risk function	λ	weight parameter
y^d	Label distribution	TN	True negative
\hat{x}	Augmented instance	$c\hat{c}v$	Mean covariance matrix
\hat{y}	Noisy label	D	Dataset
K	Constant	D^{val}	Validation dataset
TP	True positive	d	distance
cov	Covariance	ϱ	Prototype
T	Task	I	Individual regularization
D^{tr}	Training dataset		
D^{test}	Testing dataset		
τ	Temperature		
γ	Hyperparameter		

Table 3
Notations

model to learn stable representations. Formally, a domain randomization function is applied to a given input image to produce a modified image. The modified image should retain the same high-level semantics as the original image but its superficial distribution is different. This function is implemented as *amplitude mix*, where the superficial distributions of an image is perturbed through linearly interpolating its amplitude spectrum with that of another image. Alternatively, this function can be implemented as *color jitter* where variation are introduced in terms of hue, saturation and contrast distributions. The feature stability is an indicator of domain invariance, as domain randomization keeps the high-level semantics unchanged. It is defined as the sum of the channel-wise cosine distance between the original feature and its domain-randomized counterpart.

Lucieri et al. [126] presented *Amplitude-Focused Amplitude-Phase Recombination for pair samples (AF-APR-P)*³. It was proposed as a variation of the original Amplitude-Phase Recombination for Pair samples (APR-P)[31] approach to improve the robustness and performance of DL models. In APR-P, an image is augmented by replacing its amplitude spectrum with the spectrum of another

randomly selected image from the batch. The main idea is to improve the robustness of the DL model by reducing the dependence on the amplitude spectrum and enhancing the ability to capture phase spectrum. In contrast, AF-APR-P aims to enhance the model’s ability to generalize by focusing on the amplitude spectrum of the images while altering the phase spectrum. This is achieved by swapping the phase spectrum among images but retaining their original amplitude spectrum. The authors showed improved performance on binary skin lesion classification tasks on the The International Skin Imaging Collaboration (ISIC) dataset⁴ and the seven-point checklist criteria dataset [96].

Wang and Xia [203] introduced a *Domain-Ensemble Learning with Cross-domain Mixup (DELCOM)* for multi-source DG. Their proposed method collaboratively train multiple domain-specific models using the data from both source and virtual domains. To this end, they constructed virtual samples, which form a virtual mixed domain that does not belong to any source domain. In particular, they extended the conventional mixup to *cross-domain mixup* to create a virtual domain based on the data from source domains. The original mixup technique produces convex

³<https://github.com/adriano-lucieri/shape-bias-in-dermoscopy>

⁴<https://www.isic-archive.com/>

Generalizing deep learning models for medical image classification

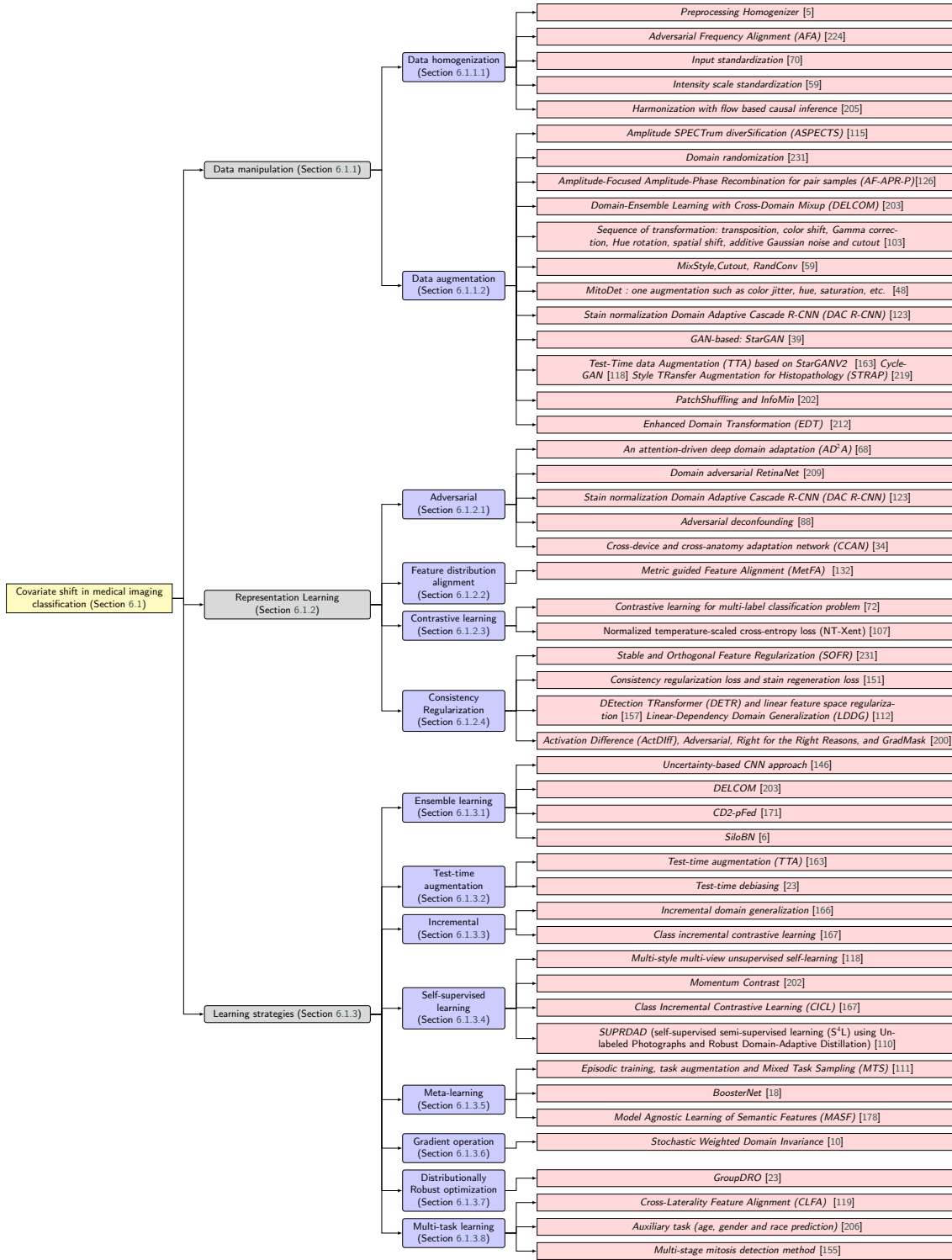


Figure 1: Literature survey tree for covariate shift

combinations of pairs of images and their labels: it interposes pairs of samples from the same domain that are drawn at random. In cross-domain mixup, one combine pairs of samples from different domains, to form a virtual domain S_{mix} that comprises virtual images (x_{mix}) and labels (y_{mix}),

as formulated in the following equations:

$$x_{mix} = \lambda x_1 + (1 - \lambda)x_2 \quad (2)$$

$$y_{mix} = \lambda y_1 + (1 - \lambda)y_2 \quad (3)$$

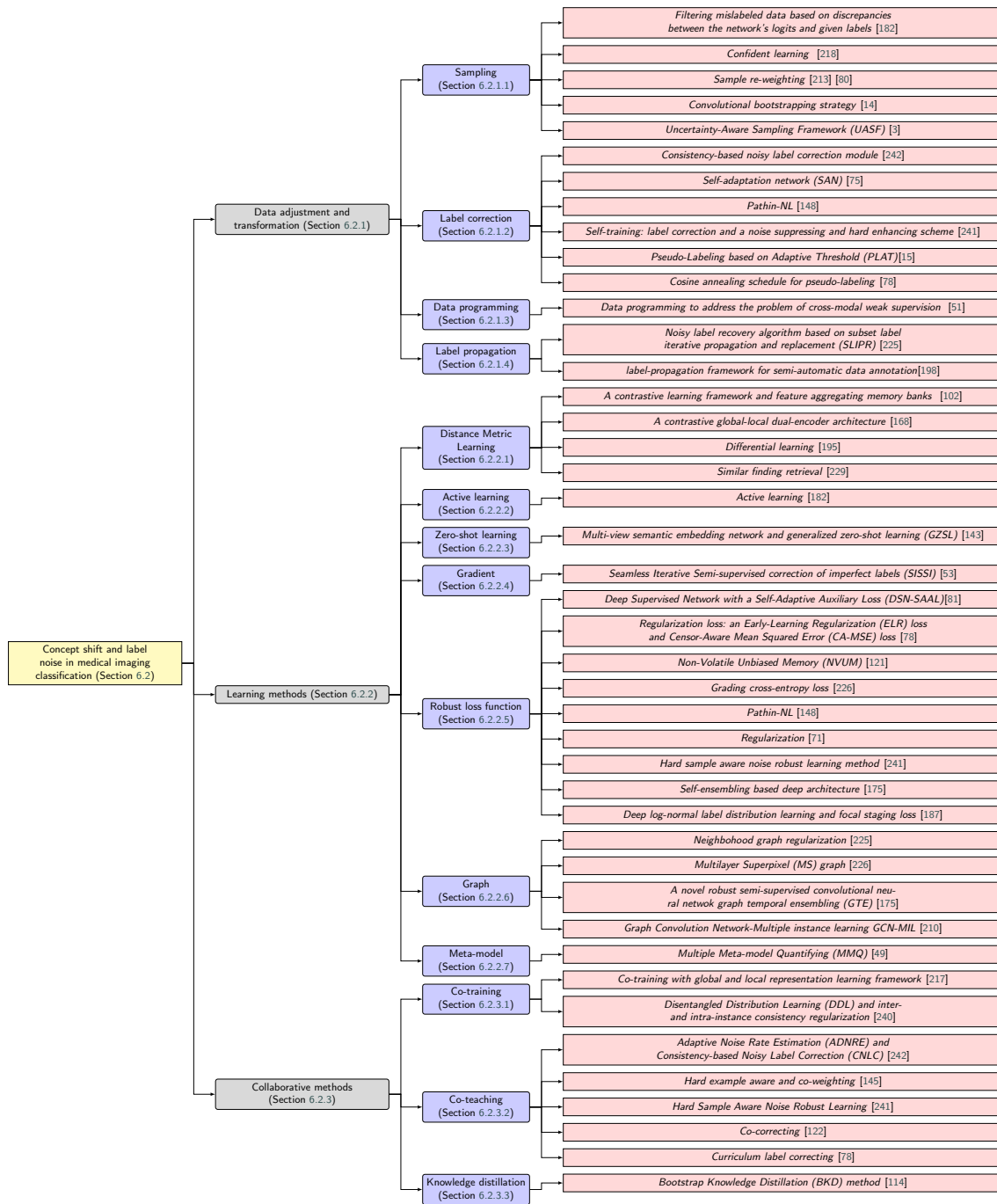


Figure 2: Literature survey tree for concept shift and label noise

where (x_1, y_1) and (x_2, y_2) denote a pair of samples from source domain S_1 and S_2 , respectively. $\lambda \sim \text{Beta}(\alpha, \alpha)$ for $\alpha \in (0, \infty)$ and $\text{Beta}(\alpha, \alpha)$ is a *Beta* distribution with two equal parameters α and α . α is set to 0.4.

Experiments performed on chest X-rays datasets for the diagnosis of thoracic diseases showed that the proposed DELCOM method outperformed ERM and six other DG approaches (CrossGrad [170], Deep Domain-Adversarial Image Generation (DDAIG) [236], Domain adaptive ensemble learning (DAEL) [237], MixStyle [237] and Exact Feature Distribution Matching (EFDMix) [232]).

Garrucho et al. [59] also studied different augmentations techniques for DG. Namely, Cutout [47], RandConv [216] and MixStyle [237]. Cutout removes square patches from training images at random locations. RandConv produces images with random local textures but consistent shapes using linear filtering. MixStyle mixes the feature statistics of two instances to synthesize new domains during the mini-batch training. In addition to these augmentation strategies, they investigated a data homogenization approach, the intensity scale standardization approach (presented in Section 6.1.1.1). They conducted experiments for mass detection

in mammography across multiple centers. Two backbones were considered: Swin Transformer and ResNet-50. They evaluated the performances of their model using one or a combination of data augmentation strategies. The results showed that the combination of intensity scale standardization and cutout data augmentation led to the best results in all unseen domains in terms of average AUC for both backbones.

To enhance their model’s generalizability to different devices, Lafarge and Koelzer [103] incorporated an extensive and aggressive data augmentation technique. They applied a sequence of transformations such as transposition, color shift, Gamma correction, Hue rotation, spatial shift, additive Gaussian noise and cutout [47]. They applied this method for mitotic figure detection in WSI from MIDOG challenge. The evaluation on the preliminary test set of the challenge resulted in a F1 score of 0.6828.

Dexl et al. [48] performed a single augmentation to each image as part as a very simple random augmentation approach, inspired by Trivial Augment [137]. These augmentations are uniformly selected from a pool of color, noise, and special transformations, with the intensity of augmentation randomly chosen within a predefined range. The pool of augmentations includes color jitter, Histogram Equalization (HE), fancy PCA, hue modification, saturation modification, equalization modification, random contrast, auto-contrast, contrast limited adaptive histogram equalization, solarize-add, sharpness, Gaussian blur, posterize, cutout, ISO noise, JPEG compression artifacts, pixel-wise channel shuffle and Gaussian noise. Each image is also randomly flipped, and the RGB channels are shuffled at random. Using this strategy, their model achieved an F1 score of 0.7138 on the preliminary test phase of the MIDOG challenge.

In the domain of histopathology, conventional stain normalization methods translate pathology images into a single target stain color style, which may limit the robustness of the detection model when confronted to new stain color appearance. To address this problem, Long et al. [123] proposed to broaden the spectrum of stain color appearances in the training images for boosting the performances of the detection model to unseen data. This is achieved by introducing randomness in selecting stain normalization techniques and target color styles. In particular, they incorporated two *stain normalization* techniques: Reinhard [156] and Vahadane [194]. Each technique is applied using a specific probability. Vahadane transfers color in accordance with the desired color appearance matrix, whilst Reinhard modifies color depending on the target mean and variance. Using the entire training set, they derive an initial range for target mean, variance, and each component of the color appearance matrix, respectively. During augmentation, target values are chosen at random from these ranges, allowing to produce images with a wide variety of color schemes. To achieve robust detection performance for variety of images, they gradually expand those ranges to provide additional training samples to the network until there is a degradation in the detection

performance. Their model, *Domain Adaptive Cascade R-CNN (DAC R-CNN)*, achieved an F1 score of 0.7500 on the preliminary test phase of the MIDOG challenge.

Chung et al. [39] proposed a *GAN-based* approach to expand the style variance of the training data. Each device type is considered as a domain that produces images with distinct ‘styles’, such as differences in hue and contrast. With the aim to develop a method to be robust on device types, they proposed to use style transfer using *StarGAN*. The generator of StarGAN [36], also referred to as the transfer module, is used to translate images into a variously styled image based on the mixing of the device characteristics, without losing morphological information (i.e., structure of a cell and nucleus) upon training. After training their transfer module, a detection network is trained using the translated images for the targeted task (mitotic figure detection). Their model achieved an F1 score of 0.7548 on the preliminary test phase of the MIDOG challenge.

Scalbert et al. [163] introduced a novel Test-Time data Augmentation (*TTA*) based on multi-domain image-to-image translation, using a more recent version of StarGAN (in contrast to Chung et al. [39]), StarGANv2 [37]. This TTA technique is based on the projection of images from unseen protocol into each source domain prior to classification, followed by an ensemble of predictions. They trained a StarGANv2 model, which a multi-domain image-to-image translation model, that can translate an input image x into any source domain without the need of the domain label of the image. The generator of StarGANv2 is given as inputs an image and a domain-dependent style vector. These vectors can either be drawn from a random latent code or from a reference image. The authors proposed to use the former method due to the lighter size and lower computational overhead. In order to preserve the structure of the input image, the perceptual domain invariant loss is used to train the StarGANv2. After training StarGANv2 and a classifier on the source data, they used TTA at inference. Specifically, the generator of StarGANv2 projects the image into each source domain. Afterwards, the predictions of the classifier and the score of the StarGANv2 discriminator can be used to obtain a final prediction. Different strategies were explored for ensembling: 1) a naive ensembling where only the predictions of the classifier are average 2) a discriminator-based top-k ensembling, where a domain discriminator score indicates how well the test image aligns with the respective source domain. Accordingly, the top k predictions linked to images with the top-k domain discriminator are combined 3) a discriminator-based weighted ensembling, where weighting the top k predictions is proposed based on their domain discriminator scores to reduce the influence of poorly projected images. The proposed method has shown good results when evaluated for two different histopathology tasks: 1) patch classification of lymph node section WSIs and 2) tissue type classification in colorectal histological images. The results of their approach were superior to those using standard/ Hematoxylin&Eosin (H&E) specific color augmentation/normalization and standard test-time

augmentation techniques. The naive ensembling technique showed slightly better performances than the two other proposed ensembling strategies.

With the aim to improve the generalization capability of DL model to various vendors, Li et al. [118] also used a GAN-based approach for style transfer. They used CycleGAN to map the images of source domain to a vendor-style domain. The augmented images are then used in their contrastive learning strategies to develop a representation with better generalization capability to various vendor domains (Section 6.1.2.3). In addition, for enhancing the sample diversity, they used different diversifying operations including random cropping, random rotation, horizontal flipping, and adjustment of brightness, contrast, and saturation.

On the other hand, instead of exploiting image-to-image translation models at training phase, Yamashita et al. [219] proposed to use it at testing phase. In particular, they presented a *Style TRansfer Augmentation for Histopathology (STRAP)*⁵, a data augmentation that employs random style transfer from non-medical style source like paintings, with the aim to achieve domain-agnostic visual representations in computational pathology. Through style transfer, the low-level texture content of an image (which is hypothesized to be domain-specific) is changed to adopt the uninformative style of a randomly selected style source image, yet its high-level semantic content (which is supposed to be more domain-invariant) remain intact.

In STRAP, the style of medical images (i.e., histopathology images), namely the texture, color and contrast are translated with the style of a selected non-medical image. However, the semantic content of the image, the global object shapes are unchanged. This is done by applying AdaIn style transfer [83], as in Geirhos et al. [60]. AdaIn style transfer creates an output image by recombining the content of an image and style of an another input image. The content and style images are encoded into a feature space by using an encoder, then the encoded representations are inputted to an AdaIN layer, which aligns the mean and variance of the content feature maps to those of the style feature maps and produces the target feature maps. The augmented image is then created from this target feature maps via a decoder. As style sources, they used different datasets, such as artistic painting from the Kaggle’s Painter by Numbers dataset⁶, natural images from the miniImageNet dataset [199], and the original Stanford-CRC dataset. They applied their method into two different problems: 1) colorectal cancer classification into two distinct genetic subtypes based on WSI in a single-DG setting and 2) identifying the presence or absence of breast cancer metastases in image patches extracted from histopathologic scans of lymph node sections in a multi-source DG setting. Their method achieved higher performances compared to stain normalization based approaches. For the specific task of classification of genetic subtype, STRAP that employed Artistic Paintings and Natural Imaging as style sources outperformed

STRAP that uses histopathologic imaging as style source. Despite promising performances, applying AdaIn as on-the-fly data augmentation is considered to be computationally expensive. Thus, stylized version of the datasets should be prepared in advance. A future perspective of this work is to apply this method to self-supervised learning, where it can be integrated as a data augmentation technique for contrastive learning framework.

Vuong et al. [202]⁷ proposed a new augmentation strategy called *PatchShuffling*, which is inspired by Pretext-Invariant Representation Learning (PIRL) [133]. This strategy aims to enable DL model to learn invariant representation, resistant to domain shift. It is used during the pre-training phase, along with another type of augmentation *InfoMin* [192]. Unlike PIRL, which starts by extracting the patch feature and then rearranging these features within the initial image, PatchShuffling directly shuffles the initial image itself. Initially, PatchShuffling randomly selects a portion from the image, ensuring it size is approximately [0.6,0.1] of the original image area. This cropped image is then resized and randomly flipped. They randomly extract 9 non-overlapping patches and assemble them as 3-by-3 grid to form a new image. On the other hand, the InfoMin augmentation constructs two views of the original image: it is designed to minimize the mutual information between the original and the augmented version of an image, while preserving any task-relevant information intact. Their proposed framework showed promising results when tested for colorectal cancer tissue classification. It outperformed other traditional histology domain-adaptation and self-supervised learning methods. As a future step, the authors proposed to investigate the combination of PatchShuffling with other domain-specific augmentation.

Xiong et al. [212] introduced *Enhanced Domain Transformation* (EDT) for improving DG on unseen images. The proposed technique is based on the idea that if a transformed color space represents the unseen data with a distribution identical to that of training data, as a result the model trained on that space should generalize more effectively. The EDT framework incorporates several image processing steps to enhance model generalization capabilities. Initially, it employs image local average subtraction, a technique inspired by Kaggle Diabetic Retinopathy (DR) winning solution [64]. Following this step, it applies average blurring for reducing high-frequency noise and Adaptive Local Contrast Enhancement (ALCE) for normalizing the images. Furthermore, it utilizes PCA color jittering which modifies the training image color with the predominant color component to simulate the color characteristics of the unseen domain. The provided image might originate from the known domain, unseen domain or even non-medical images (ImageNet, etc.). This method was applied for age regression and DR classification using fundus photographs. Despite promising results, the average blurring process can mask important features, reducing the model’s classification performance.

⁵<https://github.com/rikiyay/style-transfer-for-digital-pathology>

⁶<https://www.kaggle.com/c/painter-by-numbers>

⁷<https://github.com/trinhvg/IMPash>

6.1.2. Representation Learning

Representation learning involves training a parameterized model to learn the mapping from the raw input data to a feature vector, with the aim of uncovering more abstract and useful concepts. This process is designed to enhance the effectiveness of various downstream tasks by capturing the essential information embedded in the data [108]. In the context of DG, representation learning mainly focus on the concept of domain alignment for creating robust and generalized representations to unseen data. The goal of domain alignment is to minimize the difference among source domains for learning domain-invariant representations. It assumes that domain-invariant representation to the source domain should also be robust to unseen test domain. Recently, many methods have emerged to measure the distance between distributions and achieve domain alignment. These methods can be categorized into four main groups: adversarial learning, distance metric learning, contrastive learning, and regularization.

6.1.2.1 Adversarial learning

Adversarial learning was initially proposed by Goodfellow et al. [62] to train a generative model, which can create realistic images. In essence, the training process consists of two neural networks competing against each other: a discriminator network and a generator network. The goal of the discriminator is to differentiate between images coming from the training data and the generated data. In contrast, the generator is tasked to generate fake data so realistic that can confuse the discriminator. In DG, adversarial learning is utilized to acquire source domain-invariant features that can be effectively used on new testing domains. In this setting, the learning goal is to confuse a domain discriminator, which is trained to detect the domains using features produced by the encoder.

Guan et al. [68] presented an *Attention-driven Deep Domain Adaptation (AD²A)* approach, an adversarial learning based method. Specifically, the AD²A framework incorporates: 1) a feature encoding module (E) to extract feature representation, 2) an attention discovery module that discovers disease-related regions and 3) a domain transfer module with adversarial learning for knowledge transfer between the source and target domains. The domain transfer module includes two classifiers that are co-trained throughout the model learning process: a domain discriminator/classifier (C_D) and a category classifier (C_S). The goal of the domain discriminator is to distinguish whether features arising from an input sample are from the source or target domain. To this end, C_D is trained to minimize the cross-entropy loss to determine features from different domains:

$$\mathcal{L}(C_D) = \frac{1}{B} \sum_{k=1}^B L(C_D(E(x_k)), y_k) \quad (4)$$

where x_k are samples drawn from source and target domain, y_k are domain labels, with $y_k = 1$ indicating x_k comes from source domain and $y_k = 0$ denoting x_k comes

from target domain. $L(\cdot)$ is the cross-entropy loss. B is the number of samples in the training batch.

In contrast, the category classifier is tasked to identify diseases. The category classifier is trained using the cross entropy loss:

$$\mathcal{L}(C_S) = \frac{1}{n} \sum_{i=1}^n L(C_S(E(x_i)), y_i) \quad (5)$$

The end goal is to learn domain-invariant features across the source and target domain, that is to accurately predict labels without relying on any domain indicators. To this end, the feature extraction network is jointly trained to minimize the category classification loss (equation 5) and maximize the domain classification (equation 4) using stochastic gradient descent:

$$\mathcal{L}_{total} = \mathcal{L}(C_S) - \alpha \mathcal{L}(C_D) \quad (6)$$

where α is a hyperparameter to control the contribution of adversarial loss. In practice, given that the feature extraction network parameters are jointly updated by the backpropagation of the category classifier and domain discriminator, a self-defined *gradient reversal layer* is added to transmit negative gradient variations by the domain discriminator. Note that in the forward propagation, this layer acts as an identity transform.

By co-training the two classifiers, the model is supposed to learn domain-invariant features for both domains as well as strong classification performance for the source data, which increases the robustness of the learnt model when used for the target domain. This method has been evaluated on three benchmark neuroimaging datasets, namely, ADNI-1 [87], ADNI-2 [87], and AIBL [54] datasets, showing good results for brain dementia identification and disease progression prediction.

Similar to the previously mentioned approach, Wilm et al. [209] presented a *domain adversarial RetinaNet* approach⁸ for object detection. They incorporated a gradient reversal layer and a domain classifier to the RetinaNet model. To learn domain invariant feature, the network is trained using the domain classification loss for all source domains, the bounding box regression loss and the instance classification loss. This method was applied for mitotic figure detection in the context of the MIDOG challenge. It achieved an F1 score of 0.7183 on the challenge’s test set.

To address the same problem, another work [123] proposed *DAC R-CNN* (section 6.1.1.2), an UDA technique based on adversarial training. Their network comprises a pretrained ResNet-50 as a backbone, three cascaded detection heads for high quality detector, and a PatchGAN discriminator. The role of the PatchGAN discriminator is to address the differences between different image domains like image color and style. It is trained to distinguish features between source images and target images. At the same time, the discriminator guides the training of the network in an

⁸<https://github.com/DeepMicroscopy/MIDOG>

adversarial manner. One advantage of PatchGAN is that it can be applied to images with arbitrary sizes. In comparison to [209], their model achieved a better F1 score of 0.7500 for mitosis detection on the preliminary test phase of the MIDOG challenge.

Janizek et al. [88]⁹ proposed an *adversarial deconfounding* approach for DG for pneumonia detection using chest radiographs. In particular, they proved improved out-of-hospital generalization performance of their model by making it invariant to the view position of chest radiographs (anterior-posterior vs. posterior-anterior). The classifier is trained to detect pneumonia from a chest radiograph. It is trained using an adversarial network, which is trained to determine the view from the output score of the classifier. Both networks are trained in an alternative way, first the adversary network is optimized then the classifier is trained to fool the adversary network and to detect pneumonia. This approach does not require data from the target domain, instead it is based on domain knowledge about the causal relationships involved in the data to identify nuisance variables. These variables might relate differently to the outcome in the test domain than in the source domain. To overcome this issue, adversarial technique has shown promising results to train a classifier that is invariant to the nuisance variable.

Chen et al. [34] also presented an adversarial framework, *Cross-device and Cross-anatomy Adaptation Network (CCAN)*, for video analysis. They proposed to incorporate mutual information and multi-scale deep features to bridge the gap between high-end and low-end medical imaging devices and protocol. To overcome the problem of large anatomical variations, they used the concept of mutual information to align the distribution of multi-scale deep features in adversarial training. This was achieved by training two discriminators that focus on local and global representations. These discriminators are tasked with distinguishing whether pairs of features are related or unrelated based on their mutual information. In practice, the mutual information is computed using two binary classification losses, to detect whether two features are a positive or negative pair from the same image. The first loss, called local mutual information loss, aims to maximize mutual information between the local features (extracted from local convolutional feature maps) and the global semantic feature (the projected latent global feature representation). On the other hand, the second loss, the global mutual information loss, aims to maximize mutual information between the global semantic features, and the classifier predictions. Their approach showed promising results when evaluated for anatomy classification of ultrasound datasets. It showed significant improvement: the mean recognition accuracy increased by 20.8% and 10.0%, compared to a method without domain adaptation and a domain adaptation method based on adversarial learning (DANN), respectively.

⁹https://github.com/suinlee/cxr_adv

6.1.2.2 Feature distribution alignment

An alternative to domain adversarial learning for achieving domain-invariant representations is to match the feature distributions. This is typically achieved using information theory based technique such as Kullback-Leibler (KL) divergence. By minimizing the KL divergence, all source domain representations are aligned with a Gaussian distribution. On the other hand, other strategies such as Minimax Entropy (MME) use the principle of entropy minimization to achieve domain alignment.

Meng et al. [132]¹⁰ proposed an UDA framework based on *distance Metric guided Feature Alignment (MetFA)* to learn domain-invariant latent representations. The main idea of MetFA is to align features between the source and target domain, in order to enhance the generalization of DL models. MetFA comprises three key steps: 1) a supervised classification on the source domain, 2) feature alignment, and 3) class distribution alignment.

First, a supervised model, which is composed of an encoder, a Gaussian embedding and a classifier, is trained on source labeled domain data using a standard classification loss (i.e., cross-entropy loss). Next, features of the source and target domains are aligned according to a predefined distribution within a shared latent space. That is, features from both domains are embedded into a common latent space, where they are guided to follow a predefined distribution (i.e., a Gaussian distribution). To this end, the KL divergence is employed to align the embeddings with a Gaussian distribution. In this shared latent space, the authors proposed to estimate class representations (prototypes) to constrain the features to be domain-invariant in each class.

In essence, this technique is inspired by MME [161], a semi-supervised DA technique that identifies domain-invariant prototypes and clusters target domain features around them. In MME, a single domain-invariant prototype (a representation point) is learned for each class. The distance between the class prototypes and neighboring unlabeled target samples is then minimized to extract discriminative features. The model architecture is composed of an encoding network and a classification layer, wherein the weight vectors are treated as the class-specific prototypes. The adaptation process in MME involves two steps. In the initial step, the prototypes are transitioned from the source domain to the target domain by maximizing the conditional entropy of unlabeled target data with respect to the classifier. This step is followed by minimizing the entropy with respect to the feature extractor to cluster features around the estimated prototype.

In addition, to enhance separation between clusters of different classes in both domains, they introduced cross-domain metric learning. It aims to minimize the distance between the latent features of target data (z_T^f) and the latent features of labeled source data (z_S^f) when they belong to the same class, while maximizing the distance when they are from different classes. The metric loss is defined as follows:

¹⁰<https://github.com/qingjie99/MetFA>

$$\mathcal{L} = \frac{1}{n_{\mathcal{T}}} \sum_{i=1}^c \sum_{j=1}^{c_{\mathcal{T}_i}} \log(1 + \sum_{\substack{k \in [1, c] \\ k \neq i}} e^{d_j^i - d_j^k}) \quad (7)$$

where c is the number of classes. $n_{\mathcal{T}}$ and $c_{\mathcal{T}_i}$ are the number of all latent features of target samples and the number of latent features of target samples from class i .

Using a hard mining strategy [32], d_j^i is the distance between $z_{\mathcal{T}_j}^{f_i}$ and a same class $z_{S_i}^{f_i}$:

$$d_j^i = \max_t d(z_{\mathcal{T}_j}^{f_i}, z_{S_i}^{f_i}), t \in [1, c_{S_i}] \quad (8)$$

where c_{S_i} denotes the number of z_S^f from class i and $d(.,.)$ the squared Euclidean distance.

d_j^k is the distance between $z_{\mathcal{T}_j}^{f_i}$ and a different class $z_{S_i}^{f_k}$:

$$d_j^k = \min_t d(z_{\mathcal{T}_j}^{f_i}, z_{S_i}^{f_k}), t \in [1, c_{S_k}] \quad (9)$$

where c_{S_k} denotes the number of z_S^f from class k .

Beyond aligning individual features, MetFA also aligns the class distributions between the source and target domains. To this end, similar to Dou et al. [50], a soft label distributions with a "softened" softmax at temperature τ is computed for the target and the source domain. Specifically, for the source domain, the soft label distribution (s_{S_i}) is computed as follows: $s_{S_i} = \text{softmax}(\frac{1}{\tau_1} \frac{1}{c_{S_i}} \sum_{y=i} z_S^c) |_{(x,y) \sim \{S\}}$, where z_S^c are the pre-softmax activations from the classifier for the source domain samples and τ_1 is a temperature parameter. Similarly, $s_{\mathcal{T}_i}$ is the i^{th} class distributions in target domain such as: $s_{\mathcal{T}_i} = \text{softmax}(\frac{1}{\tau_1} \frac{1}{c_{\mathcal{T}_i}} \sum_{y=i} z_{\mathcal{T}}^c) |_{(x,y) \sim \{\mathcal{T}\}}$, $z_{\mathcal{T}}^c$ are the pre-softmax activations from the classifier for the target domain samples and $c_{\mathcal{T}_i}$ is the number of target domain samples predicted for class i . The symmetrized KL divergence is then used to define the class distribution alignment loss between s_{S_i} and $s_{\mathcal{T}_i}$.

6.1.2.3 Contrastive learning

Domain alignment based on contrastive learning has emerged as an effective strategy. These techniques often employ contrastive learning, a machine learning paradigm which can be viewed as learning by comparing. In contrastive learning, a representation is learned by comparing among the input samples. The comparison can be conducted between pairs of similar inputs (positive pairs) and pairs of dissimilar inputs (negative pairs). The method involves computing the distance between feature vectors of image pairs and deriving the loss according to this distance. An image pair is deemed sufficiently dissimilar if the computed distance exceeds a predetermined margin. Typically, most studies considered images coming from the same class as similar pairs.

Gurpinar et al. [72] proposed a DA approach based on contrastive learning with cosine distance to align data

distributions between source and target domain. Their approach consists of using the contrastive learning framework to align the embedding features, with the aim to decrease the discrepancy between the source and target domains. While the definition of positive and negative pairs is considered to be explicit in multi-class classification problem, in multi-label problem it becomes more challenging to form these pairs. To this end, Gurpinar et al. [72] used a Siamese network to learn embeddings such that samples from the same class are gathered closer and samples from different classes are pushed away. In addition, they added a new smoothing parameter, β , to the loss to make it proportional to the similarity regarding present labels.

$$\beta = \frac{|(Y_S \cup Y_{\mathcal{T}})| - |(Y_S \cap Y_{\mathcal{T}})|}{|(Y_S \cup Y_{\mathcal{T}})|} \quad (10)$$

where Y_S and $Y_{\mathcal{T}}$ denote the label vectors for a pair of source and target images, respectively. The contrastive loss is then updated as:

$$\mathcal{L}_{\text{contrastive}}(Y, d) = \frac{1}{2}(1-Y)d^2(1+\beta) + (Y)\frac{1}{2}\max(0, m-d)^2 \quad (11)$$

where d denotes the cosine distance between feature vectors extracted from the pair of images, m indicates the margin and Y represents the pair labels ($Y = 1$ for dissimilar pairs and $Y = 0$ for similar pairs). β values range between 0 and 1.

They applied this method for building a facial action unit detection model for children with hearing impairments, showing that integrating β leads to improved results between and 3% to 14%.

Le et al. [107] argue that data augmentation allows the extension of the training data but does not provide a theoretical guarantee for DG. On the other hand, invariant feature representation learning offers theoretical guarantee but the number of targeted domains that can be addressed is limited by the original training domains. To boost the performances, they proposed to combine both approaches. In particular, they applied data augmentation including random cropping, random horizontal flip, random color jitter, random grayscale, random Gaussian blur, normalization, and random erasing. To enforce invariant features, they proposed to minimize the distance between original and augmented domains using a supervised contrastive learning loss. Specifically, they adopted the contrastive loss in the form of normalized temperature-scaled cross-entropy loss (NT-Xent). The essence of this method is to minimize the distance between original and augmented domains. Positive pairs consist of pair of samples from the same class while negative pairs are from different classes.

The feature extractor was trained to optimize the cross-entropy loss and the contrastive loss while the classifier was optimized to minimize the cross-entropy loss. They used a different learning rate to update the feature extractor and the

classifier. A disadvantage of this method is it assumes that the label distribution to be roughly equal across the domains, implying the need for balanced datasets. It was assessed on the medical benchmark dataset of chest X-ray dataset and on DG benchmark PACS.

6.1.2.4 Consistency regularization

Consistency regularization methods in representation learning mainly focus on adding a loss to the learning objective for making the model robust against variations in input data that are irrelevant to the classification task such as changes in texture, color, etc.

With the aim to develop generalized representations, Zhang et al. [231] proposed a semi-supervised DG method, called *Stable and Orthogonal Feature Regularization (SOFR)*. The main idea is to make the learned representation have two characteristics: stability and orthogonality. The stability enforces the features to be domain-invariant using a data augmentation technique, domain randomization (see Section 6.1.1.2), while the orthogonality avoids overfitting by enforcing minimal redundancy.

To enforce the model to learn domain-invariant features that are orthogonal to each other, two regularization factors are integrated to the learning objective. For enforcing feature stability, a regularization based on an instance-level paradigm is used. In particular, it consisted of computing the sum of the channel-wise cosine distance between the original feature and its augmented version (its domain-randomized counterpart). The orthogonality of features is measured by cosine similarity between different channels. This method was applied for Chest X-ray diagnosis, using MIMIC [90] as the labeled source and NIH [207] and CXP [85] as unlabeled source domain. It was tested on the PadChest [28] dataset, showing promising results with a mean AUC of 0.8443.

Raipuria et al. [151] proposed a regularization loss to achieve better generalization performances in computational histopathology. They introduce a *consistency regularization loss* to constrain their model to achieve high invariance to stain color changes on unseen test data. Using this technique, the model is enforced to produce consistent predictions between original samples and their stain modified versions. This is done by minimizing the KL divergence loss:

$$\mathcal{L}_{consistency} = D_{KL}(C(F(E(x))) || C(F(E(\hat{x})))) \quad (12)$$

where C denotes the classifier, F is the projector, E is the encoder, \hat{x} is the stained altered image, D_{KL} is the symmetrized KL divergence.

In addition to the *consistency regularization loss*, *stain regeneration loss* is employed to train a decoder to regenerate the original stain color using feature representation of the stain modified images (\hat{x}). To this end, they employed the mean squared error loss between the raw image and the regenerated image. This loss is considered as an auxiliary task which helps the model to improve generalization on images with stain variation by learning shared features for

classification and regeneration task. This method was evaluated on two publicly available datasets TUPAC Mitosis Detection and Camelyon17 Tumor Metastasis Detection. It showed that stain-invariant features results in improved performance on unseen images coming from different centers.

For the purpose of DG in real-time surgical tool detection, Reiter [157] proposed to improve a transformer-based architecture, *DEtection TRansformer (DETR)* [29], by adding a latent feature space using variational encoding. This step is designed to capture the common intra-domain information by fitting the latent features to a prior distribution, a multivariate Gaussian. In addition, they employed a rank regularization to enhance the model’s ability to generalize across different domains. This approach is based on the assumption that there are linear dependencies between the latent features of different domains. This means that the latent features from one domain can be linearly related to those of another domain. In particular, it is assumed that a matrix formed from the latent features for a given label contains an influential eigenvalue related to that label. This allows the regularization of intra-class variability by constraining the rank of the latent features to the number of classes. This is done by minimizing the corresponding diagonal value in the matrix returned by singular value decomposition. The results of this method has shown improved DG performance for end-to-end detection in surgical tool detection, when assessed on three public datasets showing different instrument types and procedures.

Similarly, Li et al. [112] proposed a *Linear-Dependency Domain Generalization (LDDG)*¹¹ method to improve the generalizability of DL model for medical image classification. Similar to the aforementioned method, the authors used a linear-dependency modeling and imposed a rank regularization based on the latent feature space. Moreover, they used variational encoding for distribution alignment. To this end, they adopt KL divergence for matching the latent features from multiple source domains to a pre-defined prior distribution, which in this paper was defined as Gaussian distribution. They evaluated this approach on two challenging medical imaging classification tasks: skin lesion classification and Spinal cord gray matter segmentation.

Viviano et al. [200] investigated whether poor generalization in DL models can be visually diagnosed using *attribution (or saliency) maps*¹². The motivation behind this is that saliency maps could demonstrate if the DL model is behaving unexpectedly. For instance, instead of learning robust representation, i.e., features that denote a class, the DL model can learn spuriously-correlated image features present only in the training distribution. This behavior is also known as *shortcut learning* or *incorrect feature attribution*, where the model overfits to a set of training data. The authors hypothesized that models showing good generalization properties have attribution maps which only use the class-discriminative features to make predictions. To this end, they proposed a regularization strategy where the DL model is

¹¹<https://github.com/wyf0912/LDDG>

¹²<https://github.com/josephdiviviano/saliency-red-herring>

trained to ignore confounders (such as acquisition site or other image acquisition parameters) using attribution priors, i.e., to produce predictions using the correct anatomy (as a medical expert would). To accomplish this, they used medical datasets with auxiliary labels which consisted of masks drawn by an expert, indicating a region of the image containing relevant information to make the predictions. To make the model invariant to features arising from outside of the attribution priors, they studied two feature-aware methods: 1) the *Activation Difference (ActDiff) Approach*, which regularizes the model and penalizes the L2-normed distance between the masked and unmasked input’s latent representations, 2) *adversarial approach* which employs a discriminator to identify whether latent representations come from a masked or unmasked input. In parallel, the encoder is trained to fool the discriminator and produce discriminative representations. In addition, they explored the *saliency penalties*, where *GradMask* [181] and *Right for the Right Reasons (RRR)*[159] are applied on the input space. The idea is to penalize the model for producing saliency gradients outside of regions of interest denoting the class-discriminative feature. The results showed that although the DL models were explicitly regularized to not use features constructed from outside of the mask, the DL network still attribute features outside of the mask at test time. Therefore, the authors concluded that the proposed methods do not guarantee to negate any confounding variables that exist within the mask.

6.1.3. Learning strategies

Different learning paradigms have been proposed to enhance generalization performances. These learning techniques include: ensemble learning, test-time augmentation, incremental learning, self-supervised learning, meta-learning, gradient-operation, distributionally robust optimization, and multi-task learning.

6.1.3.1 Ensemble learning

In machine learning, ensemble methods are very common to boost generalization performance. The principle of ensemble learning is to derive a prediction given predictions from multiple models (i.e., an ensemble). This is typically implemented as a simple averaging over the ensemble predictions. In DG, more generally, ensemble learning refers to combining multiple models to enhance generalization.

Philipp et al. [146] tackled the challenge of DG in surgical instrument localization. In this context, domain shift refers to different type of surgery, illumination, types and appearances of instruments. To overcome the problem of domain shift, the authors proposed an *uncertainty-based CNN approach* which adaptively chooses the most pertinent data source by integrating its own uncertainty into the inference. In particular, they trained a dynamic CNN on a single dataset which consists of combined image and optical flow modalities. The network comprises two ensemble networks, one for each modality. In order to extract the most relevant information from both data sources, the network is guided

using uncertainty-based criteria which estimates the pixel-wise prediction quality for each modality. Pixel-wise uncertainty is defined as the standard deviation across the ensemble outputs. Next, the authors normalize these pixel-wise uncertainty to produce "uncertainty masks" ranging between 0 (high uncertainty) and 1 (high confidence). Finally, by weighting the predictions from each modality based on their respective uncertainties, the method ensures that the final output is influenced more by the most certain and relevant data. Then, a weighted linear combination of the predictions is computed. The proposed method was evaluated on different surgical datasets, i.e., eye and laparoscopic surgeries. It showed good generalization performances across different surgical domains.

Wang and Xia [203] proposed to use a *consistency regularization loss* in *Domain-Ensemble Learning with Cross-Domain Mixup (DELCOM)*. Specifically, they consider the predicted probability vector z_i^c of a domain-specific model f_i as a pseudo label to supervise the learning of non-domain specific model $f_j (j \neq i)$. Given M domains, an ensemble of the predictions from all non-domain-specific model is computed $z_i^{c(ens)} = \frac{1}{M-1} \sum_{j=1, j \neq i}^M z_i^{c(j)}$. In order to enforce the consistency between the predictions made by non-domain-specific models and the pseudo label, a consistency regularization loss is defined as follows:

$$\mathcal{L}_{CR} = \sum_{i=1}^N ||z_i^{c(ens)} - z_i^c||^2 \quad (13)$$

Each domain is selected in turn, supervised learning is applied for domain-specific model and consistency regularization learning is performed for non-domain-specific models. To enhance the consistency regularization loss, weak transformations are employed to augment the inputs of f_i such as standard flip-and-shift transformation. In contrast, strong transformations are used to augment the inputs of $f_{j \neq i}$ by using a combination of RandAugment [44] and flip-and-shift transformation. This method was applied for thoracic disease classification in unseen domains and showed that it outperformed the state-of-the-art DG methods on unseen datasets.

Shen et al. [171] proposed *CD2-pFed*, a novel Cyclic Distillation-guided Channel Decoupling framework, to personalize the global model in federated learning. To address the non-IID data across different clients, they presented a *channel decoupling strategy* for model personalization. The goal is to train a collection of k models clients to effectively adapt to their local dataset without exchanging their data. The network of each client i is composed of private personalized parameters θ_i , and global shared parameters θ_0 . Specifically, they applied a vertical decoupling strategy consisting of assigning an adaptive proportion of learnable personalized weights at each layer from the target model, moving from the top layers to the bottom layers. A uniform personalization partition rate, ranging between zero and one, is defined to determine the precise proportion of the personalized channels in each layer. At the initial stage, it

is set to a small value to facilitate learning global representation for faster convergence, and afterwards gradually increase its value. Moreover, to enhance the collaboration between private and shared weights, they used a novel *Cyclic Distillation (CD)* scheme to impose a consistent regularization between the local and global model representations to avoid divergence. For each input sample, they used the KL divergence to impose an consistency regularization between the θ_i and θ_0 guiding the predictions from θ_i and θ_0 denoted by \hat{y}_i^L and \hat{y}_i^G to align to each other:

$$\mathcal{L}_{CD} = \frac{1}{2}(KL(\hat{y}_i^L, \hat{y}_i^G) + KL(\hat{y}_i^G, \hat{y}_i^L)) \quad (14)$$

They tested their approach on Histo-FED, a medical image dataset, consisting of both public and private H&E stained histological WSI of human Colorectal Cancer (CRC) and normal tissue. They showed that guided by cyclical distillation, their channel decoupling framework can deliver more accurate and generalized results, outperforming the baselines.

For the purpose of training DL models robust to data heterogeneity in a federated learning setting, Andreux et al. [6] presented a *SiloBN*, a novel federated learning approach that uses local-statistic Batch Normalization (BN) layers. The premise of this method is that BN layers can be employed to discriminate between local and domain-invariant data. An input tensor x is normalized using a BN layer, as described in the following equation:

$$BN(x) = \gamma \frac{x - \mu}{\sqrt{\sigma^2 + \epsilon}} + \beta \quad (15)$$

where γ and β are learned affine renormalization parameters along the channel axis (learned parameters), μ and σ^2 denote the running means and variances of each channel computed across both spatial and batch dimensions, respectively (BN statistics).

In particular, the statistics from BN and its trained parameters serve distinct purposes. While the training parameters may be used across other domains, BN statistics reflect local domain peculiarities. Andreux et al. [6] proposed to take into account the separate roles of BN statistics and learned parameters. In *SiloBN*, only the learned BN parameters are shared across centers, whereas BN statistics remain local. This approach is considered as model personalization method as a model per center is learned, rather than one global model. To generalize the resulting models to unseen center, similar to AdaBN [116], the authors proposed to recompute BN statistics on a data batch from the target domain and keep the other model parameters frozen from the federated learning. This approach has shown promising out-of-domain generalization performances when assessed on real-world multicentric histopathology datasets.

6.1.3.2 Test-time augmentation

Inspired by ensemble methods and adversarial examples, *Test-Time Augmentation (TTA)* stands as a straightforward

approach for estimating predictive uncertainty. This technique involves generating multiple augmented versions of each test sample by applying various data augmentation methods. These augmented images are then inputted to the model which returns an ensemble of predictions. In DG, this method can be used to project images to the source domains and then ensemble their predictions. It can also be used to select robust features for inference.

Scalbert et al. [163]¹³ integrated TTA to their DG framework based on multi-domain image-to-image translation model StarGANv2 (which was detailed in Section 6.1.1.2). At test time, this method projects testing images to the source domains, classify the projected images and ensemble their predictions. This method does not rely on any prior on the domain shifts, it learns them directly from the training data. Given an unseen image, the authors sample M (where M is the number of source domains) random latent code vectors with respective domain label. Then, different style vectors are generated by feeding the random latent code and its domain label to a mapping network. Finally, given the testing image with the style vectors, the StarGanV2 generator translates the image to different source domains. The conducted experiments on different histopathology datasets showed that the method is more efficient than previous color augmentation/normalization, train-time data augmentation and DG methods (including CORAL[186], IRM [8], Group DRO [160] and FISH [176]).

On the other hand, recent studies have shown that test-time feature selection can achieve significant gains in performance, even when spurious correlations are learned [24]. Bissoto et al. [23]¹⁴ proposed to use this concept in their framework. They employed *test-time debiasing*, where most relevant features are selected to boost the performances. More particularly, they applied *NoiseCrop* procedure which removes the background information, replaces it with a uniform noise, and resizes the lesion to occupy the whole image. The proposed approach was applied for skin lesion detection. For better generalization assessment, the data was partitioned into levels of increasingly higher biased training and testing sets. The results showed that their approach outperformed the baseline ERM approach and other DG methods such as RSC and GroupDRO with an AUC of 0.74 on a strong biased test set (referred to as trap test). For out-of-distribution sets, the gain of performances using debiasing depends on the similarity between the artifacts present in the testing subset and those in training, used to partition domains. Despite promising performances, *test-time debiasing* requires domain knowledge of the task.

6.1.3.3 Incremental learning

Incremental learning also known as lifelong learning or continual learning, is a machine learning process where data arrives in sequence, or in a number of steps instead of

¹³<https://gitlab.com/vitadx/articles/test-time-i2i-translation-ensembling>

¹⁴<https://github.com/alceubissoto/artifact-generalization-skin>

having access to all the training data as in classical scenarios. With the continued emergence of novel medical devices and procedure protocols, incremental learning has gained interest in DG. It allows the model to learn new domain shifts, without the need to retrain the model from scratch.

In the context of surgical scene understanding, Seeni-vasan et al. [166] proposed *incremental domain generalization*¹⁵ on scene graphs to predict instrument-tissue interaction during robot-assisted surgery. First, a Feature Extraction Network (FEN) ResNet18 is trained to classify the instruments and tissues in the source dataset (a nephrectomy surgery dataset). For the task of human-object interaction detection, the authors employed a graph network. After extracting the visual features of tissues and instruments using the FEN, these features are embedded in a visual graph. In parallel, nodes and node names are embedded in a semantic graph. After node aggregation in both graphs, these graphs are merged to form a combined graph G_c . Once G_c is aggregated, its edge features are processed by a readout function to estimate interaction logits.

In order to extend the model to the target domain (transoral robotic surgery), the authors employed incremental DG which incorporates the *incremental learning* and the *knowledge distillation*. Whereas the incremental learning is used to include novel instruments in the target domain, the knowledge distillation technique is adopted to generalize the model to domain shift in the target domain. To this end, the FEN is enhanced with incremental learning to include new instruments. Since each scene is considered as a sparse graph and the graph network is robust in handling various numbers of nodes without a fixed sequence, novel instruments can be incorporated by training the graph network on the target domain data without changing the network architecture.

To handle domain shifts, the authors integrated an enhanced graph network with a teacher-student model-based knowledge distillation. In particular, the teacher network is a network trained on the source domain using the multi-label soft margin loss between the network output and the ground truth. In contrast, the student network is a copy of the teacher network. It is trained on the whole target domain dataset and on a sample of the source domain dataset using the multi-label soft margin loss. In addition, the student network is regularized using a *knowledge distillation loss* between the teacher and student network logits. This loss allows the student network to retain on the source domain while generalizing to the target domain. Despite promising performances, this method showed limited performances on the target domain. Thus, further improvement are required for real-world applications.

In line with the previously mentioned paper, the authors [167] designed a multi-task learning model¹⁶ to perform tool-tissue interaction detection and scene caption. The model consists of: 1) a shared feature extractor 2) a mesh-transformer branch for scene captioning and 3) a graph attention branch for tool-tissue interaction detection.

To deal with domain shift, the authors proposed a *class incremental contrastive learning* approach for surgical scene understanding. In addition, *curriculum learning* is applied by using Laplacian of Gaussian (LOG) based curriculum by smoothing across all three modules to enhance model learning. In particular, curriculum by smoothing is adopted. The authors used LOG kernels, instead of the standard Gaussian kernel, to achieve better feature representation learning and highlight the instrument contours.

6.1.3.4 Self-supervised learning

Self-supervised learning is a paradigm in machine learning aiming to construct robust image representations via pretext tasks that do not require semantic annotations. Within the context of DG, self-supervised learning based on contrastive learning has recently emerged. In self-supervised learning, the focus shifts from relying on class labels to leveraging the structure within the data itself. Typically, it uses a pre-train strategy wherein a DL model is encouraged to develop generalized representations. It achieves this by optimizing for similarity across different augmented versions of the same image within the training dataset. These methods mostly use contrastive learning to produce pre-text invariant representations, without the supervision of annotations.

For instance, Li et al. [118] proposed to learn invariant features to various vendor-device styles by training a network with a multi-style and multi-view unsupervised self-learning scheme using contrastive learning. In their self-supervised framework¹⁷, an encoder is trained to learn representations using contrastive learning, without the supervision of annotations. The end goal is to pre-train a model for various downstream tasks.

In order to form the pairs for self-supervised learning, the input mini-batch (B) is augmented into $2B$ samples using random augmentations such as cropping, and rotation. Using the augmented mini-batch, two samples from the same image source are considered as a positive pair (i, j) while the other samples within the mini-batch are regarded as negative pairs. The contrastive loss in self-supervised learning scheme, is defined as:

$$\mathcal{L}_{i,j} = -\log \frac{\exp(\text{sim}(z_i^f, z_j^f)/\tau)}{\sum_{k=1}^{2B} \mathbb{1}_{k \neq i} \exp(\text{sim}(z_i^f, z_k^f)/\tau)} \quad (16)$$

where z^f denotes the extracted features, $\text{sim}(\cdot)$ is the dot product, $\mathbb{1}_{k \neq i} \in \{0, 1\}$ is an indicator function equals to 1 when $k \neq i$ and τ is a temperature parameter.

Through maximizing the agreement for the positive pairs, the learned representations should be more general and robust to the augmentations or operations performed. The authors used this concept to explore the generalization for various vendor styles and the domains of CC and MLO views in mammography. More specifically, to achieve the aim of generalization to multiple vendor styles, the authors used

¹⁵<https://github.com/lalithjets/Domain-Generalization-for-Surgical-SceneGraph>

¹⁶<https://github.com/lalithjets/Domain-adaptation-in-MTL>

¹⁷<https://github.com/lizheren/MSVCLMICCAI2021>

a CycleGAN to create multiple vendor style images from a single source image. Positive pairs for multi-style contrastive learning are formed by randomly selecting two images derived from the same source image (including the original and its transformed versions). The other combinations are treated as negative pairs. In addition, they employed multi-view contrastive learning where the CC and MLO views of the same breast are considered positive views while the other combinations are negative pairs. After pre-training with contrastive loss, the backbone is used for the main task of lesion detection. The proposed method was assessed with mammograms from four vendors and one unseen public dataset. It has shown that it can help to significantly improve lesion detection on both seen and unseen domains.

Similarly, Vuong et al. [202] proposed to use a self-supervised approach using contrastive learning for achieving a domain-shift robust representation. For achieving good image representation, contrastive learning method requires to process a large batch size, which is computationally demanding, a high GPU memory is needed. To overcome this issue, Vuong et al. [202] employed *Momentum Contrast (MoCo)* [74] which enables the construction of a consistent dictionary of negative samples in near-linear scaling. The authors designed two dedicated momentum branch for using MoCo for both InfoMin and PatchShuffling augmentations (described in Section 6.1.1.2). Each branch encodes and stores a dictionary of image representations of the corresponding studied augmentation. They employed an extended version of InfoNCE loss [141], where the mutual information across positive pairs resulting from an encoder and its momentum version is maximized. In contrast, the similarity between the representation of the current view of the image and the representations of other negative samples, as encoded by the momentum encoder, is minimized.

For the application of surgical scene understanding, Seenivasan et al. [167] proposed to use *Class Incremental Contrastive Learning (CICL)* to address intensity shift and novel class appearance in the target domain. Inspired by Xu et al. [214], they integrated supervised contrastive loss, also known as SupCon loss [98], in their framework. This technique also applies extensive augmentation to the input and maximizes the mutual information for different views. However, it also minimizes the distance between the same label inputs across domains and pushes apart the samples with different labels in the feature embedding space.

For boosting representation learning and improving the recognition of low-prevalent diseases, Lee and Song [110] proposed *Self-supervised semi-supervised learning (S^4L) using Unlabeled Photographs and Robust Domain-Adaptive Distillation (SUPRAD)*. It consists of three main components: 1) supervised learning on labeled data for Extended Single Label (ESL) baseline 2) Self-Supervised Semi-Supervised Learning (S^4L) with an additional auxiliary head, and 3) UDA followed by Domain-Adaptive Distillation (DAD).

The ESL task learning aims to learn generic feature representation from a more difficult task. In ESL, images are

re-labeled by assigning a separate single label to images that belongs to multiple diseases. A DL model is then trained on the re-labeled images using the cross-entropy loss and a class-balanced loss technique.

The S^4L component consists of retraining the model using consistency regularization on unlabeled data. In order to enforce the model to predict with confidence on the perturbed data, they used a consistency regularization loss (\mathcal{L}_{cr}) for unlabeled data. It consisted of a combination of Virtual Adversarial Training (VAT) [134] loss and Conditional Entropy Minimization (CEM) [66] loss. In addition, they integrated a self-supervised learning loss where they adopted rotation pretext task. To this end, they augmented images in the dataset by creating four rotated copies from x by $\{0^\circ, 90^\circ, 180^\circ, 270^\circ\}$ degrees, and trained an auxiliary head to predict the rotation task.

Finally, to address domain divergence, they employed MUDA [109], an UDA framework where they considered the labeled domain as source domain and unlabeled domain as the target domain. This approach constraints the model to contain more robust features by minimizing the predictive uncertainty associated with the models. It leverages the potential distribution shifts between labeled and unlabeled data. Further enhancing this approach, the framework uses a distillation process where knowledge from an ensemble of ESL, S^4L and UDA is distilled to an identical student model.

6.1.3.5 Meta-learning

Meta-learning, also known as learning to learn, is a paradigm aiming to learn from episodes derived from related tasks to enhance the efficacy of future learning. The motivation for incorporating meta-learning in DG stems from the objective to expose the DL model to domain shift during training, thereby improving the model adaptability to domain shift when encountering unseen data [235].

In this context, a popular approach applying meta-learning in DG is *Model-Agnostic Meta-Learning (MAML)* [57]. The main idea of MAML is to transfer the knowledge from previous training tasks to facilitate the learning of new testing tasks. It uses the principle of *episodic training* to optimize the model according to its performance on the virtual test domain, which reflects its generalization ability. In episodic training, a simulation of domain shift is done by dividing the source domains into "meta-train" and "meta-test" domains, also called virtual training and virtual testing domains. Specifically, to enhance the generalization performance, this framework optimizes the model according to its performance on a virtual test domain. The meta-task T_i is produced using *Task Sampling (TS)* strategy, i.e., it is episodically sampled from the set $T = \{T_1, T_2, \dots, T_K\}$. Depending on T_i , M source domains are split into $M - 1$ D_i^{tr} meta-train and the held-out meta-test D_i^{te} . The model is trained using two loops of optimization. First, it is updated in *inner optimization*, using one or more steps of gradient descent on D_i^{tr} with a task loss (i.e., cross-entropy loss). Second, an *outer optimization* is applied to evaluate the

generalization performance. To be specific, in addition to the task loss, a meta-learning objective is added to emphasize certain properties among D_i^{tr} and D_i^{te} .

Despite promising performances of MAML, Li et al. [111] argued that in clinical applications, only a few source domains are available, which may limit the capacity of training task generation and increase the risk of overfitting. To address this issue, they proposed another DG framework based on meta-learning. Their approach uses the concept of episodic training with task augmentation on medical imaging classification. To reduce task-level overfitting, the authors proposed *Mixed Task Sampling (MTS)* strategy which enhances the variety for the training task simulation. In comparison to the TS strategy, the meta-test domains are acquired by the interpolation among all the source domains.

Furthermore, to regularize the deep embedding of training domains, they proposed a novel "meta-objective", which regularizes the cross-domain alignment from both sample-wise and prototype-wise.

In this context, prototype refers to the centroid of the embedding for same-class samples. In particular, sample-wise alignment is used to make the features of the same class closer to each other while the features of different class far apart. The loss of sample-wise alignment uses contrastive learning and cosine distance based decision boundary. It is defined as follows:

$$\begin{aligned} \mathcal{L} = & \sum_{x_j^l \in (D_i^{tr}, D_i^{te})} \{(1 - \text{Cosine}(F(E(x_j^l)), \phi_1^g)) \\ & + \sum_{t=1}^c \mathbb{1}(t \neq l) \text{Cosine}(F(E(x_j^l)), \phi_t^g)\} \end{aligned} \quad (17)$$

where $\mathbb{1}(\cdot)$ is an indicator function, E is the encoder and F is a projection layer for feature extraction. $\phi^g = [\phi_1^g, \phi_2^g, \dots, \phi_c^g]$ is the set of *domain-general prototypes*, defined as the weight vectors of the classifier C .

In addition, they introduced *domain-specific prototypes*. For each class in each domain, a prototype is calculated as the centroid of the feature embeddings of samples belonging to that class. For instance, for domain i , the centroid of class l is computed as $\phi_l^i = \frac{1}{n_l^i} \sum_{(x_j^i, y_j^i=l) \in D_i} F(E(x_j^i))$; where n_l^i denotes the number of samples belonging to class l in domain i . The prototypes of all classes are represented by $\phi^i = [\phi_1^i, \phi_2^i, \dots, \phi_c^i]$. Given these prototypes, the prediction scores of an input sample are obtained by computing the cosine distance between feature embedding and prototypes. For a query sample from meta-test, M prediction scores are computed based on the $M - 1$ domain specific prototypes and the domain-general prototypes. Finally, a prototype-wise alignment based on KL divergence is proposed to enforce the prediction scores across different prototypes to be consistent with each other.

The proposed approach was validated on two tasks 1) epithelium-stroma classification using histopathological images and 2) liver segmentation on abdominal CT image.

For the first task, it showed promising performances, outperforming the ERM baseline approach raising the accuracy from 88.43% to 91.77% on average.

Bayasi et al. [18] also proposed an episodic training based on meta-learning to tackle the problem of DL model generalization. In particular, they addressed the problem of shortcut learning and feature suppression, wherein a DL model tends to only learn a subset of features and ignore the other features resulting in shortcut decision rules. They proposed *BoosterNet*, an auxiliary network that can be added to any arbitrary core network to enhance its generalizability without the need to change its training procedure or its architecture. Their approach combats shortcut learning using the concept of feature culpability. It uses episodic learning to learn from the most culpable features (referred to as confusion features) in the core network, that is features which are linked with erroneous predictions, and to learn from the most predictive characteristics of the data, named least culpable features or discriminant features. *BoosterNet* was validated for detecting skin lesions, where the authors showed improved generalization performance compared to other benchmark DG approaches including data augmentation based DG, adversarial training, and feature alignment.

Sikaroudi et al. [178] studied a *Model Agnostic Learning of Semantic Features (MASF)* strategy in DG. MASF was inspired by the MAML approach, it aims to learn a latent space representation suitable for generalization to an unseen test domain. The architecture consists of layers of feature extractor, classification and metric embedding.

MASF also uses episodic training process. In each iteration, a batch of the source domain is split into meta-train and meta-test batches. The DL model is trained with the cross-entropy loss for supervised learning and hard class separation. In addition, for enhancing soft class separation and promoting domain-independent class-specific cohesion and separation of instance, a metric loss is added. Specifically, the metric loss is the average triplet loss for a batch of triplets, which is formed from an anchor, positive and negative instances from all the source domain dataset. The triplet loss compares a reference input (referred to as anchor, x_A^b) to a matching input (positive instance belonging to the same class as x_A^b , denoted by x_P^b) and a non-matching input (negative instance belonging to a different class than x_A^b , denoted by x_N^b). The distance from the anchor to the positive instances is minimized, while the distance from the anchor to the negative instances is maximized. The triplet loss is formulated as follows:

$$\begin{aligned} \mathcal{L}_{triplet} = & \frac{1}{B} \sum_{b=1}^B \max(\|F(E(x_A^b)) - F(E(x_P^b))\|_2^2 - \\ & \|F(E(x_A^b)) - F(E(x_N^b))\|_2^2 + \alpha, 0) \end{aligned} \quad (18)$$

where $\|\cdot\|_2$ is the l_2 norm, α is a margin between positive and negative pairs, B denotes number of instances in a batch, E denotes the sub-network feature extractor that outputs a

latent space representation, and F is a projection layer which lower the dimension of the representation layer.

Finally, to enforce representation alignment, the authors employed the KL divergence. Given two source domains S_i and S_j , this loss can be formulated as follows:

$$\mathcal{L}_{alignment}(S_i, S_j) = \frac{1}{c} \sum_{k=1}^c \frac{1}{2} [D_{KL}(s_k^{(i)} || s_k^{(j)}) + D_{KL}(s_k^{(j)} || s_k^{(i)})] \quad (19)$$

where D_{KL} represents the symmetrized Kullback-Leibler divergence, $s_k^{(i)}$ denotes the soft confusion matrix, which is computed by applying softmax function with temperature $\tau > 1$ on the output of classification network.

The training process consists of first updating the weights of the classifier and the feature extractor using the cross-entropy loss. Then, the meta loss is computed using a weighted sum of the alignment loss ($\mathcal{L}_{alignment}$) and the triplet loss ($\mathcal{L}_{triplet}$). It is combined to the cross-entropy loss. Next, two gradient descent steps are done to update the network according to 1) the meta loss and the cross-entropy loss and 2) to the triplet loss.

They applied this method for Renal Cell Carcinoma (RCC) subtypes classification in WSI. The results showed that this method outperformed the baseline, which was training on only cross-entropy loss on three hold-out trial sites.

6.1.3.6 Gradient operation

Some DG strategies focus on operating on gradients to develop robust models with generalized representations.

In order to reduce gradient variance from different domains, Atwany and Yaqub [10] presented a method¹⁸ that encourages seeking a flatter minima while imposing a regularization. Their method is inspired by *Stochastic Weight Averaging Densely* (SWAD) [30] and *Fishr* [152].

Inspired by the concept of *Stochastic Weight Averaging* (SWA) [86], SWAD seeks a flat minimum by averaging the weights "densely", i.e., by iterations (rather than by epochs). In addition, to avoid overfitting, the start and the end iterations for collecting the weights to be averaged are determined based on the validation loss. Specifically, the start iteration is defined as the iteration where the validation loss first reaches a local minimum while the end iteration is defined as the iteration when the validation loss no longer decreases but keeps increasing. This method enables averaging weights only from specific iterations where the validation loss decreases. It has shown promising performances for DG.

On the other hand, *Fishr* [152] is a regularization approach that enforces domain invariance in the space of the gradients of the loss. In particular, the domain-level variances of gradients are matched across training domains. This regularization enhances the out-of-distribution generalization properties by aligning the domain-level loss landscapes

at convergence. It uses the gradient covariance, the Hessian of the loss and Fisher information relationship. Fishr constrains domain invariance to the classifier's weights using an exponential moving average after a predetermined warm-up phase, where the network learns predictive features. Once the warm-up phase is finished, Fishr regularization enforces the domain-level gradient invariance in the classifier by aligning the gradient covariances at the domain level. The Fishr loss is thus formulated as follows:

$$\mathcal{L}_{Fishr} = \frac{1}{M} \sum_{i=1}^M ||cov_i - c\hat{v}||_F^2 \quad (20)$$

where cov_i denotes the covariance matrix for each S^i domain for $i = \{1, \dots, M\}$ and $c\hat{v}$ is the mean covariance matrix, $c\hat{v} = \frac{1}{M} \sum_{i=1}^M cov_i$

The total loss is then formulated as:

$$\mathcal{L}_{Total} = \frac{1}{M} \sum_{i=1}^M R_i + \lambda \mathcal{L}_{Fishr} \quad (21)$$

where λ is a hyperparameter and R_i denotes the average empirical risk averaged for all training domains.

Atwany and Yaqub [10] adopted *Stochastic Weighted Domain Invariance* where they used Fishr loss for constraining invariance based on the difference in covariance matrices. After the warm-up phase, that is when the Fishr regularization is activated, they used exponential moving average to compute stable gradient variances and applied a penalty anneal iteration coefficient to help moderate the update speed at each time-step. They also integrated in their framework stochastic weighted averaging.

6.1.3.7 Distributionally Robust optimization

Distributionally Robust Optimization (DRO) [160] attempts to learn a model at worst-case distribution scenario. In comparison to ERM which minimizes the global average risk, DRO minimizes the maximum risk for all groups (or domains). This enforces the model to focus on high-risk groups, which usually comprise those with correlations underrepresented in the dataset. The risk in DRO is computed as follows: $R_{DRO} = \max_{i \in \{1, \dots, M\}} \mathbb{E}_{S_i} [\mathcal{L}(x, y, \theta)]$ [160].

Bissoto et al. [23] proposed a DG approach based on DRO. This approach assume the presence of multi-domain data. To this end, their pipeline consisted of first preparing the data. They partitioned the data into biased training and test sets (named trap sets) to better assess model generalization. In this context, "trap set" refers to datasets whose training and test splits present high and opposite correlations between the annotated artifacts and target label (malignant vs. benign). Afterwards, the training set is divided into artifact-based domains. Data are grouped according to the presence of specific artifact, such as dark corners or drawing of rulers. In other words, each training source domain contains the same set of artifacts. Next, these training source domains are used to train a robust learning algorithm, the *Group Distributional Robust Optimization (GroupDRO)*

¹⁸<https://github.com/BioMedIA-MBZUAI/DRGen>

[160] algorithm, which consists of minimizing the loss of the worst-case training source environment. In the last phase, the authors employed a test-time debiasing procedure to reduce the influence of spurious features in the inference images. The experimental results for skin lesion detection showed that GroupDRO allows learning more robust features.

6.1.3.8 Multi-task learning

Multi-task learning is a learning paradigm where models are jointly optimized on several related tasks. In DG, the premise is that the model’s generalization performance on classification task should be enhanced by learning robust representations, that are shared among different tasks. Therefore, multi-task learning can be viewed as a strategy for domain alignment, it makes possible learning of generic features by sharing parameters.

To improve the model generalizability, Lin et al. [119]¹⁹ proposed a multi-task network for cardiovascular disease risk (CVD) estimation using fundus photographs. Inspired by the DG research and contrastive learning, they proposed a *Cross-Laterality Feature Alignment (CLFA)* for CVD estimation in fundus images. They hypothesized that fundus photographs share invariant representation for the CVD risk over the two eyes. A DL model identifying the invariant representation, would have a better generalization capability. Therefore, they proposed to adopt a Siamese network and pre-train it using the left and right fundus photographs for each patient as positive sample pairs. They added a supervised learning branch to their Siamese network where they jointly trained the model on WHO-CVD score and on seven clinical variables explicitly correlated with WHO-CVD such as age, systolic blood pressure, total cholesterol, body massive index, gender, smoking status and diabetes status. They also integrated a feature-level knowledge distillation. Given two input images (left and right fundus photographs) from a single patient, the feature with the smallest supervised learning loss is considered as the teacher whereas the other as the student. For the teacher-level features, they performed stop-gradient operation when updating the feature extractor. The results showed that CLFA pre-training reduced the feature-space discrepancy between the UK biobank dataset collected using the Topcon 3D OCT-1000 MKII and the other cameras (Mediwork portable camera).

In contrast to the domain-invariant methods, Wang et al. [206] embraced the disharmony in data and developed a simple framework to cope with domain shift problem. The main idea is to design a pre-trained classifier using the source data and adapt it to new data. For adaptation, they studied scenarios where we do not have access to ground-truth label of the target domain. They used auxiliary task (predicting age, gender and race) and integrated them in their framework. Specifically, their method consisted of four stages: 1) pre-training a classifier (composed of a feature extractor, an auxiliary task network and a primary task network) using the source data on the primary task and

the auxiliary labels, 2) adapting the feature extractor: fine-tuning the feature extractor and the auxiliary task network for the auxiliary tasks using data from the target domain while constraining the feature extractor not to change significantly, 3) adapting the primary task classifier, the primary classifier is fine-tuned on the source data to correctly classify the primary task (i.e., classification) based on the modified features, 4) inference, inference on data coming from the target domain is performed using the updated weights of the feature extractor and the primary classifier. The authors showed improvement of performances when tested on 3D brain MRI dataset for the classification task of Alzheimer’s disease and schizophrenia.

For MIDOG challenge, Razavi et al. [155] proposed a *multi-stage mitosis detection method* based on a *Cascade RCNN*. This method was developed to be sequentially more selective against false positives. The Cascade-RCNN comprises a sequential detectors with increasing intersection over union to reduce false positives which may be attributed to the hard to detect mitotic cells. It consists of two-stage: 1) a region proposal network that detects candidate region and 2) a region proposal network and a classification network that performs classification on the candidate regions. This method achieved a F1 score of 0.7492 on the MIDOG testing set. This ends our presentation of DG solutions to address covariate shift.

6.2. Concept shift and label noise in medical imaging

The quality of annotations has a crucial role on the model generalizability, which is usually evaluated by applying the model to an independent test dataset. Nevertheless, the annotation process can be subjective, and the issue of label noise is sometimes unavoidable. In addition, the quality of annotations can differ among various annotators. To improve prediction performances, DL methods have been proposed to address the problem of noisy labels and concept shift. These methods can be categorized into two main classes: **data-centric** methods and **model-centric** methods. Data-centric methods focus on *data adjustment and transformation* (Section 6.2.1). These methods focus on identifying noisy samples and correcting their labels. Model-centric methods include *learning methods* (Section 6.2.2) and *collaborative methods* (Section 6.2.3). Learning methods propose an optimization framework based on loss functions (i.e., regularization), architecture (e.g., graphs) and learning strategies (active learning, zero-shot learning, meta-learning, etc.). On the other hand, collaborative methods exploit the cooperation between models to boost DL performances.

6.2.1. Data adjustment and transformation

Data adjustment and transformation based methods are proposed to mitigate the problem of inconsistency of medical data annotation. These methods focus on adjusting the labels using techniques such as sampling, label correction, data programming, or label propagation.

¹⁹<https://github.com/linzhilalala/CVD-risk-based-on-retinal-fundus-images>

6.2.1.1 Sampling

Sampling-based methods aim to identify samples with inaccurate labels and then proceed to either correct these labels or remove the samples entirely.

Son et al. [182] proposed a method to filter mislabeled data based on discrepancies between the network’s logits and given labels. More precisely, their method uses the softmax outputs to judge the correctness of the given labels. After filtering suspected mislabeled data, they masked the loss function computed over such samples.

They evaluated their method for detecting referable diabetic retinopathy using Kaggle 2015 dataset. The dataset was split into three subsets: a training subset, a validation subset and a testing subset. The training set was corrupted by randomly flipping referable DR to non-referable and vice versa with probabilities ranging between 0 and 0.8. To detect mislabeled samples in the training stage, they introduced a filtration network that is trained on top of the classification network. More formally, the filtration network is trained to minimize the logistic regression loss over validation data. It is only trained at each validation step (one training epoch) in the training phase, it does not contribute in the testing stage. Since the filtration network is trained on clean labels, it is able to detect clean positive data by assigning high values on positive images with clean labels and assigning low values for negative images. The authors thus examine the classifier’s confidence to perform data filtration and reduce the effect of the incorrect annotations. The filtration network is used to mask the loss values for suspected noisy samples. They showed that their proposed strategy outperformed state-of-the-art methods such as S-model and Bootstrap when noise ratio is 0.2.

Xue et al. [218] used the principle of Confident Learning (CL) [139] to identify noisy samples in the training data. It estimates label uncertainty which is the joint distribution between the noisy and true labels. To this end, similar to the previously mentioned approach, it employs the predicted probability outputs from a classification DL model. In CL, the class imbalance and heterogeneity in predicted probability distributions across classes are addressed by using a per-class threshold when calculating the confident joint. To further enhance the precision, Xue et al. [218] proposed an ensemble strategy. It consists of training three different classification networks and selecting the candidates that were jointly identified as noisy using CL. The proposed approach was assessed for automated visual evaluation for precancer screening. It achieved good performances with a kappa score of 0.687 when using cleaned train and validation sets compared to a score of 0.682 using the original train and validation sets.

To address the problem of weak label, *Uncertainty-Aware Sampling Framework (UASF)*²⁰, was proposed by Aljuhani et al. [3]. Example of weak labels include diagnosis of WSI-level labels obtained from patient records, where there is minimal annotation indicating the specific regions

within these images that justify the diagnosed label at the WSI-level. The UASF comprises two stages. The first stage comprises a screening stage, where a screening model, a Resnet18 backbone with modifications for uncertainty estimation via Monte Carlo dropout, is trained on all available training tiles to screen for informative tiles. Next, in order to identify the most relevant tiles, an informative sampling is employed. The second stage, an uncertainty-guided model, is trained on the refined training dataset.

The informative sampling algorithm operates on the principle that tiles most predictive of their WSI level label exhibit high prediction probability and low uncertainty. It utilizes a model’s output, combining prediction probabilities from the overall model and uncertainty measures derived from Monte Carlo inference, to identify these tiles. To achieve this, the algorithm first models uncertainty as a quadratic function of prediction confidence for each WSI. It aims to identify a selection threshold for identifying the most relevant tiles. To this end, a threshold is determined based on the overall uncertainty measure of the WSI samples and the variability of tile predictions. The algorithm computes the difference between the True Predicted Rate (TPR) and the False Predicted Rate (FPR) at each threshold level, selecting the minimum threshold value as optimal.

In the area of genomics and computational biology, Bai et al. [14]²¹ proposed a novel method for calling genotypes from next-generation sequencing data, specifically targeting deletions. Their method is called *Cnn geno*, it converts sequencing data into images for genotypes classification. It adopts a *convolutional bootstrapping strategy* to improve its ability to handle noisy labels in the data. First, the authors manually selected a set of highly reliable seeds (i.e., a subset of samples) as training set and trained their model until convergence. After the initial training, the model is used to classify the remaining samples in the dataset. The process involves selecting samples with higher classification confidence into a seed set, and this selection process is based on a set classification confidence level, which is set at 0.8. The expansion of the seed set is repeated until no new seeds are added, and the final trained model is then used for classifying genotypes.

Xu and Chen [213] tackled the problem of label noise in neural decoding. They proposed a deep neural network based on *sample re-weighting* method. In their work, they assume that the training set is noisy while the validation set is small but accurately labeled. The sample re-weighting strategy consists of assigning weights to training samples to minimize the loss on a clean unbiased validation dataset to solve the problem of label noise and improve prediction performance. The process involves adjusting the weights of the training samples in such a way that samples which are likely to be correctly labeled have a higher weight, while those that are likely mislabeled are down-weighted. The proposed method was assessed on simulated neural activity data and calcium imaging data of anterior lateral motor cortex. It has shown that it correctly predicted the behavioral

²⁰<https://github.com/machiraju-lab/UA-CNN>

²¹<https://github.com/BRF123/Cnn geno>

variable even with 36% of samples in the training set are mislabeled in the simulated data. On the anterior lateral motor cortex study, the proposed method, which was trained with 48% of training mislabeled samples, can predict trial types with an F1 score of around 0.85.

Similar to Xu and Chen [213], to effectively alleviate the disturbance from data labeling errors, Hu et al. [80] adopted a *sample re-weighting*²² strategy, where higher weights are assigned to clean samples and lower weights to noisy samples. First, the output features of the encoder are grouped into k groups (where k was set to 2) according to the channel layer. Next, a linear projection is performed on the grouped results after global average pooling. Finally, they applied a *group weighted learning* on the results of the two groups after ReLU activation. They evaluated their approach on the automatic classification of retinal Arteries and Veins, which is essential for diagnosing cardiovascular and eye-related diseases. The proposed method showed good results achieving an accuracy of 97.47%, 96.91%, 97.79%, and 98.18% on AV-DRIVE, HRF, LES-AV and a private dataset, respectively. Therefore, the sample re-weighting strategy effectively alleviates the influence of noisy labels due to the subjective judgment of annotator.

6.2.1.2 Label correction

Label correction methods focus on adjusting (re-labeling) the labels of suspected noisy samples.

Hermoza et al. [78]²³ proposed a method for predicting survival time from medical images using both censored and uncensored data. Censored data are cases where the event of interest (such as death) has not occurred by the end of the study. These data are typically ignored in previous studies, resulting in an under-utilization of the training data. To leverage these incomplete observations, the authors used the concept of pseudo labels, i.e., using the output of the network to estimate the label. For each censored data point, a pseudo label is estimated, which represents a lower-bound survival time. The authors argue that the quality of generated pseudo-labels depends on the training procedure stage: during the first epochs, the pseudo-labels are less accurate than the ones at the last epochs. Therefore, they proposed to control the ratio of censored sample labels to be replaced with pseudo labels at each epoch using a cosine annealing schedule. Using this strategy, no pseudo-labels are produced at the beginning of the training and by the end of the training all censored data with their pseudo labels are produced. The evaluation of their proposed method on pathology and X-ray images from the TCGAGM and NLST datasets showed good prediction survival accuracy on both datasets.

Bai et al. [15] proposed a label correction method in a semi-supervised approach. Specifically, they generate new high quality labels from unlabeled data. They used the concept of adaptive threshold to reduce noisy labels and

retain the effective information. Their method called Pseudo-Labeling based on Adaptive Threshold (PLAT) reduces the generation of noisy labels and therefore enhance the generalizability of the models. It is inspired by epistemic uncertainty [97]. Unlabeled images are inputted to the model k times using Monte Carlo Dropout. This will result into k predictions. Uncertainty of pixels is computed by calculating the variance of k predictions. Finally, a normalization step is achieved by dividing the results with the largest variance among all predictions. The normalized result is used as an adaptive threshold. Compared to model trained only on labeled images, this method showed a gain of 9%-13% in terms of F1 score. These performances are comparable to a model trained using supervised learning paradigm.

Qiu et al. [148] proposed a self-training strategy consisting of noisy label cleaning optimization. First, the model is pretrained using the initial noisy labels, with a large fixed learning rate. This strategy assumes that the network does not overfit the label noise and maintain high performance when using a high learning rate. Then, noise-free labels (soft labels) are initialized based on the pretrained model. These labels are computed using the softmax output of the current model. In each iteration, first the soft labels are fixed to update the model parameters; then the model parameters are fixed and the soft labels used in the next iteration are updated. This method achieved good performances for pathology image classification.

He et al. [75] proposed a *Self-Adaptation Network (SAN)* using facial images to improve uncertain labeling for automatic depression estimation. Their architecture comprises: 1) an encoder for extracting deep features, 2) a self-attention module for learning the weights from the mini-batch and assigning lower weight to uncertain images, 3) a square ranking regularization module where the attention weights are ranked in descending order of importance and grouped into a high partition and a low partition, and 4) a re-label module for re-labeling the uncertain annotations for automatic depression estimation in the low partition. In the re-labeling module, for each image, the authors compute the softmax probabilities, which give the predicted probability distribution over all possible labels. For each image, the maximum value of the predicted probability is compared with the probability value of the provided label in the dataset. If the predicted probability is greater than the probability of the given label by a threshold value, the sample is assigned a new pseudo-label, which is based on the model's prediction (the index of the maximum value of the predicted probability). Extensive experience on AVEC2013 and AVEC2014 demonstrated the efficiency of their proposed method.

Zhu et al. [241] employed a *hard sample aware self-training*²⁴ strategy to correct and update labels. Their method comprises two phases: 1) a label correction and 2) a noise suppressing and hard enhancing scheme. The first phase produces "almost clean data" from noisy data. This is done by using an architecture consisting of 1) a classification/correction model, 2) an Easy/Hard/Noisy (EHN)

²²<https://github.com/TwistedW/MIAV>

²³<https://github.com/renato145/CASurv>

²⁴<https://github.com/bupt-ai-cz/HSA-NRL/>

detection scheme based on the sample training history and 3) a post-processing component. The main idea is to employ the prediction history for each sample as guiding information for differentiating hard from noisy samples. First, a classification network is trained on noisy data. The prediction history for one sample can then be stored for a specific number of epochs. The EHN detection module is then used to separate the data into easy, hard and noisy samples. In particular, the authors find that the normalized probability is easier to analyze than the loss value, a criteria used by previous state-of-the-art methods to detect clean samples. They propose to use the mean prediction value of the sample training history for detecting clean samples (clean samples have higher mean prediction probabilities than the noisy ones). They inject noise to the easy samples and retrain the classification model on the simulated noisy data. Based on the mean prediction probability value, they select hard and noisy samples. Next, a multi-layer perceptron classifier is trained on the training history of the initial classifier to distinguish noisy from hard samples. The correction model which is the same as the initial classification model is then trained on the easy and hard samples. After this step, the correction model is used to correct noisy labels. The labels of hard and noisy samples are corrected using the pseudo-labels produced by the correction model, which correspond to the class with the highest probability model output. These steps are repeated to further purify the dataset. Finally, in the post-processing step, the noisy data which can not be corrected are dropped out. In addition, hard samples whose labels were changed were also dropped out. The second phase employs a co-learning strategy based on co-teaching to train a noise robust model using the "almost clean data" (the second phase is detailed in Section 6.2.3.2). In Co-teaching, two DL networks are trained simultaneously, each DL network teach its peer network by selecting possibly clean data, data with small loss.

Similar to Zhu et al. [241], Zhu et al. [242] proposed a co-teaching method to address noisy labels (see Section 6.2.3.2). Their framework includes a consistency-based noisy label correction module to detect noisy labels and correct them. It is a two-stage algorithm: 1) two networks are used to select clean samples according to their loss ranking, samples with the smallest loss are considered to be clean samples, 2) among the remaining suspected noisy data, samples that have consistent predictions on both networks are corrected. Specifically, they computed a prediction confidence score per network for the suspected noisy data. Samples are relabeled if they have the same predicted labels using both networks and the prediction confidences are larger than a predefined threshold. This means that if both networks agree on the classification of a sample and the confidence of this classification is high enough, the sample is assigned a new label based on this prediction. The new label (pseudo-label) is the class that both networks most strongly agree upon, under the condition that their prediction confidence surpasses the predetermined threshold. The rest uncorrected data are dropped and not used for training.

6.2.1.3 Data programming

Creating large labeled datasets is expensive and challenging in some applications. To address this issue, Ratner et al. [154] introduced data programming, a paradigm for the programmatic creation of training sets in weak supervision. It uses a generative modeling step to create weak training labels by combining unlabeled data with heuristics provided by domain experts that may overlap, conflict, and be arbitrarily correlated.

Inspired by this concept, Dunnmon et al. [51] proposed a framework for applying data programming to address the problem of cross-modal weak supervision in medicine, wherein weak labels derived from an auxiliary modality (text) are used to train models over a different target modality (images). In their proposed cross-modal data programming, users provide two inputs: 1) unlabeled cross-modal data points (i.e., an imaging study and the corresponding text report), 2) a set of Labeling Functions (LFs), which are user-defined functions (pattern-matching rules, existing classifiers) that take in an auxiliary modality data as input (e.g., text reports) and either output a label or abstain. In the phase of offline model training, these LFs are employed on unstructured clinical reports to be combined and produce probabilistic (confidence-weighted) training labels for training a classifier on the target modality (radiograph). Then, a discriminative text model, for instance, a Long Short-Term Memory (LSTM) network, is trained to align the raw text with the output of the generative model. They employed a simple heuristic optimization to determine if it is more efficient to train the final model of the target modality directly with the probabilistic labels from the generative model or if the model's performance could be enhanced by using the probabilistic labels from the trained LSTM. During test time, the final model only takes input from the target modality and provides predictions.

This framework presents a powerful approach for reducing the reliance on hand-labeled datasets. It has shown promising results when applied to different applications spanning radiography, CT, and EEG. However, it also brings challenges related to dependence on auxiliary data, the quality of labeling functions, and potential biases.

6.2.1.4 Label propagation

Label propagation allows to take advantage of the few labeled samples to automatically annotate unlabeled samples. Given a dataset with a large number of unlabeled samples and a small number of labeled samples, this approach is based on estimating a probabilistic transition matrix that depends on the neighborhood size and a quality threshold.

Vindas et al. [198] proposed to estimate this transition matrix through K-Nearest Neighbor (KNN) and local quality measures. Their approach involves four steps. First, features are extracted using an auto-encoder in an unsupervised manner. Second, they used t-distributed Stochastic Neighbor Embedding (t-SNE) algorithm, a dimensionality reduction technique, to project the features into a 2D space. In this step,

the optimal projection is selected based on the silhouette score, which compares the similarity of a sample between the samples of its own class and the samples of the other classes. The best projection is based on the highest silhouette score. This is because for label propagation using KNN strategies, it is ideal to increase the inter-cluster distance and to reduce the intra-class distance; annotation errors mainly come from samples that are located at the boundaries of close class clusters, or from samples located in the wrong class cluster. Note that only labeled samples are used for this computation. Third, they perform automatic label propagation where the labels of high-quality labeled samples are propagated to high-quality unlabeled samples using KNN strategy and local quality metrics. This allows to increase the size of the training set. Fourth, for classification purposes, to compensate for the noise introduced by the automatic label propagation they used a robust loss function *a generalized cross-entropy loss* [233], formulated as follows:

$$\mathcal{L}(f(x), y_i) = \frac{1 - f_i(x)^v}{v} \quad (22)$$

where y_i and $f_i(x)$ are the i -th components of the true label y and the predicted label $f(x)$, v is a hyperparameter which allows control of the noise tolerance and the convergence speed; when $v \rightarrow 1$ we get the mean absolute error loss function whereas when $v \rightarrow 0$ we get the cross-entropy loss function. In their framework, v was set to 0.7. They evaluated their framework on three tasks: emboli classification, organ classification and digit classification.

Similarly, Ying et al. [225] introduced label propagation for label recovery in the presence of noisy labels. They proposed a *noisy label recovery algorithm based on Subset Label Iterative Propagation and Replacement (SLIPR)* for dealing with noisy labels in COVID chest X-ray images classification. This algorithm aims to recover label and train the CNN on the label-recovered training set. It employs techniques such as principal component analysis, low-rank representation, and neighborhood graph regularization, followed by the kNN algorithm for classifying samples and recovering noisy labels through iterative label propagation and replacement. The first stage of their framework is a feature extraction and classification phase where they utilize a low-rank representation and a neighborhood graph regularization to extract both global and local features of the samples and KNN for classification purposes. The second stage consists of multi-level propagation and replacement of labels. In this stage, the concept of label propagation is used to select and replace the labels of the samples. In addition, they introduced a selection strategy for high confidence samples. Inspired by majority voting, the framework select high confidence samples as the training set based on the sample optional labels: a sample is considered to be high confidence sample if the majority result suggests that it should belong to the same type of label. For applying this principle, we should define the proportion of high confidence samples selected for training of the CNN, that is the minimum number of samples required for the classification model divided by the

total number of samples. Based on this proportion, they followed these steps to select high confidence samples: 1) in each round of "label propagation and replacement", they counted the optional labels of the samples 2) they ranked the confidence of the samples according to the majority voting principle, and 3) they selected the required number of high confidence samples.

6.2.2. Learning methods

Learning-based methods are among the most used strategies to overcome the problem of noisy datasets and improve the generalizability of DL networks. They use an optimization framework to enhance the robustness of DL networks. These methods include distance metric learning, active learning, zero-shot learning, gradient, robust loss function, graph and meta-model.

6.2.2.1 Distance metric learning

Distance Metric Learning (DML) aims to learn a discriminative embedding in which similar samples are closer together, and dissimilar samples are separated [52]. DML emerged from the concept of contrastive loss, which turns this principle into a learning objective [16]. Unlike classification losses, which learn a class logit vector, the contrastive loss in DML captures the relationships among samples: it trains a Siamese Network, which consists of two identical subnetworks whose architecture, configurations, and weights are the same, to predict whether two inputs are from the same class. This is achieved by putting their embedding close to each other (for the same class) and far apart (for different classes) [16, 52].

In particular, DML based approach can be effective to overcome the issue of poor generalization performances of DL models caused by annotation bias problems. For instance, Zhang et al. [229] used similar finding retrieval based on DML to improve DL models generalizability. Their method requires an extra "clean" dataset with pathological-proven labels to re-label a noisy dataset according to similar finding retrieval. First, a Siamese Network is trained on randomly selected pairs of images from the clean dataset. Each pair is assigned a label depending on whether the two images of this pair belong to the same class. The model is trained under the assumption that if two images belong to the same class, their feature vectors should be close in the feature space, and if they belong to different classes, their feature vectors should be far apart. To enforce this, a contrastive loss is applied over the Euclidean distance metric (similarity score) induced by the malignancy representation. Next, during the re-labeling phase, each sample from the clean dataset used in training is paired with an "under-labeled" sample from the noisy dataset. These noisy samples are then sorted based on their similarity scores with their corresponding clean sample. The new label for each sample from the noisy dataset is determined by averaging the labels of the top 20% of its partner samples in the ranking list of similarity scores. This process aims to provide more accurate labels for the noisy label samples based on their

similarity to pathologically confirmed samples in the clean dataset. In addition, taking the average labels of top-ranked similarity samples is intended to increase the confidence of label propagation.

Zhang et al. [229] applied the aforementioned method using the Lung Image Database Consortium and Image Database Resource Initiative (LIDC-IDRI) [9], a prominent source of public dataset of thoracic Computed Tomography (CT) image data. Despite its popularity, the LIDC-IDRI dataset is considered a noisy dataset because of the absence of clinical information. More precisely, four qualified thoracic radiologists assessed nodule characteristics and provided a rating of malignancy rating (from 1 to 5). A thorough examination of the dataset revealed that the 'likelihood of malignancy' characteristic was subjective since it was established based on the assumption of a 60-year-old male smoker, due to the absence of any clinical information about the patients. To challenge the low confidence labels of LIDC, the authors proposed to use a pathological-proven labeled dataset, the SCH-LND [230] dataset. This extra dataset includes 180 solid nodules (90 benign / 90 malignant). The idea is to apply this dataset to transfer pathological knowledge for various clinical indications. To this end, two re-labeling methods were explored to obtain new ground-truth labels on the LIDC database. The first method produces the malignancy label using a machine annotator: a nodule classifier that was pre-trained on LIDC data and fine-tuned on SCH-LND data. The second method uses a machine comparator to rank the top nodules' labels: a metric-based network computes the correlation between pairs of nodules. According to this study, relabeling through metric learning outperformed the general supervised model. It suggests that the input pairs produced by random sampling provide a data augmentation effect to learning with limited data.

With the aim of being robust to inherent observer-variability in training labels, Van Woudenberg et al. [195] also employed the DML based approach in another form within the differential learning approach. The differential learning consists of training the model on an auxiliary comparison task, i.e., determining whether a clinical parameter is significantly different between two patients. This task is considered to be an easier task and less prone to subjectivity. It is modeled using a Siamese Network to compare the estimated clinical parameter that are sufficiently apart from each other based on the generated representations. The proposed approach showed good results in the assessment of left ventricle measurements in echocardiography cine series. In this context, differential learning was integrated as an auxiliary task by computing whether there is a significant difference in Ejection Fraction (EF) between two patients (normal vs severe EF). It showed enhanced performances when evaluated on 1) a large cart-based dataset consisting of 28,577 echo cines obtained from 23,755 patients and 2) 51 echo cines acquired from 23 heart-failure patients using a Point-Of-Care Ultrasound (POCUS).

While the aforementioned methods tackled the problem of noise in labels in form of subjective interpretations between readers, Seibold et al. [168] addressed inconsistent labels generated from unstructured medical reports via text classifiers, typically by using classifiers which may not perfectly capture the nuances of the medical terminology and context. The authors argued that traditional methods rely on a predefined set of categories extracted from medical reports which can cause some limitations and inaccuracies. To overcome this problem, they proposed a contrastive language-image pre-training on report-level approach to learn directly from the unstructured medical reports. They applied a contrastive global-local dual-encoder architecture to learn concepts directly from unstructured medical reports while maintaining its ability to perform free-form classification. In contrast to the previously mentioned approach, DML is combined with self-supervision, by integrating SimSiam [35]. In this framework, two augmented versions of the same input image are created. These images are then processed through a backbone network, a three-layer encoder-head, and a two-layer prediction-head, to enforce similarity between the two views. Furthermore, they use the augmented images from the pre-training objective to mirror their text-image objectives to the augmented samples. Their approach performed on par with direct label supervision approach when evaluated on the large-scale chest X-ray datasets MIMIC-CXR [90], CheXpert [85], and ChestX-Ray14 [207] for disease classification.

Finally, similar to [168], Kurian et al. [102] employed a DML method in conjunction with a self-supervised approach. Their method is based on a contrastive learning framework and feature aggregating memory banks to identify and increase the emphasis on clean training samples. In essence, it consists of 1) a warm-up phase that includes contrastive learning following a weight update based on cross-entropy, 2) a weight calculation phase in which the weights of the training samples are adjusted in accordance with their similarity to the features preserved in the memory bank and 3) a final classification training phase which consists of training the model using a weighted cross entropy loss function. The method uses ResNet-18 neural architecture trained using SimCLR, a self-supervised training. In the warm-up phase, training involves both cross-entropy loss and contrastive loss. A maximum loss miner function, using the contrastive loss, identifies 'hard-pairs' and noisy labels based on cosine similarity. The subset with maximum contrastive loss represents the hard pairs, all the feature vectors except the hard-pairs are updated class-wise into a memory bank, which is limited to a fixed size. The features are thus appended in this memory bank in a FIFO manner. In the weight calculation phase, sample weights are computed using cosine similarities with memory bank features of the same class. Next, a K-medoids computation for the features in the memory bank is carried out to evaluate the cosine similarity between the samples and the medoids. Exponential of the similarity scores are normalized between 0 and 1. In the final classification training phase, these scores are applied as

weights for the cross-entropy loss. The authors demonstrated the effectiveness of their approach when evaluated on two histology datasets: 1) the ICIAR 2018 Grand Challenge dataset called Breast Cancer Histology (BACH) dataset [7] and 2) the basal versus Luminal A PAM50 subtype classification from H&E stained WSI extracted from TCGA-BRCA dataset.

6.2.2.2 Active learning

Active learning can be combined with noisy labels for improving DL performances.

In this context, Son et al. [182] proposed this strategy²⁵ to enhance the model's learning efficiency for detecting a rare disease. Their method involved assigning "normal" pseudo-labels to a large number of publicly available unlabeled images. This set was combined with a small set of labeled images (having the targeted rare disease) for initial training. The authors thus introduced noise in the pseudo-labels as it is likely that some of the images pseudo-labeled as "normal" actually contain the targeted disease. After the CNN is initially trained on the pseudo-labeled dataset, it is used to identify images that it predicts as rare disease with high confidence (greater than 0.5). This step effectively filters out a significant portion of the noise by focusing on cases where the model has high confidence, thereby reducing the need to manually inspect a vast number of images. This process significantly narrows down the number of images to be manually reviewed for the rare disease. The active learning process allows to screen for the positive selected cases. It helps in correcting the initial noise introduced by pseudo-labeling. The refined dataset is then used for training. This strategy attained an AUC of 0.9993 on the PALM competition, ranking first on the off-site validation set.

6.2.2.3 Zero-shot learning

Zero-shot learning (ZSL) is a technique enabling machine learning algorithms to recognize objects belonging to new, previously unseen classes, using semantic descriptions. ZSL fundamentally relies on auxiliary information about seen and unseen classes in the form of semantic description. A key advancement in this field is the Generalized Zero-Shot Learning (GZSL), where the test data may originate from either seen or unseen classes, posing a more realistic and challenging scenario. In ZSL, the process involves mapping a visual feature vector extracted from an input image to a semantic space created using auxiliary information. This mapping is crucial for bridging the gap between the visual and semantic domains, enabling the recognition of unseen classes.

Based on these principles, Paul et al. [143] proposed a GZSL for the diagnosis of chest radiographs. Their approach is based on a Multi-View Semantic Embedding (MVSE) network, which integrates three distinct semantic spaces: one derived from X-ray reports, another from CT radiology

reports, and a third based on visual traits used by radiologists. The inclusion of the CT semantic space is particularly insightful, as most diseases identifiable from chest X-rays are also diagnosable from chest CTs, which provide richer information. The methodology involves a two-branch auto-encoder for performing semantic embeddings into these X-ray and CT semantic spaces. Each branch is supplemented with a novel guiding network that leverages the trait-based semantic space, thereby enhancing the model's ability to interpret complex medical images. To improve performance for unseen classes, the framework incorporates a self-training strategy. This process begins by creating a self-training set comprising unlabeled X-ray images from both seen and unseen classes. The self-training is executed in two steps: initial inference and model fine-tuning. Initially, class probabilities for unlabeled images from the self-training set are computed using the trained MVSE network. Images are then selected for both seen and unseen classes based on the highest confidence scores. Subsequently, the model is fine-tuned with this selectively chosen data for each class. This refined model is then deployed for generalized zero-shot diagnosis of chest X-rays. During testing, for a given X-ray image that may belong to either seen or unseen classes, the model computes distances in both the X-ray and CT semantic spaces from the respective class signatures. The final class probability is determined by dynamically balancing the importance assigned to the X-ray and CT branches. Then authors showed that their model achieved robust generalization capabilities when tested on NIH Chest X-ray dataset (NIH), hand-labeled subset of NIH dataset (NIH-900), Open-i dataset, PubMed Central dataset (PMC) and the CheXpert dataset.

6.2.2.4 Gradient

The *Balanced Gradient Contribution* (BGC) strategy is a training approach designed to manage the significant statistical differences between domains [158]. This method addresses the issue of large variance in gradients that occurs due to the distinct nature of data from each domain. In the context of domain generalization, the BGC method could be employed to balance the learning from different domains by adjusting the contribution of gradients from each domain during the training process.

This strategy was integrated in the work of Elbatel et al. [53]. They proposed a *Seamless Iterative Semi-supervised correction of imperfect labels* (SISSI)²⁶, a novel framework for training object detection models with noisy and missing annotations. They introduced a range of image processing and deep learning methods to make iterative label correction. They applied a domain adaptation strategy to address noisy labels by exploiting a source labelled dataset (Cellpose), to enhance training on a target noisy dataset (CellLab). In the early phase, they used a mixed-batch training combining both training datasets to train a Faster R-CNN mode using BGC [158], which generates stable gradient directions. To

²⁵https://bitbucket.org/woalstdnd/codes_and_data

²⁶<https://github.com/marwankefah/SISSI>

determine the end of this phase, they used ADELE method which permits to detect when the network starts memorizing the initial noisy annotations. Next, they applied a semi-supervised phase for each cycle. They used label correction strategy. To this end, they used test-time augmentation and weighted box fusion techniques to filter potential bounding boxes and hence producing confident bounding boxes. They also proposed to use synthetic like image adaptation according to pseudo labels. This method would solve the problem of undetected cells in the pseudo labels which would affect the training negatively. Thus, the authors generated dynamically synthetic-like images for continual training.

6.2.2.5 Robust loss function

Robust loss functions focus mainly on improving the loss to build robust DL network.

To address the problem of model overfitting due to label ambiguity and noisy labels, Sun et al. [187] proposed to use *deep log-normal label distribution learning* and *focal loss*. The concept of *deep log-normal label distribution learning* is inspired by the paradigm of *label distribution learning* [61, 58], where an instance is assigned a label distribution, aiming to learn a mapping from instance to label distribution. For the targeted application of pneumoconiosis staging on chest radiographs, the construction of the label distribution is to estimate the tolerance of each stage of pneumoconiosis. The authors modeled the label distribution using asymmetric log-normal distribution.

$$y^d = \frac{p(y_i|\mu, \delta)}{\sum_j p(y_j|\mu, \delta)} \quad (23)$$

$$p(y_i|\mu, \delta) = \frac{1}{y_i \sqrt{2\pi\delta}} \exp\left(-\frac{(\log(y_i) - \mu)^2}{2\delta^2}\right) \quad (24)$$

y^d is the probability distribution (label distribution) with $y^d \in [0, 1]$. In normal label distribution, the label y_i starts from 1, μ is the mean value equal to $\log(y_i)$, and δ is an hyperparameter.

To enforce label distribution learning, the KL Divergence loss is employed using the label distribution and the prediction of the staging network. This loss aims to measure the distance between two continuous distributions: the label distribution (y^d) and the network prediction after the Softmax function.

In addition, the authors added a regularization term, the cross-entropy loss, to strengthen the learning abilities of the model on unambiguous samples and deal with subjective inconsistency. Combining both loss, the KL divergence loss and the cross-entropy loss, constitute the focal staging loss. However, using the aforementioned loss together results in an optimization inconsistency. To solve this issue, an instance-level drop parameter was introduced to skip samples with better predicted results during the optimization process.

Zhu et al. [241] employed the focal loss to enhance the training process by emphasizing hard samples. It is defined as follows:

$$\mathcal{L}_{focal} = -(1 - q(y|x))^\gamma \log(q(y|x)) \quad (25)$$

where $q(y|x)$ is the predicted probability and γ is a hyperparameter. To reduce the relative loss for well-classified examples and put more focus on hard, misclassified examples, the parameter γ in the focal loss function was set to 2. This technique aims at improving the robustness of the model against noisy labels and ensuring that the model learns effectively from the most challenging parts of the data.

Hu et al. [81] proposed a robust training method for solving the classification problem with imbalanced data. The targeted application was the diagnosis from imbalanced CT images. Their framework, called *Deep Supervised Network with a Self-Adaptive Auxiliary Loss (DSN-SAAL)*, consisted of integrating a novel loss function. The loss function tackles both the effects of data overlap between CT slices and noisy labels. In order to consider the effects of data overlap between CT slices, they propose adjusting the weight of samples in the Cross-Entropy (CE) loss function as follows:

$$\mathcal{L}_{CE} = - \sum_{i=1}^c \frac{1 - \alpha}{1 - \alpha^{k_i}} p(y_i|x) \log(q(y_i|x)) \quad (26)$$

where $q(y|x)$ denotes the output of the classifier and $p(y|x)$ represents the ground-truth distribution over labels for sample x . k_i is the number of samples in the k^{th} class and α is a learnable parameter which represents the effective sample factor to measure the ratio of the effective number of samples. In addition, they introduced a regularization term, called *Reverse Cross Entropy (RCE)* to combat noisy labels:

$$\mathcal{L}_{RCE} = - \sum_{i=1}^c \frac{1 - \alpha}{1 - \alpha^{k_i}} q(y_i|x) \log(p(y_i|x)) \quad (27)$$

In this setting, since some labels are incorrect and $p(y|x)$ does not represent the true class distribution, they employed $q(y|x)$ as the ground truth and $p(y|x)$ as the class probability of the outputs, hence the name reverse cross-entropy. Finally, the proposed *self-adaptive auxiliary loss* can be formulated by combining the aforementioned losses (Equations 26 and 27) while adding a weighting hyperparameter β to balance between them. The authors showed that their approach outperformed the state-of-the-art methods when evaluated on COVID19-Diag and three public COVID-19 diagnosis datasets.

To handle the subjectivity of annotation, Yu et al. [226] proposed a *Grading Cross Entropy (GCE) loss*. The loss is designed to account for the feature continuity of disease grades and the inherent progression of disease, recognizing that misclassifications are more likely to occur between adjacent grades rather than distant ones. It is defined as

follows:

$$\mathcal{L}_{GCE} = - \sum_i p(y_i|x) \log \left(1 - \prod_{j \in \mathbb{N}(i)} (1 - q(y_j|x))^{w_{ij}} \right) \quad (28)$$

where $p(y_i|x)$ is the i -th element of the one-hot encoded label of the input x , $\mathbb{N}(i)$ the neighboring indexes of grade i , $q(y_j|x)$ denotes the j -th element of the model predictions and w_{ij} represents the weight of grade j with the annotated label i . This weighting system allows the GCE loss to be more flexible than the CE loss in handling noise by setting different weights to neighboring labels and the annotated label. Therefore, GCE can effectively reduce overfitting to noisy data.

Hermoza et al. [78] tackled the problem of predicting survival time from medical images using both censored and uncensored data. They proposed an *Early-Learning Regularization (ELR) loss* regularization loss to handle pseudo label noise. ELR is designed to mitigate the impact of noisy pseudo labels in the survival time prediction setting. It is used to ensure that training continues for samples where the model's prediction aligns with the temporal ensembling momentum (considered "clean" pseudo-labeled samples) and is minimized for noisy pseudo-labeled samples. The temporal ensembling momentum is a blend of the current and previous predictions. The ELR loss is defined as follows:

$$\mathcal{L}_{ELR}(z_i^c) = \log(1 - \frac{1}{c}(\sigma(z_i^c)^T \sigma(\tilde{z}_i^c))) \quad (29)$$

where $\tilde{z}_i^{c(e)} = \phi \tilde{z}_i^{c(e-1)} + (1 - \phi)z_i^{c(e)}$ is the temporal ensembling momentum of the prediction with e denoting the training epoch and $\phi \in [0, 1]$. σ is the sigmoid function, z^c is the output of the model, and c denotes the number of classes.

Liu et al. [121] proposed a similar approach based on a *new training module called Non-Volatile Unbiased Memory (NVUM)*²⁷, which non-volatility stores running average of model logits. The authors proposed a regularization loss based on this memory module to minimize the differences between the model's current logits and those from its initial learning phase. In essence, the model f_θ is trained on noisy labeled dataset using binary cross-entropy loss. In addition to the binary cross-entropy loss, they integrated the following regularization term:

$$\mathcal{L}_{REG}(\tilde{z}_i^c, z_i^c) = \log(1 - \sigma((\tilde{z}_i^c)^T \sigma(z_i^c))) \quad (30)$$

where \tilde{z} is a memory module that stores an unbiased multi-label running average of the predicted logits of all training samples and \tilde{z}^c employs the class prior distribution π for updating, denoted by $\pi(j) = \frac{1}{n} \sum_{i=1}^n \hat{y}(j)$ for $j \in \{1, \dots, c\}$, where n is the total number of sample in the noisy dataset, and \hat{y} denotes a one-hot noisy label.

Initially, \tilde{z} is initialized with zeros, it is updated in every epoch using the following formula:

$$\tilde{z}_i^{c(e)} = \beta \tilde{z}_i^{c(e-1)} + (1 - \beta)(z_i^{c(e)} - \log \pi) \quad (31)$$

where $\beta \in [0, 1]$ is a hyperparameter controlling the volatility of the memory storage. β is set to 0.9 representing a non-volatile memory. Since in the early stage of training the model is considered to be robust to noisy label, this regularization enforces consistency between the current model logits and the logits produced at the beginning of the training. The NVUM approach was evaluated on new benchmarks, where training is performed on noisy multi-label imbalanced chest X-ray (CXR) training sets, formed by Chest-Xray14 and CheXpert, and the testing is performed on the clean multi-label CXR datasets OpenI and PadChest. Their approach outperformed previous state-of-the-art CXR classifiers and previous methods that can deal with noisy labels on all evaluations.

Shi et al. [175] proposed a semi-supervised deep learning approach that leverages the semantic information of annotated images and explores the information hidden in unlabeled data, while being robust to noisy labels. Their approach is based on *self-ensembling based deep architecture*. It is inspired by Temporal Ensembling (TE) [105], which produces an ensemble target for each label prediction of training samples. This is done by applying *Exponential Moving Average (EMA)* to the predictions within several previous training epochs and then minimizing the difference between the label prediction and its ensemble target. Shi et al. [175] proposed *Graph Temporal Ensembling (GTE)* to improve TE. GTE creates ensemble targets for feature and label predictions of each training sample and forms consensus predictions under different configurations. Using a graph, the ensemble targets within the same class are mapped into a cluster so that they are further enhanced. Next, a consistency loss is utilized to form consensus predictions under different configurations.

$$\mathcal{L} = \frac{\tau(t)}{c|B|} \sum_{i,j \in B} \left(\lambda_1 \left\| z_i^f - \sum_{j=1}^{|B|} w_{ij} \hat{z}_j^f \right\|_F^2 + \lambda_2 \left\| z_i^c - \sum_{j=1}^{|B|} w_{ij} \hat{z}_j^c \right\|_F^2 \right), \quad (32)$$

where B denotes the batch of selected images, $|B|$ represents the number of selected images, c is the number of classes. The prediction for image i is given by z_i^c , while y_i is the true label. The time-dependent weighting function to gradually enhance the weight of the consistency cost is represented by $\tau(t)$, and λ_1 and λ_2 are non-negative constants that balance the terms in the loss function. The feature representation for image i is z_i^f , and \tilde{z}_j^f is obtained by applying EMA to feature representations within multiple previous training epochs, i.e., $\hat{z}_j^f = \frac{z_j^f}{(1-\alpha)^t}$, where $\tilde{z}_i^f = \alpha \tilde{z}_i^f + (1-\alpha)z_i^f$ where α is an ensembling momentum term to control how far the ensemble \tilde{z}_j^f reaches into the training history, and t is the current number of training epochs. Similarly, \tilde{z}_j^c is obtained by applying EMA to label predictions within multiple previous epochs, i.e., $\hat{z}_j^c = \frac{z_j^c}{(1-\alpha)^t}$, where $\tilde{z}_i^c =$

²⁷<https://github.com/FBLADL/NVUM>

$\alpha z_i^c + (1 - \alpha)z_i^c$. The weighting factor between images i and j is w_{ij} . The authors validated the proposed method with extensive experiments on lung and breast cancer datasets that contain thousands of images.

Gündel et al. [71] proposed a novel training strategy to handle label noise in chest radiography abnormality classification. They addressed the issue of label noise originating from natural language processed medical reports. Prior label probabilities were measured on a subset of training data re-read by 4 board-certified radiologists and were used during training to enhance the robustness of the model to label noise. These probabilities were used to adjust the weights in the loss function, making it more robust to inaccuracies in the original labels.

This is done by computing the sensitivity and specificity of the original dataset labels based on the subset of the re-read labels. Specifically, the sensitivity, s_{sens} is computed as follows $s_{sens} = TP/P$ where TP is the number of original positive labels which are correctly labeled based on the re-read subset and P stand for the total number of positive samples in the re-read samples. s_{spec} denoting specificity score $s_{spec} = TN/N$ where TN is the number of original negative labels which are correctly labeled based on the re-read subset and N stand for the total number of negative samples in the re-read samples.

To increase the robustness of the model, a regularization term \mathcal{L}_{noise} is added to the original binary cross-entropy loss function during training.

$$\mathcal{L}_{noise} = - \sum_{j=1}^n \sum_{i=1}^c [\lambda_{noise} [I_P^{(i)} w_N^{(i)} (1 - p(y_i|x_j)) \log q(y_i|x_j) + I_N^{(i)} w_P^{(i)} p(y_i|x_j) \log(1 - q(y_i|x_j))] \quad (33)$$

I_P and I_N denote the individual regularization weights for positive and negative examples, where $I_P^{(i)} = 1 - s_{sens}^i$ and $I_N^{(i)} = 1 - s_{spec}^i$. $w_P^{(i)}$ and $w_N^{(i)}$ are additional weight constants to address the problem of imbalance. $w_P^{(i)} = \frac{P^{(i)} + N^{(i)}}{P^{(i)}}$ and $w_N^{(i)} = \frac{P^{(i)} + N^{(i)}}{N^{(i)}}$, λ_{noise} is a weight parameter defining the overall influence of the regularization term.

In addition to the \mathcal{L}_{noise} , the authors proposed to exploit the correlation between labels observed in chest radiography and incorporate this information in the original loss function to further reduce the impact of label noise.

Qiu et al. [148] incorporated a regularization loss in their self-training framework, called *Pathin-NL*. In particular, their approach regularizes the classification model by using the KL divergence to enforce the similarity between the soft label distribution, estimated using the softmax output of the model's current predictions, and the estimated noise free label distribution, which was computed using the softmax of the model's output for the previous iteration. In addition, it was assumed that even in the presence of noisy labels, the majority of images were initially

correctly labeled. Therefore, the original unmodified labels were also used for training their model using the standard cross-entropy loss. This will enforce the estimated label distribution not to be completely different from the initial noisy labels. They validated their approach for pathology image classification, using glioma and lung cancer datasets from The Cancer Genome Atlas (TCGA). They modeled this task as a noise label problem. In fact, each WSI is divided into multiple patches and each patch is assigned to the WSI label. Therefore, even if the WSI is labeled to be a tumor WSI, it still contains some patches of normal tissue, which are considered to be noisy samples. The results showed that the proposed method achieved an AUC of 0.872 and 0.977 on these two datasets respectively.

6.2.2.6 Graph

Graph-based methods aim to model relationships between images [175, 225] or between patches [210, 226] in feature space to better detect label noise.

Xiang et al. [210] proposed a weakly supervised model *Graph Convolution Network-Multiple instance learning (GCN-MIL)* for prostate cancer grading. It consists of 1) a self-supervised CNN model to conduct feature extraction, 2) a graph convolution network and attention pooling model to aggregate features. For self-supervised learning, they used contrastive loss on unlabeled patches (histopathological images) extracted from WSIs. For the second phase, a graph is developed based on the embedding vectors and their spatial position in the slide. DeepGCN convolution is conducted on the graph-structure data to pass information among nodes. To output a final grading prediction, the authors used attention pooling over all nodes. Since the labels are imperfect, the training process iteratively filters out noisy labels using uncertainty estimation. Noisy samples are identified based on the assumption that noisy labels samples have a large loss and uncertainty compared with clean samples. At each iteration, only clean samples within the uncertainty boundary are selected to update the GCN-MIL model.

As described in Section 6.2.2.5, Shi et al. [175] proposed a novel robust semi-supervised convolutional neural network Graph Temporal Ensembling (GTE). In particular, graph-based approach is used to map labeled samples of each class into a cluster, it is shown to be more beneficial than feature consistency which aims to form consensus predictions of feature representations. In contrast, feature consistency has shown significant improvement for combating noisy labels.

Yu et al. [226] presented a novel framework for pathological cancer grading. Their method takes into account space noise and level noise which tackles annotating inaccurate scope of cancerous area and cancerous level, respectively. A global-to-local rectifying strategy is used to solve the space noise. First, the ultra-large image is converted into a *Multilayer Superpixel (MS) graph* for data compressing. This is done using a space-aware branch which reduces

the size while preserving the global features. After generating the multilayer superpixel graphs, a Graph Convolution Network (GCN) is used for preliminary classification into binary labels (positive and negative) and for generating K pseudo masks by MS graphs. These graphs are used to cover category-independent regions. They are inputted into a CNN network in order to fine-tune classification results. A level-aware branch adopts different grouped kernels and a novel grading loss function to handle level noise. Finally, a bidirection co-operation are conducted to synthesize the information of the aforementioned two denoising branches which permits the assistance of the space-aware branch in grading and the feedback from the level-aware branch.

Ying et al. [225] employed *neighborhood graph regularization* after reducing data dimensionality using PCA. Their aim was to perform manifold learning for ensuring that the reduced-dimensional data retains its original local structure.

6.2.2.7 Meta-model

Few-shot meta-learning aims to train a model that can quickly adapt to a new task using only a few data-points and training iterations [57]. To this end, in meta-learning, the model is trained on a set of tasks in a way that the model can quickly adapt to new tasks using only a small number of examples. In the context of DG, meta-learning can tackle the problem of label noise by leveraging the uncertainty of predicted scores and producing meta-models that contain robust features.

Do et al. [49] presented a new *Multiple Meta-model Quantifying (MMQ)*²⁸ method that effectively learns meta-annotation and leverages meaningful features to the medical Visual Question Answering (VQA) task. Their framework consists of three modules : 1) *Meta-training* for training a meta-model to extract image features used in medical VQA, 2) *Data refinement* which uses auto-annotation to increase the training data and deals with the noisy label by using the uncertainty of predicted score, and 3) *Meta-quantifying* for selecting meta-models whose robust to each others and have high accuracy during inference phase of model-agnostic tasks.

For doing meta-training, they followed *Model-Agnostic Meta-Learning (MAML)* [57]. Considering a model f with its θ parameters. When adapting to a new classification task T_i and its associated dataset $\{D_i^{tr}, D_i^{val}\}$, the updated parameter vector (θ^i) can be written as follows:

$$\theta^i = \theta - \eta \nabla_{\theta} \mathcal{L}_{T_i}(f_{\theta}(D_i^{tr})) \quad (34)$$

where η is a learning rate. The model parameters are trained by optimizing for the performance of f_{θ^i} with respect to θ across all tasks. At the end of each iteration, the meta-model parameters are updated using validation sets of all tasks to learn the generalized features. Formally, the meta-objective is as follows:

$$\theta = \theta - \beta \nabla_{\theta} \sum_{T_i} \mathcal{L}_{T_i}(f_{\theta^i}(D_i^{val})) \quad (35)$$

where β is a learning rate.

Once the meta-training phase is done, the weights of the meta-models are used for refining the dataset. The goal of this data refinement is to update (increase) the meta-data for meta-training and remove samples that are suspected to be noisy labels or hard-to-learn. This is done by comparing the predicted scores to a predefined uncertainty threshold. If the predicted score is lower than threshold, the sample is considered noisy.

In order to identify candidate meta-models that are useful for the medical VQA task, they proposed a meta-quantifying phase. In this phase, they compute a fuse score S_F which quantify the performance during the validating process for each meta-model :

$$S_F = \gamma S_P + (1-\gamma) \sum_{t=1}^m 1 - \text{Cosine}(z_c^f, z_t^f) \quad \forall z_c^f \neq z_t^f \quad (36)$$

where S_F stands for the fuse score, γ is the effectiveness-robustness balancing hyperparameter. S_P is the predicted score over ground-truth label. The summation runs over all m models, where t is the index of the model. z_c^f is the feature extracted from the current meta-model. m denotes the number of candidate meta-models. z_t^f is the feature extracted from the t -th model of the list of meta-models. Cosine represents the cosine similarity function used for checking the similarity between two features.

6.2.3. Collaborative methods

DL methods are prone to overfitting on incorrect labels, which can affect their ability to generalize. To overcome this issue, some approaches have focused on incorporating regularization into the loss function [134]. However, in some cases, these methods prevent the classifier from achieving optimal performance. On the other hand, some strategies have attempted to estimate the transition matrix [142], a technique that avoids a regularization bias and has the potential to enhance classifier performance. However, accurately estimating transition matrix is challenging, in particular with datasets that are imbalanced. A promising solution to avoid the complexities of estimating the noise transition matrix involves focusing on training with a subset of carefully selected samples. This approach aims to filter out clean instances from the noisy data for network training. In this context, collaborative methods via training two or more models leverages the cooperation between models for improving the performances of DL models. These methods encompass co-training, co-teaching, and knowledge distillation.

6.2.3.1 Co-training

Co-training is a machine learning technique where two or more models are trained separately on distinct views of the

²⁸https://github.com/aioz-ai/MICCAI21_MMQ

data, and their predictions are used to enhance each other's learning process.

Zhou et al. [240] addressed the challenges of concept shift and noisy labels in medical imaging datasets using co-training. With the aim to tune a single target network for disease classification, they proposed to pre-train multiple reference networks to account of the uncertainty and inconsistency of the original labels. To co-optimize the target network and reduce the influence of label uncertainty, they introduced a *Disentangled Distribution Learning (DDL)* strategy which disentangle the multiple reference models predictions into a hard *Majority Confident Label (MCL)* vector (a pseudo cleaned ground-truth) and a soft *Description Degree Score (DDS)* vector. The MCL vector was computed by counting the number of networks giving positive and negative predictions for the corresponding disease label. The DDS vector was computed using the average over all the predictions. To optimize the target network, they employed the KL divergence based on the confidence-weighted relative entropy of the hard majority label vector with respect to the predictions of the target network. Moreover, to enforce the target network to provide consistent predictions for images with similar medical findings, the authors proposed *inter- and intra-instance consistency regularization*. To this end, K -nearest neighbor smoothing modules and image augmentation were proposed. K nearest neighbors of an image (the anchor image) were computed based on the fixed soft label distribution. Then, the target network was constrained to produce similar predictions for the anchor image and its K nearest neighbors. On the other hand, the anchor image was also augmented into different views and the target network was constrained to have the same prediction to these views. Experiments performed on chest X-ray and fundus image dataset, showed that the proposed approach is outperforming state-of-the-art methods.

Xue et al. [217] proposed a *co-training with global and local representation learning framework*. Their self-ensemble co-training scheme consisted of training two independent teacher-student networks simultaneously. To ensure having different weight parameters for both networks, different image augmentation, initialization strategy were used. After one epoch of training, a Noisy Label Filter (NLF) was used to divide the data into clean and noisy samples based on the teacher encoder's predictions. Specifically, for the NLF, a two-component Gaussian Mixture Model (GMM) is adopted. The cross-entropy loss is computed for training data, which is then inputted to the GMM. The latter fits the max-normalized loss of the training data using the Expectation-Maximization algorithm. Then, the divided clean and noisy samples are crossly sent to the peer student-teacher network as new input data. Once the noisy label detection procedure is done, rather than removing the noisy labeled sample, the authors proposed a *self-supervised learning strategy*.

To learn robust representation, the *local contrastive loss* is applied on noisy samples and the *global relation loss* is

applied using both clean and noisy samples. For local contrastive loss, the network is encouraged to learn robust representation by creating two augmented images of the same data and regularizing the network to minimize the difference between positive pairs (two augmented views of the same source image) and maximize the difference from negative pairs (augmented images from different source). The global inter-sample relationship alignment ensures that for each batch of noisy data, the predictions of the student network and the teacher network maintain the same relationships. To this end, an inter-sample relation matrix is computed between each sample within a mini-batch. Then a global inter-sample relationship loss is added to align the inter-sample relationship of samples between the teacher and student model. Through extensive experiments on datasets such as the Histopathologic Lymph Node dataset, ISIC Melanoma dataset, the Gleason 2019 dataset, CXP dataset, the proposed approach consistently outperformed other state-of-the-art methods, especially in scenarios with high noise ratios.

6.2.3.2 Co-teaching

Co-teaching is a paradigm where two models are jointly trained with each model selecting the instances to train the other model. Since each model is initialized differently, each model learns a different decision boundary, resulting in different selection of training instances.

Zhu et al. [242] presented a robust *co-teaching* paradigm which cross-trains two DL networks simultaneously to select small-loss samples for training. Their proposed approach comprises two modules: 1) an *Adaptive Noise Rate Estimation (ADNRE)* module for estimating the dataset's noise rate, and 2) a *Consistency-based Noisy Label Correction (CNLC)* module which aims to select probably clean samples based on their loss ranking and relabel highly suspected noisy samples using consistent predictions. In ADNRE, two DL networks are trained using training data and evaluated using an evaluation subset (i.e., validation subset). To estimate the noise rate of the dataset, the maximum validation accuracy is used. In CNLC, the models are initialized using the previously trained models. This module comprises two stages. In the first stage, *the noisy label detection*, both networks are used to select probably clean samples based on their loss ranking. In the second stage, *label correction*, samples with greater credible prediction are selected from suspected noisy data and relabeled, while the others are removed. To this end, at each training epoch, for estimated noisy samples, samples with the same predicted labels on both networks as well as the prediction confidences that are larger than a certain threshold, are relabeled. The idea stems from the observation that samples with consistent predictions on different models have greater credibility. Finally, the corrected samples are aggregated with small-loss samples into "a corrected set" which is used for training the network in the next iteration. The authors showed promising performance of their proposed approach to handle noisy labels, when tested on

public skin lesion datasets ISIC-2017, and ISIC-20019 and a constructed thyroid ultrasound image dataset.

One drawback of co-teaching is that ordering data based on their loss may overlook difficult examples that may be correctly labeled but hard to train. In other words, cases which have similar characteristics to noisy ones but are needed for improving model performances. To overcome this issue, Peng et al. [145] proposed an improvement on co-teaching, called co-weighting.

Similar to co-teaching, two DL networks are trained simultaneously, teaching each other given every mini-batch. However, in co-weighting, each network feeds forward all data and re-weight samples of the current batch dynamically. In this approach, noisy samples are identified and excluded by analyzing the statistical features of predictive history and only hard informative samples are retained. The history of prediction, i.e., all the output in the former iterations are stored in H_i^{t-1} and is used to store the learning events that correspond to an increase of the predictions between two consecutive updates (associated with the numerical value of 1) and forgetting events that correspond to a decrease of the predictions between two consecutive updates (-1), denoted by K_i^{t-1} . It is assumed that noisily-labeled samples are forgettable in contrast clean samples undergo fewer forgettable events. Based on K_i^J , where J is the max step of iterations, the number of forgetting events can be identified, hence the noisy samples are identified. Next, they adopted Noisy cross-validation [33] to estimate noise ratio (ϵ). The reserved samples (with a ratio of $1 - \epsilon$) underwent a ranking process.

Experiments on DigestPath2019 and the colorectal tumor dataset were conducted and showed high average accuracy (> 0.915) of 5-fold cross-validation. The results outperformed co-teaching.

Zhu et al. [241] also proposed an improvement over co-teaching framework. Similar to Peng et al. [145], the authors argued that by selecting small loss samples, co-teaching framework overlooks hard samples, which may be considered as noisy. To overcome this problem, they proposed a *hard sample aware noise robust learning method*. Their framework²⁹ is composed of two phases: a *label correction* phase and a *Noise Suppressing and Hard Enhancing* (NSHE) phase. The label correction phase produces an "almost clean dataset" which is then used as input in the second phase. This stage pre-discard most of the noisy samples using a self-training strategy, as described in Section 6.2.1.2. The NSHE phase takes the obtained "almost clean dataset" as input and outputs the final noise-robust classification model. In this phase, the authors adopted a co-learning architecture to enhance the hard samples while suppressing the few existing noisy ones. First, two DL networks, $f_1(x, \theta_1)$ and $f_2(x, \theta_2)$, are initialized with the same backbone and parameters. Both networks are updated using back-propagation and momentum manner. Inspired by MoCo [74], the parameters of the first DL network θ_1 are updated by back-propagation. While the parameters of the

second DL network θ_2 are updated by:

$$\theta_2 \leftarrow m\theta_2 + (1 - m)\theta_1 \quad (37)$$

where $m \in [0, 1)$ denotes a momentum coefficient. θ_2 evolve more smoothly than θ_1 . At each epoch, f_2 selects training data for f_1 by ranking samples according to their prediction values, i.e., samples with small prediction probabilities are not used for back-propagation. The proposed method showed good performances, outperforming state-of-the-art methods across all noise ratios in tests on both medical scenario datasets (DigestPath2019 and Camelyon16) and toy computer vision datasets (CIFAR-10 and Webvision).

Co-correcting strategy [122]³⁰, inspired also by co-teaching, aims to address the issue of noisy labels through the simultaneous training of two deep learning networks with identical architecture (also called dual-network architecture). The parameters of DL networks are updated using the principle "updated by agreement". This strategy assumes that instances with small losses are clean and collect their gradients when agreement occurs (mutual learning). The framework consists of three modules: the dual-network module based on mutual learning, the curriculum learning module, and the label updating module. The dual-network is trained by selecting clean samples based on small losses and mutual agreement. The correction of labels is based on curriculum learning, in which co-correcting introduces a label correction strategy by increasing difficulty from easy tasks to harder ones. This avoids premature label modification which modifies noise-free samples incorrectly. Finally, for the label updating module, a probabilistic estimation of whether the label is noise-free (label distribution) is done like in the PENCIL framework [223]. The idea is to update both network parameters and label estimations as label distributions. The estimated label distribution serves as a pseudo-label, it is initialized based on the noisy labels and continuously updated using backpropagation. This method was evaluated on PatchCamelyon and ISIC datasets, under different level of noise. It outperformed other state-of-the-art methods such as PENCIL, Reweight, DivideMix, Co-teaching, Co-teaching+, and Joint Optim.

6.2.3.3 Knowledge distillation

Knowledge distillation is a paradigm which refers to transforming knowledge from one model to the other. A student model trained from noisy labels is guided by a teacher model. Specifically, first an initial teacher model is trained on a clean dataset. In parallel, a student model is trained using a combination of original noisy labels and the output predictions of current teacher, which serves as pseudo labels to guide the training process of the student model. As the training progresses, better guidance is provided to the student model since the prediction of the teacher model becomes more reliable.

Li and Xu [114] proposed a novel *Bootstrap Knowledge Distillation (BKD) method*, which seeks to improve the label

²⁹<https://github.com/bupt-ai-cz/HSA-NRL/>

³⁰<https://github.com/JiarunLiu/Co-Correcting>

qualities gradually, therefore degrade the noise level of the whole dataset. The idea is to transform the distribution of noisy labels to be closer to the distribution of real labels without estimating a noise transition matrix. They applied their method for lung disease classification on CXR images using the CheXpert dataset and the Chest X-ray14 dataset. For the CheXpert dataset, they used the certain part of data to train the teacher model. At the next steps, they employed various strategies to train it on the entire dataset. For handling uncertain labels, they adopted three different strategies they mapped all uncertain labels to 0 (U-Zeros), to 1 (U-Ones), or to the output probability of an auxiliary model (U-SelfTrained). They compared their method with a baseline method which trains a CNN and takes the ensemble of 30 checkpoint using the mean of the output probabilities. They showed that their method which is based on self-train strategy outperformed the baseline method. In particular, despite the fact that the U-SelfTrained strategy seems to be outperforming the other strategies particularly for the “Cardiomegaly” and “Consolidation” detection, the U-ones strategy showed the best results for atelectasis detection, indicating that most of uncertain labels are likely to be positive. For Chest X-ray14 dataset, they used a pre-trained model to select the clean subset. They have chosen the samples whose output probability is larger than 0.55 and ground truth is 1 as certain positive and those whose output probability is smaller than 0.45 and ground truth label is 0 as certain negative while the rest was considered as uncertain labels. When comparing the results of their approach to 3 different published methods, they showed that their method outperformed these baseline methods on most pathologies.

7. Discussion

One of the ultimate goals of DL models in healthcare is to achieve good generalization performances for wider deployment. This desideratum is of critical importance for the DL models to be employed in real world. However, domain shift is almost inevitable in the medical field. This is mainly because medical data is heterogeneous, exhibiting significant variability due to diverse imaging modalities, patients demographics, and disease characteristics. These factors cause what is called *covariate shift*. Besides, the data is typically collected in diverse scenarios (e.g., mass screening, city consultations, hospital appointments, etc.), possibly in different countries, implying different annotation guidelines, levels of expertise, etc. These factors cause what we call *concept shift*. For these reasons, we suspect domain shifts are particularly strong in the medical domain, compared to general-purpose computer vision tasks, where imaging devices (typically cameras) are more homogeneous and concepts (animal species, building types, etc.) are more universal. Facing this domain shift, it is crucial to ensure that DL will perform robustly, reliably and fairly when making predictions about data different from the training data. In this paper, we have presented state-of-the-art strategies for the development of generalized method for medical image classification. Depending on the type of shift, two main

categories of methods were identified: covariate shift-based methods and concept shift-based methods.

Hereafter, we will first draw conclusions on the benefits of current DG methods, through the analysis of their results on challenge data (Section 7.1). We will then examine the recent trends in DG development (Section 7.2). Furthermore, we will discuss connections with other research fields (federated learning, fair AI, causal AI, etc.) (Section 7.3). Afterward, we give practical issues to implement and evaluate a DG method (libraries, evaluation strategies, etc.) (Section 7.4). Finally, we end with future directions and promises (subpopulation shift, open DG, etc.) (Section 7.5).

7.1. Lessons learnt from challenges

In histopathology, 17 methods were submitted for the MIDOG challenge [12] final test. These methods were compared to a reference DG approach [209] which reduces covariate shift in the feature space by using adversarial training, belonging to “Representation learning– Adversarial category” in our taxonomy (detailed description of this approach can be found in Section 6.1.2.1). In addition, a non-DG baseline was considered, named CNN baseline, with the same network topology as the reference approach but only trained using standard image augmentation. Among the submitted methods, three methods [39, 103, 123] were described in this survey and belong to the “Data manipulation– Data augmentation” category (Section 6.1.1.2).

The findings from the MIDOG 2021 competition suggest that through the use of effective augmentation techniques and sophisticated DL architecture models, domain shift between different whole slide imaging scanners can be addressed to some extent. Despite promising overall performances, the results on unseen Scanners were considerably weaker, indicating that domain shift is not completely covered by the algorithms. This highlights that the problem of DG is not solved yet: there is a need for developing more robust algorithms.

Regarding the recent challenge UBC-OCEAN³¹ which aims to classify ovarian cancer subtypes based on histopathology images, Owkin’s team has won the competition³². Their solution consisted of using Phikon, Owkin’s foundation model for digital pathology. It is a self-supervised foundation model [56], which consists of a ViT-Base pre-trained with iBOT on 40 million tiles from the TCGA dataset. Specifically, they trained an ensemble of Chowder [43] models (multiple instance learning models) on top of Phikon tile embeddings. Then, they used high entropy predictions to detect outliers. These results suggest that the development of foundation models in the medical field pave the way for improving the generalizability of DL models. In particular, the pre-training strategies are important for enhancing the performances of DL models.

³¹<https://www.kaggle.com/competitions/UBC-OCEAN>

³²<https://www.kaggle.com/code/jbschiratti/winning-submission>

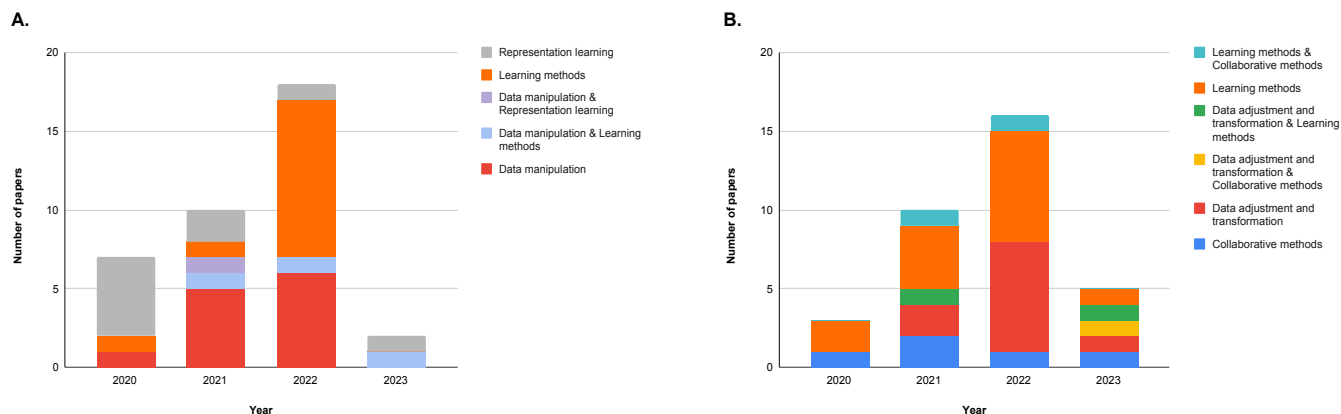


Figure 3: Number of paper per year for covariate shift methods (A) and concept shift methods (B). Publications up to April 2023. A unique category is created for papers belonging to multiple categories simultaneously.

7.2. Trends in DG

Figure 3 shows the number of papers per category for methods dealing with covariate shift (Figure 3 A) and methods with concept shift (Figure 3 B). In both graphs, the number of papers tends to increase over the years, suggesting that the generalization research in the medical field is emerging (the decrease in 2023 simply indicates that the reviewed period ends in April 2023). For the methods dealing with covariate shift, it can be seen that learning based methods are showing a significant increase over the years. Data manipulation based methods are showing a smooth increased evolution. On the other hand, we note a slight decreasing evolution for representation learning method.

For methods dealing with concept shift, we also noted that the number of papers employing learning methods is increasing through the years. We note that some methods use two categories simultaneously (i.e., "data manipulation" and "representation learning", "data adjustment and transformation" and "learning methods"). This suggests that combining methods could be also studied in future research to enhance the results.

Indeed, learning methods, more precisely based on self-supervised learning, are becoming more and more prominent in the field of generalization research. In this context, a promising avenue for DG is the development of foundation models, a large AI model developed using a massive amount of unlabeled data on a large scale, that can be customized for a wide range downstream tasks.

For example, in the field of ophthalmology, a foundation model for retinal images, RETFound [239], was proposed. It underwent pre-training on 1.6 million unlabeled retinal images through self-supervised learning, leveraging the weights from a model that was trained on natural images from ImageNet using the same self-supervised learning strategy. RETFound has achieved increased generalization performances in the diagnosis and prognosis of sight-threatening eye diseases on unseen datasets, when compared

to other pretraining strategies. These pretraining strategies used the same model architecture and the fine-tuning process but only differed with the pretraining process. For instance, one classical pretraining strategy consisted of pre-training the model on natural images by means of supervised learning. Other more sophisticated strategies employed self-supervised learning pretraining scheme using either natural images or retinal images.

In histopathology, many foundation models have been proposed [2, 104, 56, 222]. Among these models, [56] was adopted for the UBC-OCEAN competition and was the winner.

7.3. Related research to DG

This section presents the link between generalization research and other learning methods such as federated learning, fairness, and causality.

7.3.1. Federated learning

Several algorithms [171, 6, 116] described in this paper used Federated Learning (FL) in their framework. FL, notably, can be regarded as one of the most practical application of DG in medical imaging. The distributed, heterogeneous data in FL, renders it an appealing scenario for implementing DG in FL applications. In this context, the medical data is distributed across multiple domains (organizations/hospitals), where each domain corresponds to one organization. FL offers privacy preserving guarantee in distributed scenarios while DG ensures that the developed model can generalize well to unseen data. The use of FL in DG is more challenging in practice since the data is inaccessible in this setting. Hence, the assessment of the type of domain shift is harder in this case. The collected data may differ in terms of data acquisition systems, demographics, medical conditions, and treatment protocols. Researcher should choose the most appropriate DG strategy depending on the assumed domain shift (covariate shift or concept shift).

Notwithstanding this difficulty, federated domain generalization [117] is a promising research area and one perspective would be to extend more DG algorithms in this context. One line of research is to use FL mechanisms for improving DG. For instance, Matta et al. [130] used FL to study two main factors which affect DL generalizability: the difference in terms of collected imaging data (screening centers) and the difference of annotation between readers (graders). The targeted application was the detection of diabetic retinopathy using fundus photographs. To this end, they have developed two FL algorithms: 1) a cross-center FL algorithm, using data distributed across centers and 2) a cross-grader FL algorithm, using data distributed across the graders. The study has shown that the cross-grader FL algorithm has outperformed the cross-center FL algorithm and centralized learning (a learning paradigm where all data is pooled in a centralized repository). It suggests that the averaging mechanism used in FL allows to give equal weight to all graders, leading to a more generalized model.

7.3.2. Fairness

In the context of covariate shift, some work have proposed to study the performance by attributes. This permits to gain a better understanding of the model biases caused by different dataset shift. For instance, in the mammography field, mass detection performances were analyzed according to mass status, mass size, age, and breast density [59]. Using this analysis, the authors observed that the model seems to have a bias towards masses smaller than five millimeters in diameter and bounding boxes with a high height-to-width ratio, possibly because these samples were not represented in the training dataset.

In histopathology, Graham et al. [65] proposed to develop a DL algorithm to screen for colon cancer based on WSI. To investigate potential biases and ensure fairness in the model’s predictions, the authors assessed model performances across different demographic subgroups, including sex, age, ethnicity and anatomical site of the biopsy. The differences in model performance based on sex and ethnicity are minimal, but the impact of age on performance is more significant. This variation could stem from several sources, including the data selected for training the model and possible differences in how diseases manifest across different age groups.

In radiology and dermatology, Brown et al. [26] investigated unfairness of DL models due to shortcut learning, a phenomenon where DL models make predictions based on incorrect correlations found in the training data. In their experiment on X-ray dataset, the authors have shown that the performances of the DL models varies with age. In addition, these models learn to encode age even though the models were trained to do so. To identify the presence of shortcut learning when attributes might be causally related to the outcome (such as age), they proposed ShorT, an approach based on adversarial learning. It applies an intervention that modifies the amount of age encoding in the feature extractor and assess the effect of this intervention on model fairness.

7.3.3. Causality

Causal machine learning [91] is a learning paradigm that utilizes causal knowledge about the to-be-modeled system. Essentially, causal inference offers a framework for formalizing structural knowledge about the data generating process via Structural Causal Models (SCMs). SCMs permit to estimate the impact on data when changes (called interventions) are applied to its generating process. Moreover, they also allow us to model the consequences of changes in hindsight while taking into account what happened (called counterfactuals).

One of the most promising areas where causal machine learning can be applied is DG. Causality aware DG aims to reduce dependency on spurious correlations by addressing and adjusting for confounding variables [174]. For additional information about these methods, readers are invited to refer to the survey on DG and causality available in the literature, in Sheth et al. [174], Sheth and Liu [173] and a survey of causality in medical image analysis [201].

7.4. Implementation in generalization research

In this section, we present generalization libraries, model selection strategies, and evaluation research, for the purpose of readers intending to start employing DG approaches.

7.4.1. Generalization libraries

A few general-purpose libraries exist for covariate shift, concept shift and noisy label management. These libraries implement multiple algorithms and benchmarking mechanisms and can therefore be useful to develop DG approaches.

- **DomainBed**³³ [69], a testbed for domain generalization, is a PyTorch suite containing benchmark datasets (mainly computer vision datasets) and algorithms for DG. Initially, it includes seven multi-domain datasets, nine baseline algorithms, and three model selection criteria.
- **Cleanlab**³⁴ is a popular library for noisy label management. It implements various data-centric AI algorithms, in which noisy labels are “cleaned” before training. Benchmarking relies on a noise generation module.
- **DeepDG**³⁵, inspired by DomainBed, DeepDG is a PyTorch based toolkit for DG. It is a simplified version of DomainBed while it adds new features to enhance functionality.
- **Dassl**³⁶ [237] is a PyTorch toolbox developed to support research in domain adaptation and generalization. It comprises methods for single-source domain adaptation, multi-source domain adaptation, domain generalization and semi-supervised learning.

³³<https://github.com/facebookresearch/DomainBed>

³⁴<https://github.com/cleanlab/cleanlab>

³⁵<https://github.com/jindongwang/transferlearning/tree/master/code/DeepDG>

³⁶<https://github.com/KaiyangZhou/Dassl.pytorch>

- **ClinicalDG**³⁷ A Modified version of DomainBed framework.

7.4.2. Model selection

Following Gulrajani and Lopez-Paz [69], two potential selection methods can be used as model selection policy, *Training-domain validation set* and *Leave-one-domain-out cross-validation*:

- **Training-domain validation set** consists of splitting the data for each source domain into a training subset and a validation subset. The validation subsets are pooled across all source domains to form an overall validation set. Finally, the model maximizing the score performance on the overall validation set is selected.
- **Leave-one-domain-out cross-validation** This strategy assumes the presence of at least two source domains. Therefore, it is applicable in multi-source DG. It consists of leaving one source domain for the validation while using the others for training.

7.4.3. Evaluation

Some studies have focused on the evaluation of the key driver of covariate shift such as the effect of the physical generation process, i.e., Physical Imaging Parameters (PIPs), on model generalization [99]. Regarding the concept shift, evaluating the models when the test data contains noisy labels has gained interest in the last few years. For instance, Lovchinsky et al. [125] tackled this problem and proposed the *discrepancy ratio* as an evaluation metric. In this section, we present common metrics used for evaluation in the generalization research.

F1 score F1 score was used as a metric for evaluating mitotic figure detections in the MIDOG challenge [12]. Overall F_1 is computed as follow using the counting of all True Postives (TP), False Positives (FP) and False Negatives (FN) detections on slide i for all the k processed slides:

$$F_1 = \frac{2 \sum_i^k TP_i}{2 \sum_i^k TP_i + \sum_i^k FP_i + \sum_i^k FN_i} \quad (38)$$

Quadratic Cohen's Kappa This metric [41] compares the performance of the algorithms with the reference standard. It reflects the degree of disagreement, in such a way that more emphasis is given to bigger differences among ratings than to minor differences [180]. It is suitable for multi-category ordinal classification. It was used to assess the algorithms in the PANDA challenge [27].

Balanced accuracy It is defined as the average of recall obtained on each class. This metric was used for assessing the algorithms performances in the ISIC challenge.

A-distance A-distance measures the distribution discrepancy[21]. The smaller the A-distance, the more domain-invariant the features are. Therefore, it is an indicator of how efficient a method is to reduce cross-domain divergence [34].

Representation shift The *representation shift* (R) is used to quantify the statistical difference between the datasets in the evaluation of DG methods [18, 184]. It computes the differences in the distribution of layer activations of a model between datasets from two domains, capturing the model perceived similarity between the two datasets. The distributions between the two dataset are likely to be similar (small distances) if the model had learnt domain-invariant features.

7.5. Future promises

In this section, we discuss future possibilities for generalization research in medical imaging. We include perspectives for exploring important research area related to DG including datasets, subpopulation shift, open DG, continual DG and unified benchmarking.

7.5.1. Datasets in DG

Regarding DG datasets, Kilim et al. [99] encouraged to include medical image generation metadata in open source datasets. The goal of using metadata measured with standard international units is to establish a universal standard between distributions generated across the world for all current and future imaging modalities. In addition, future work can use these meta-data describing the generative process of an image in unsupervised and self-supervised algorithms. Also, leveraging such metadata to develop models that are agnostic to physical imaging parameters would be an interesting future direction towards more robust models. Indeed, these metadata could be used as a tool for predicting the worst case generalization scenario.

In comparison to multi-DG, where the information related to domains is needed, single-DG is more easy to tackle in practice since it only requires one single source dataset. In this scenario, it is easier for industries to obtain the rights to access this data. Moreover, the problem of missing domain information (i.e., data's originating center) could be solved using single-DG algorithms.

For a safe deployment, AI systems in health undergo thorough evaluations for validation purposes. In general, it is assumed that the ground truth is fixed (certain). However, in healthcare, the ground truth may be uncertain. Standard evaluations of AI models often overlook this aspect, which can lead to serious repercussions, such as an overestimation of the models' future performance [63]. This is particularly concerning in the medical field, because a lack of robustness may translate into patient risk.

7.5.2. Subpopulation shift

Subpopulation shift refers to changes in the proportion of some subpopulations between training and deployment

³⁷<https://github.com/MLforHealth/ClinicalDG>

[221]. In these contexts, DL models may have high overall performance yet still underperform in rare subgroups. Subpopulations shift can be categorized into spurious correlations, attribute imbalance, class imbalance and attribute generalization. Spurious correlations refers to non-causal relationships between the input and the label that may shift in deployment (non-robust features, namely, image backgrounds or texture). Another type of subpopulation shift is attribute imbalance in which certain attributes are sampled with a much smaller probability than others in the training. Class imbalance occurs when class labels exhibit imbalanced distributions, which may cause lower preference for minority labels. Attribute generalization denotes the setting where some attribute are totally missing in the training domain but present in the testing domain.

7.5.3. Open DG

In conventional DG, it is assumed that the label space is the same between the source domain and the target domain. However, this assumption does not hold in real applications. Open DG [177] addresses the problem of DG when the training and test label spaces are not the same. It is a promising approach to tackle the problem where the label taxonomy is not the same between source datasets. This problem is often encountered in medical image analysis. For example, for developing a multi-disease AI system, Matta et al. [131] analyzed the labels of different datasets and converted them into a unified labeling system.

A special form of open DG is open-set DG, in which the label space on the source domain is considered a subset of that on the target domain. For instance, Zheng et al. [234] proposed an open-set single-DG based on multiple cross-matching method. Their approach consists in generating auxiliary samples that fall outside the category space of the source domain, thereby enhancing the identification of an unknown class (i.e., class that does not belong to the source domain). Crucially, these produced auxiliary samples do not necessarily align with the novel classes within the target domain.

7.5.4. Continual DG

Conventional DG assumes that multiple source domains are accessible and the domain shift is abrupt. However, this is not universally applicable to all real-world applications where the data distribution may gradually change over time, especially, in the medical field. In this context, new disease or new biomarkers may arise. As the domain continues to evolve, new domains will consistently emerge. Re-training DL models, under the conventional scheme of DG, to keep-to-date with both new and existing domains can be both resource-intensive and inefficient. Continual learning, on the other hand, permits the model to continuously learn from a sequence of tasks over time while maintaining performances on all experienced tasks. Combining continual learning and DG would enable to model the evolutionary patterns of temporal domains and leveraging these patterns to palliate the distribution shift in the future domains. Recent work [211]

proposed a continual domain generalization over temporal drifts, where the goal is to generalize on new unseen domain given that only data from the current domain is accessible at any given time, while information from past domains is unavailable.

7.5.5. Unified Benchmarking

From this survey, we can see that there is a variation in the targeted application (histopathology, Xray, fundus photographs, ultrasound). In addition, the training protocol differ from one paper to another (architecture, augmentation strategies, etc) or even in datasets (not the same split was used). This makes the comparison between methods challenging and unfair. A practical solution for this problem is to organize challenges in domain generalization for medical image classification. This help in ensuring the testing data is the same. However, this strategy does not ensure that the main differences in methods come from other factors such as the backbone used. Therefore, for a better assessment of these methods, there is a need for a unified framework like in DomainBed, or like benchmarking framework used in federated learning for medical field such as Flamby [190] and MedPerf-FeTS [92].

In the benchmarking framework, researcher could also state what problem of shift they are targeting to solve. In this work, we have identified two main categories of methods based on the shift type: covariate and concept shift. However, in the medical field, the domain shift problem is very complex and both shifts can appear simultaneously. While it is more challenging to tackle both problems, future work handling full shift (covariate shift and concept shift) holds great potential for the clinical world.

8. Conclusion

In the medical field, data exhibit different sources of variation: images may be collected from multiple countries and different ethnic group (causing covariate shift), data can be gathered using different criteria (different screening programs), annotations differences, etc. (causing concept shift). To mitigate these challenges, we reviewed state-of-the-art methods for the generalization of DL models in medical image classification and discussed challenges and future research trends for this line of research. We hope that this work will help the research community to tackle the problem of generalization in a variety of applications.

Acknowledgement

This work was supported by the French National Research Agency under the LabCom program (ANR-19-LCV2-0005 - ADMIRE project).

References

- [1] AlBadawy, E.A., Saha, A., Mazurowski, M.A., 2018. Deep learning for segmentation of brain tumors: Impact of cross-institutional training and testing. *Medical physics* 45, 1150–1158.
- [2] Alfasy, S., Nejat, P., Hemati, S., Khan, J., Lahr, I., Alsaafin, A., Shafique, A., Comfere, N., Murphree, D., Meroueh, C., et al., 2024.

- Foundation models for histopathology—fanfare or flair. *Mayo Clinic Proceedings: Digital Health* 2, 165–174.
- [3] Aljuhani, A., Casukhela, I., Chan, J., Liebner, D., Machiraju, R., 2022. Uncertainty aware sampling framework of weak-label learning for histology image classification, in: *International Conference on Medical Image Computing and Computer-Assisted Intervention*, Springer. pp. 366–376.
- [4] Allan, M., Shvets, A., Kurmann, T., Zhang, Z., Duggal, R., Su, Y.H., Rieke, N., Laina, I., Kalavakonda, N., Bodenstedt, S., et al., 2019. 2017 robotic instrument segmentation challenge. *arXiv preprint arXiv:1902.06426*.
- [5] Almahfouz Nasser, S., Kurian, N.C., Sethi, A., 2021. Domain generalisation for mitosis detection exploiting preprocessing homogenizers, in: *International Conference on Medical Image Computing and Computer-Assisted Intervention*, Springer. pp. 77–80.
- [6] Andreux, M., du Terrail, J.O., Beguier, C., Tramel, E.W., 2020. Siloed federated learning for multi-centric histopathology datasets, in: *Domain Adaptation and Representation Transfer, and Distributed and Collaborative Learning: Second MICCAI Workshop, DART 2020, and First MICCAI Workshop, DCL 2020, Held in Conjunction with MICCAI 2020, Lima, Peru, October 4–8, 2020, Proceedings 2*, Springer. pp. 129–139.
- [7] Aresta, G., Araújo, T., Kwok, S., Chennamsetty, S.S., Safwan, M., Alex, V., Marami, B., Prastawa, M., Chan, M., Donovan, M., et al., 2019. *Bach: Grand challenge on breast cancer histology images. Medical image analysis* 56, 122–139.
- [8] Arjovsky, M., Bottou, L., Gulrajani, I., Lopez-Paz, D., 2019. Invariant risk minimization. *arXiv preprint arXiv:1907.02893*.
- [9] Armato III, S.G., McLennan, G., Bidaut, L., McNitt-Gray, M.F., Meyer, C.R., Reeves, A.P., Zhao, B., Aberle, D.R., Henschke, C.I., Hoffman, E.A., et al., 2011. The lung image database consortium (lidc) and image database resource initiative (idri): a completed reference database of lung nodules on ct scans. *Medical physics* 38, 915–931.
- [10] Atwany, M., Yaqub, M., 2022. Drngen: Domain generalization in diabetic retinopathy classification, in: *International Conference on Medical Image Computing and Computer-Assisted Intervention*, Springer. pp. 635–644.
- [11] Aubreville, M., Bertram, C., Breininger, K., Jabari, S., Stathonikos, N., Veta, M., 2022. Mitosis domain generalization challenge (2021), in: *25th International Conference on Medical Image Computing and Computer Assisted Intervention (MICCAI 2022)*.
- [12] Aubreville, M., Stathonikos, N., Bertram, C.A., Klopffleisch, R., Ter Hoeve, N., Ciompi, F., Wilm, F., Marzahl, C., Donovan, T.A., Maier, A., et al., 2023a. Mitosis domain generalization in histopathology images—the midog challenge. *Medical Image Analysis* 84, 102699.
- [13] Aubreville, M., Wilm, F., Stathonikos, N., Breininger, K., Donovan, T.A., Jabari, S., Veta, M., Ganz, J., Ammeling, J., van Diest, P.J., et al., 2023b. A comprehensive multi-domain dataset for mitotic figure detection. *Scientific Data* 10, 484.
- [14] Bai, R., Ling, C., Cai, L., Gao, J., 2021a. Cnngeno: A high-precision deep learning based strategy for the calling of structural variation genotype. *Computational Biology and Chemistry* 94, 107417.
- [15] Bai, T., Zhang, Z., Zhao, C., Luo, X., 2021b. A novel pseudo-labeling approach for cell detection based on adaptive threshold, in: *Bioinformatics Research and Applications: 17th International Symposium, ISBRA 2021, Shenzhen, China, November 26–28, 2021, Proceedings 17*, Springer. pp. 254–265.
- [16] Balestriero, R., Ibrahim, M., Sobal, V., Morcos, A., Shekhar, S., Goldstein, T., Bordes, F., Bardes, A., Mialon, G., Tian, Y., et al., 2023. A cookbook of self-supervised learning. *arXiv preprint arXiv:2304.12210*.
- [17] Batista, F.J.F., Diaz-Aleman, T., Sigut, J., Alayon, S., Arnay, R., Angel-Pereira, D., 2020. Rim-one dl: A unified retinal image database for assessing glaucoma using deep learning. *Image Analysis and Stereology* 39, 161–167.
- [18] Bayasi, N., Hamarneh, G., Garbi, R., 2022. Boosternet: Improving domain generalization of deep neural nets using culpability-ranked features, in: *Proceedings of the IEEE/CVF Conference on Computer Vision and Pattern Recognition*, pp. 538–548.
- [19] Beck, A.H., Sangoi, A.R., Leung, S., Marinelli, R.J., Nielsen, T.O., Van De Vijver, M.J., West, R.B., Van De Rijn, M., Koller, D., 2011. Systematic analysis of breast cancer morphology uncovers stromal features associated with survival. *Science translational medicine* 3, 108ra113–108ra113.
- [20] Bejnordi, B.E., Veta, M., Van Diest, P.J., Van Ginneken, B., Karssemeijer, N., Litjens, G., Van Der Laak, J.A., Hermsen, M., Manson, Q.F., Balkenhol, M., et al., 2017. Diagnostic assessment of deep learning algorithms for detection of lymph node metastases in women with breast cancer. *Jama* 318, 2199–2210.
- [21] Ben-David, S., Blitzer, J., Crammer, K., Kulesza, A., Pereira, F., Vaughan, J.W., 2010. A theory of learning from different domains. *Machine learning* 79, 151–175.
- [22] Bertram, C.A., Veta, M., Marzahl, C., Stathonikos, N., Maier, A., Klopffleisch, R., Aubreville, M., 2020. Are pathologist-defined labels reproducible? comparison of the tupac16 mitotic figure dataset with an alternative set of labels, in: *Interpretable and Annotation-Efficient Learning for Medical Image Computing: Third International Workshop, iMIMIC 2020, Second International Workshop, MIL3ID 2020, and 5th International Workshop, LABELS 2020, Held in Conjunction with MICCAI 2020, Lima, Peru, October 4–8, 2020, Proceedings 3*, Springer. pp. 204–213.
- [23] Bissoto, A., Barata, C., Valle, E., Avila, S., 2022. Artifact-based domain generalization of skin lesion models, in: *European Conference on Computer Vision*, Springer. pp. 133–149.
- [24] Borji, A., 2021. Contemplating real-world object classification. *arXiv preprint arXiv:2103.05137*.
- [25] Boucher, M., Qian, J., Brent, M., Wong, D., Sheidow, T., Duval, R., Kherani, A., Dookeran, R., Maberley, D., Samad, A., et al., 2020. Evidence-based canadian guidelines for tele-retina screening for diabetic retinopathy: recommendations from the canadian retina research network (cr2n) tele-retina steering committee. *Canadian Journal of Ophthalmology* 55, 14–24.
- [26] Brown, A., Tomasev, N., Freyberg, J., Liu, Y., Karthikesalingam, A., Schrouff, J., 2023. Detecting shortcut learning for fair medical ai using shortcut testing. *Nature Communications* 14, 4314.
- [27] Bulten, W., Kartasalo, K., Chen, P.H.C., Ström, P., Pinckaers, H., Nagpal, K., Cai, Y., Steiner, D.F., Van Boven, H., Vink, R., et al., 2022. Artificial intelligence for diagnosis and gleason grading of prostate cancer: the panda challenge. *Nature medicine* 28, 154–163.
- [28] Bustos, A., Pertusa, A., Salinas, J.M., De La Iglesia-Vaya, M., 2020. Padchest: A large chest x-ray image dataset with multi-label annotated reports. *Medical image analysis* 66, 101797.
- [29] Carion, N., Massa, F., Synnaeve, G., Usunier, N., Kirillov, A., Zagoruyko, S., 2020. End-to-end object detection with transformers, in: *European conference on computer vision*, Springer. pp. 213–229.
- [30] Cha, J., Chun, S., Lee, K., Cho, H.C., Park, S., Lee, Y., Park, S., 2021. Swad: Domain generalization by seeking flat minima. *Advances in Neural Information Processing Systems* 34, 22405–22418.
- [31] Chen, G., Peng, P., Ma, L., Li, J., Du, L., Tian, Y., 2021. Amplitude-phase recombination: Rethinking robustness of convolutional neural networks in frequency domain, in: *Proceedings of the IEEE/CVF International Conference on Computer Vision*, pp. 458–467.
- [32] Chen, G., Zhang, T., Lu, J., Zhou, J., 2019a. Deep meta metric learning, in: *Proc. IEEE Int. Conf. Comput. Vis.*, pp. 9547–9556.
- [33] Chen, P., Liao, B.B., Chen, G., Zhang, S., 2019b. Understanding and utilizing deep neural networks trained with noisy labels, in: *International Conference on Machine Learning*, PMLR. pp. 1062–1070.
- [34] Chen, Q., Liu, Y., Hu, Y., Self, A., Papageorgiou, A., Noble, J.A., 2020. Cross-device cross-anatomy adaptation network for ultrasound video analysis, in: *Medical Ultrasound, and Preterm, Perinatal and Paediatric Image Analysis: First International Workshop, ASMUS 2020, and 5th International Workshop, PIPPI 2020*,

- Held in Conjunction with MICCAI 2020, Lima, Peru, October 4-8, 2020, Proceedings 1, Springer. pp. 42–51.
- [35] Chen, X., He, K., 2021. Exploring simple siamese representation learning, in: Proceedings of the IEEE/CVF conference on computer vision and pattern recognition, pp. 15750–15758.
- [36] Choi, Y., Choi, M., Kim, M., Ha, J.W., Kim, S., Choo, J., 2018. Stargan: Unified generative adversarial networks for multi-domain image-to-image translation, in: Proceedings of the IEEE conference on computer vision and pattern recognition, pp. 8789–8797.
- [37] Choi, Y., Uh, Y., Yoo, J., Ha, J.W., 2020. Stargan v2: Diverse image synthesis for multiple domains, in: Proceedings of the IEEE/CVF conference on computer vision and pattern recognition, pp. 8188–8197.
- [38] Chowdhury, M.E., Rahman, T., Khandakar, A., Mazhar, R., Kadir, M.A., Mahbub, Z.B., Islam, K.R., Khan, M.S., Iqbal, A., Al Emadi, N., et al., 2020. Can ai help in screening viral and covid-19 pneumonia? *Ieee Access* 8, 132665–132676.
- [39] Chung, Y., Cho, J., Park, J., 2021. Domain-robust mitotic figure detection with style transfer, in: International Conference on Medical Image Computing and Computer-Assisted Intervention, Springer. pp. 23–31.
- [40] Codella, N.C., Gutman, D., Celebi, M.E., Helba, B., Marchetti, M.A., Dusza, S.W., Kallou, A., Liopyris, K., Mishra, N., Kittler, H., et al., 2018. Skin lesion analysis toward melanoma detection: A challenge at the 2017 international symposium on biomedical imaging (isbi), hosted by the international skin imaging collaboration (isic), in: 2018 IEEE 15th international symposium on biomedical imaging (ISBI 2018), IEEE. pp. 168–172.
- [41] Cohen, J., 1960. A coefficient of agreement for nominal scales. *Educational and psychological measurement* 20, 37–46.
- [42] Cohen, J.P., Hashir, M., Brooks, R., Bertrand, H., 2020. On the limits of cross-domain generalization in automated x-ray prediction, in: Medical Imaging with Deep Learning, PMLR. pp. 136–155.
- [43] Courtiol, P., Tramel, E.W., Sanselme, M., Wainrib, G., 2018. Classification and disease localization in histopathology using only global labels: A weakly-supervised approach. *arXiv preprint arXiv:1802.02212*.
- [44] Cubuk, E.D., Zoph, B., Shlens, J., Le, Q.V., 2020. Randaugment: Practical automated data augmentation with a reduced search space, in: Proceedings of the IEEE/CVF conference on computer vision and pattern recognition workshops, pp. 702–703.
- [45] De Fauw, J., Ledsam, J.R., Romera-Paredes, B., Nikolov, S., Tomasev, N., Blackwell, S., Askham, H., Glorot, X., O’Donoghue, B., Visentin, D., et al., 2018. Clinically applicable deep learning for diagnosis and referral in retinal disease. *Nature medicine* 24, 1342–1350.
- [46] Demner-Fushman, D., Kohli, M.D., Rosenman, M.B., Shooshan, S.E., Rodriguez, L., Antani, S., Thoma, G.R., McDonald, C.J., 2016. Preparing a collection of radiology examinations for distribution and retrieval. *Journal of the American Medical Informatics Association* 23, 304–310.
- [47] DeVries, T., Taylor, G.W., 2017. Improved regularization of convolutional neural networks with cutout. *arXiv preprint arXiv:1708.04552*.
- [48] Dexl, J., Benz, M., Bruns, V., Kuritcyn, P., Wittenberg, T., 2021. Mitodet: Simple and robust mitosis detection, in: International Conference on Medical Image Computing and Computer-Assisted Intervention, Springer. pp. 53–57.
- [49] Do, T., Nguyen, B.X., Tjiputra, E., Tran, M., Tran, Q.D., Nguyen, A., 2021. Multiple meta-model quantifying for medical visual question answering, in: Medical Image Computing and Computer Assisted Intervention–MICCAI 2021: 24th International Conference, Strasbourg, France, September 27–October 1, 2021, Proceedings, Part V 24, Springer. pp. 64–74.
- [50] Dou, Q., Coelho de Castro, D., Kamnitsas, K., Glocker, B., 2019. Domain generalization via model-agnostic learning of semantic features. *Adv. Neural Inf. Process. Syst.* 32.
- [51] Dunmon, J.A., Ratner, A.J., Saab, K., Khandwala, N., Markert, M., Sagreya, H., Goldman, R., Lee-Messer, C., Lungren, M.P., Rubin, D.L., et al., 2020. Cross-modal data programming enables rapid medical machine learning. *Patterns* 1.
- [52] Dutta, U.K., Harandi, M., Shekhar, C.C., 2021. Semi-supervised metric learning: A deep resurrection, in: Proceedings of the AAAI Conference on Artificial Intelligence, pp. 7279–7287.
- [53] Elbatel, M., Bornberg, C., Kattel, M., Almar, E., Marrocco, C., Bria, A., 2022. Seamless iterative semi-supervised correction of imperfect labels in microscopy images, in: MICCAI Workshop on Domain Adaptation and Representation Transfer, Springer. pp. 98–107.
- [54] Ellis, K.A., Bush, A.I., Darby, D., De Fazio, D., Foster, J., Hudson, P., Lautenschlager, N.T., Lenzo, N., Martins, R.N., Maruff, P., et al., 2009. The australian imaging, biomarkers and lifestyle (aibl) study of aging: methodology and baseline characteristics of 1112 individuals recruited for a longitudinal study of alzheimer’s disease. *Int. Psychogeriatr.* 21, 672–687.
- [55] Esteva, A., Kuprel, B., Novoa, R.A., Ko, J., Swetter, S.M., Blau, H.M., Thrun, S., 2017. Dermatologist-level classification of skin cancer with deep neural networks. *Nature* 542, 115–118.
- [56] Filiot, A., Ghermi, R., Olivier, A., Jacob, P., Fidon, L., Mac Kain, A., Saillard, C., Schiratti, J.B., 2023. Scaling self-supervised learning for histopathology with masked image modeling. *medRxiv*, 2023–07.
- [57] Finn, C., Abbeel, P., Levine, S., 2017. Model-agnostic meta-learning for fast adaptation of deep networks, in: International conference on machine learning, PMLR. pp. 1126–1135.
- [58] Gao, B.B., Xing, C., Xie, C.W., Wu, J., Geng, X., 2017. Deep label distribution learning with label ambiguity. *IEEE Transactions on Image Processing* 26, 2825–2838.
- [59] Garrucho, L., Kushibar, K., Jouide, S., Diaz, O., Igual, L., Lekadir, K., 2022. Domain generalization in deep learning based mass detection in mammography: A large-scale multi-center study. *Artificial Intelligence in Medicine* 132, 102386.
- [60] Geirhos, R., Rubisch, P., Michaelis, C., Bethge, M., Wichmann, F.A., Brendel, W., 2018. Imagenet-trained cnns are biased towards texture; increasing shape bias improves accuracy and robustness. *arXiv preprint arXiv:1811.12231*.
- [61] Geng, X., 2016. Label distribution learning. *IEEE Transactions on Knowledge and Data Engineering* 28, 1734–1748.
- [62] Goodfellow, I., Pouget-Abadie, J., Mirza, M., Xu, B., Warde-Farley, D., Ozair, S., Courville, A., Bengio, Y., 2014. Generative adversarial nets. *Advances in neural information processing systems* 27.
- [63] Gordon, M.L., Zhou, K., Patel, K., Hashimoto, T., Bernstein, M.S., 2021. The disagreement deconvolution: Bringing machine learning performance metrics in line with reality, in: Proceedings of the 2021 CHI Conference on Human Factors in Computing Systems, pp. 1–14.
- [64] Graham, B., 2015. Kaggle diabetic retinopathy detection competition report. University of Warwick 22, 17.
- [65] Graham, S., Minhas, F., Bilal, M., Ali, M., Tsang, Y.W., Eastwood, M., Wahab, N., Jahanifar, M., Hero, E., Dodd, K., et al., 2023. Screening of normal endoscopic large bowel biopsies with interpretable graph learning: a retrospective study. *Gut* 72, 1709–1721.
- [66] Grandvalet, Y., Bengio, Y., 2004. Semi-supervised learning by entropy minimization. *Advances in neural information processing systems* 17.
- [67] Guan, H., Liu, M., 2021. Domain adaptation for medical image analysis: a survey. *IEEE Transactions on Biomedical Engineering* 69, 1173–1185.
- [68] Guan, H., Yang, E., Yap, P.T., Shen, D., Liu, M., 2020. Attention-guided deep domain adaptation for brain dementia identification with multi-site neuroimaging data, in: MICCAI Workshop on Domain Adaptation and Representation Transfer, Springer. pp. 31–40.
- [69] Gulrajani, I., Lopez-Paz, D., 2020. In search of lost domain generalization. *arXiv preprint arXiv:2007.01434*.
- [70] Gunasinghe, H., McKelvie, J., Koay, A., Mayo, M., 2022. Domain generalisation for glaucoma detection in retinal images from unseen

- fundus cameras, in: Asian Conference on Intelligent Information and Database Systems, Springer. pp. 421–433.
- [71] Gündel, S., Setio, A.A., Ghesu, F.C., Grbic, S., Georgescu, B., Maier, A., Comaniciu, D., 2021. Robust classification from noisy labels: Integrating additional knowledge for chest radiography abnormality assessment. *Medical Image Analysis* 72, 102087.
- [72] Gurpinar, C., Takir, S., Bicer, E., Uluer, P., Arica, N., Kose, H., 2022. Contrastive learning based facial action unit detection in children with hearing impairment for a socially assistive robot platform. *Image and Vision Computing* 128, 104572.
- [73] Halling-Brown, M.D., Warren, L.M., Ward, D., Lewis, E., Mackenzie, A., Wallis, M.G., Wilkinson, L.S., Given-Wilson, R.M., McAvinchey, R., Young, K.C., 2020. Optimam mammography image database: a large-scale resource of mammography images and clinical data. *Radiology: Artificial Intelligence* 3, e200103.
- [74] He, K., Fan, H., Wu, Y., Xie, S., Girshick, R., 2020a. Momentum contrast for unsupervised visual representation learning, in: Proceedings of the IEEE/CVF conference on computer vision and pattern recognition, pp. 9729–9738.
- [75] He, L., Tiwari, P., Lv, C., Wu, W., Guo, L., 2022. Reducing noisy annotations for depression estimation from facial images. *Neural Networks* 153, 120–129.
- [76] He, X., Zhang, Y., Mou, L., Xing, E., Xie, P., 2020b. Pathvqa: 30000+ questions for medical visual question answering. *arXiv preprint arXiv:2003.10286*.
- [77] Hegde, N., Hipp, J.D., Liu, Y., Emmert-Buck, M., Reif, E., Smilkov, D., Terry, M., Cai, C.J., Amin, M.B., Mermel, C.H., et al., 2019. Similar image search for histopathology: Smily. *NPJ digital medicine* 2, 56.
- [78] Hermoza, R., Maicas, G., Nascimento, J.C., Carneiro, G., 2022. Censor-aware semi-supervised learning for survival time prediction from medical images, in: International Conference on Medical Image Computing and Computer-Assisted Intervention, Springer. pp. 213–222.
- [79] Hong, W.Y., Kao, C.L., Kuo, Y.H., Wang, J.R., Chang, W.L., Shih, C.S., 2020. Cholecseg8k: a semantic segmentation dataset for laparoscopic cholecystectomy based on cholec80. *arXiv preprint arXiv:2012.12453*.
- [80] Hu, J., Wang, H., Wu, G., Cao, Z., Mou, L., Zhao, Y., Zhang, J., 2022. Multi-scale interactive network with artery/vein discriminator for retinal vessel classification. *IEEE Journal of Biomedical and Health Informatics* 26, 3896–3905.
- [81] Hu, K., Huang, Y., Huang, W., Tan, H., Chen, Z., Zhong, Z., Li, X., Zhang, Y., Gao, X., 2021. Deep supervised learning using self-adaptive auxiliary loss for covid-19 diagnosis from imbalanced ct images. *Neurocomputing* 458, 232–245.
- [82] Hu, Q., Abramoff, M.D., Garvin, M.K., 2013. Automated separation of binary overlapping trees in low-contrast color retinal images, in: Medical Image Computing and Computer-Assisted Intervention–MICCAI 2013: 16th International Conference, Nagoya, Japan, September 22–26, 2013, Proceedings, Part II 16, Springer. pp. 436–443.
- [83] Huang, X., Belongie, S., 2017. Arbitrary style transfer in real-time with adaptive instance normalization, in: Proceedings of the IEEE international conference on computer vision, pp. 1501–1510.
- [84] Hupkes, D., Giulianelli, M., Dankers, V., Artetxe, M., Elazar, Y., Pimentel, T., Christodoulopoulos, C., Lasri, K., Saphra, N., Sinclair, A., et al., 2023. A taxonomy and review of generalization research in nlp. *Nature Machine Intelligence* 5, 1161–1174.
- [85] Irvin, J., Rajpurkar, P., Ko, M., Yu, Y., Ciurea-Ilcus, S., Chute, C., Marklund, H., Haghighi, B., Ball, R., Shpanskaya, K., et al., 2019. Chexpert: A large chest radiograph dataset with uncertainty labels and expert comparison, in: Proceedings of the AAAI conference on artificial intelligence, pp. 590–597.
- [86] Izmailov, P., Podoprikin, D., Gariipov, T., Vetrov, D., Wilson, A.G., 2018. Averaging weights leads to wider optima and better generalization. *arXiv preprint arXiv:1803.05407*.
- [87] Jack Jr, C.R., Bernstein, M.A., Fox, N.C., Thompson, P., Alexander, G., Harvey, D., Borowski, B., Britson, P.J., L. Whitwell, J., Ward, C., et al., 2008. The alzheimer’s disease neuroimaging initiative (adni): Mri methods. *Journal of Magnetic Resonance Imaging: An Official Journal of the International Society for Magnetic Resonance in Medicine* 27, 685–691.
- [88] Janizek, J.D., Erion, G., DeGrave, A.J., Lee, S.I., 2020. An adversarial approach for the robust classification of pneumonia from chest radiographs, in: Proceedings of the ACM conference on health, inference, and learning, pp. 69–79.
- [89] Javed, S., Mahmood, A., Fraz, M.M., Koohbanani, N.A., Benes, K., Tsang, Y.W., Hewitt, K., Epstein, D., Snead, D., Rajpoot, N., 2020. Cellular community detection for tissue phenotyping in colorectal cancer histology images. *Medical image analysis* 63, 101696.
- [90] Johnson, A.E., Pollard, T.J., Berkowitz, S.J., Greenbaum, N.R., Lungren, M.P., Deng, C.y., Mark, R.G., Horng, S., 2019. Mimic-cxr, a de-identified publicly available database of chest radiographs with free-text reports. *Scientific data* 6, 317.
- [91] Kaddour, J., Lynch, A., Liu, Q., Kusner, M.J., Silva, R., 2022. Causal machine learning: A survey and open problems. *arXiv preprint arXiv:2206.15475*.
- [92] Karagyris, A., Umeton, R., Sheller, M.J., Aristizabal, A., George, J., Wuest, A., Pati, S., Kassem, H., Zenk, M., Baid, U., et al., 2023. Federated benchmarking of medical artificial intelligence with medperf. *Nature Machine Intelligence* 5, 799–810.
- [93] Karimi, D., Dou, H., Warfield, S.K., Gholipour, A., 2020. Deep learning with noisy labels: Exploring techniques and remedies in medical image analysis. *Medical image analysis* 65, 101759.
- [94] Kather, J.N., Krisam, J., Charoentong, P., Luedde, T., Herpel, E., Weis, C.A., Gaiser, T., Marx, A., Valous, N.A., Ferber, D., et al., 2019. Predicting survival from colorectal cancer histology slides using deep learning: A retrospective multicenter study. *PLoS medicine* 16, e1002730.
- [95] Kather, J.N., Weis, C.A., Bianconi, F., Melchers, S.M., Schad, L.R., Gaiser, T., Marx, A., Zöllner, F.G., 2016. Multi-class texture analysis in colorectal cancer histology. *Scientific reports* 6, 27988.
- [96] Kawahara, J., Daneshvar, S., Argenziano, G., Hamarneh, G., 2018. Seven-point checklist and skin lesion classification using multitask multimodal neural nets. *IEEE journal of biomedical and health informatics* 23, 538–546.
- [97] Kendall, A., Gal, Y., 2017. What uncertainties do we need in bayesian deep learning for computer vision? *Advances in neural information processing systems* 30.
- [98] Khosla, P., Teterwak, P., Wang, C., Sarna, A., Tian, Y., Isola, P., Maschinot, A., Liu, C., Krishnan, D., 2020. Supervised contrastive learning. *Advances in neural information processing systems* 33, 18661–18673.
- [99] Kilim, O., Olar, A., Joó, T., Palicz, T., Pollner, P., Csabai, I., 2022. Physical imaging parameter variation drives domain shift. *Scientific Reports* 12, 21302.
- [100] Koh, P.W., Sagawa, S., Marklund, H., Xie, S.M., Zhang, M., Balsubramani, A., Hu, W., Yasunaga, M., Phillips, R.L., Gao, I., et al., 2021. Wilds: A benchmark of in-the-wild distribution shifts, in: International Conference on Machine Learning, PMLR. pp. 5637–5664.
- [101] Kumari, S., Singh, P., 2023. Deep learning for unsupervised domain adaptation in medical imaging: Recent advancements and future perspectives. *Computers in Biology and Medicine*, 107912.
- [102] Kurian, N.C., Varsha, S., Bajpai, A., Patel, S., Sethi, A., 2022. Improved histology image classification under label noise via feature aggregating memory banks, in: 2022 IEEE 19th International Symposium on Biomedical Imaging (ISBI), IEEE. pp. 1–5.
- [103] Lafarge, M.W., Koelzer, V.H., 2021. Rotation invariance and extensive data augmentation: A strategy for the mitosis domain generalization (midog) challenge, in: International Conference on Medical Image Computing and Computer-Assisted Intervention, Springer. pp. 62–67.

- [104] Lai, J., Ahmed, F., Vijay, S., Jaroensri, T., Loo, J., Vyawahare, S., Agarwal, S., Jamil, F., Matias, Y., Corrado, G.S., et al., 2023. Domain-specific optimization and diverse evaluation of self-supervised models for histopathology. arXiv preprint arXiv:2310.13259 .
- [105] Laine, S., Aila, T., 2016. Temporal ensembling for semi-supervised learning. arXiv preprint arXiv:1610.02242 .
- [106] Lau, J.J., Gayen, S., Ben Abacha, A., Demner-Fushman, D., 2018. A dataset of clinically generated visual questions and answers about radiology images. *Scientific data* 5, 1–10.
- [107] Le, H.S., Akmeliawati, R., Carneiro, G., 2021. Combining data augmentation and domain distance minimisation to reduce domain generalisation error, in: 2021 Digital Image Computing: Techniques and Applications (DICTA), IEEE. pp. 01–08.
- [108] Le-Khac, P.H., Healy, G., Smeaton, A.F., 2020. Contrastive representation learning: A framework and review. *Ieee Access* 8, 193907–193934.
- [109] Lee, J., Lee, G., 2020. Model uncertainty for unsupervised domain adaptation, in: 2020 IEEE International Conference on Image Processing (ICIP), IEEE. pp. 1841–1845.
- [110] Lee, J., Song, S.J., 2021. Suprad: A robust feature extractor better recognizes low-prevalent retinal diseases, in: 2021 20th IEEE International Conference on Machine Learning and Applications (ICMLA), IEEE. pp. 534–540.
- [111] Li, C., Lin, X., Mao, Y., Lin, W., Qi, Q., Ding, X., Huang, Y., Liang, D., Yu, Y., 2022a. Domain generalization on medical imaging classification using episodic training with task augmentation. *Computers in biology and medicine* 141, 105144.
- [112] Li, H., Wang, Y., Wan, R., Wang, S., Li, T.Q., Kot, A., 2020. Domain generalization for medical imaging classification with linear-dependency regularization. *Advances in neural information processing systems* 33, 3118–3129.
- [113] Li, J., Yang, S., Huang, X., Da, Q., Yang, X., Hu, Z., Duan, Q., Wang, C., Li, H., 2019. Signet ring cell detection with a semi-supervised learning framework, in: Information Processing in Medical Imaging: 26th International Conference, IPMI 2019, Hong Kong, China, June 2–7, 2019, Proceedings 26, Springer. pp. 842–854.
- [114] Li, M., Xu, J., 2021. Bootstrap knowledge distillation for chest x-ray image classification with noisy labelling, in: Image and Graphics: 11th International Conference, ICIG 2021, Haikou, China, August 6–8, 2021, Proceedings, Part II 11, Springer. pp. 704–715.
- [115] Li, Y., He, N., Huang, Y., 2022b. Single domain generalization via spontaneous amplitude spectrum diversification, in: MICCAI Workshop on Resource-Efficient Medical Image Analysis, Springer. pp. 32–41.
- [116] Li, Y., Wang, N., Shi, J., Liu, J., Hou, X., 2016. Revisiting batch normalization for practical domain adaptation. arXiv preprint arXiv:1603.04779 .
- [117] Li, Y., Wang, X., Zeng, R., Donta, P.K., Murturi, I., Huang, M., Dustdar, S., 2023. Federated domain generalization: A survey. arXiv preprint arXiv:2306.01334 .
- [118] Li, Z., Cui, Z., Wang, S., Qi, Y., Ouyang, X., Chen, Q., Yang, Y., Xue, Z., Shen, D., Cheng, J.Z., 2021. Domain generalization for mammography detection via multi-style and multi-view contrastive learning, in: Medical Image Computing and Computer Assisted Intervention–MICCAI 2021: 24th International Conference, Strasbourg, France, September 27–October 1, 2021, Proceedings, Part VII 24, Springer. pp. 98–108.
- [119] Lin, Z., Shi, D., Zhang, D., Shang, X., He, M., Ge, Z., 2022. Camera adaptation for fundus-image-based cvd risk estimation, in: International Conference on Medical Image Computing and Computer-Assisted Intervention, Springer. pp. 593–603.
- [120] Linder, N., Konsti, J., Turkki, R., Rahtu, E., Lundin, M., Nordling, S., Haglund, C., Ahonen, T., Pietikäinen, M., Lundin, J., 2012. Identification of tumor epithelium and stroma in tissue microarrays using texture analysis. *Diagnostic pathology* 7, 1–11.
- [121] Liu, F., Chen, Y., Tian, Y., Liu, Y., Wang, C., Belagiannis, V., Carneiro, G., 2022. Nvum: Non-volatile unbiased memory for robust medical image classification, in: International Conference on Medical Image Computing and Computer-Assisted Intervention, Springer. pp. 544–553.
- [122] Liu, J., Li, R., Sun, C., 2021. Co-correcting: noise-tolerant medical image classification via mutual label correction. *IEEE Transactions on Medical Imaging* 40, 3580–3592.
- [123] Long, X., Cheng, Y., Mu, X., Liu, L., Liu, J., 2021. Domain adaptive cascade r-cnn for mitosis domain generalization (midog) challenge, in: International Conference on Medical Image Computing and Computer-Assisted Intervention, Springer. pp. 73–76.
- [124] Lopez, M.G., Posada, N., Moura, D.C., Pollán, R.R., Valiente, J.M.F., Ortega, C.S., Solar, M., Diaz-Herrero, G., Ramos, I., Loureiro, J., et al., 2012. Bcdr: a breast cancer digital repository, in: 15th International conference on experimental mechanics, pp. 113–120.
- [125] Lovchinsky, I., Daks, A., Malkin, I., Samangouei, P., Saeedi, A., Liu, Y., Sankaranarayanan, S., Gafner, T., Sternlieb, B., Maher, P., et al., 2019. Discrepancy ratio: Evaluating model performance when even experts disagree on the truth, in: International Conference on Learning Representations.
- [126] Lucieri, A., Schmeisser, F., Balada, C.P., Siddiqui, S.A., Dengel, A., Ahmed, S., 2022. Revisiting the shape-bias of deep learning for dermoscopic skin lesion classification, in: Annual Conference on Medical Image Understanding and Analysis, Springer. pp. 46–61.
- [127] Luo, H., Xu, G., Li, C., He, L., Luo, L., Wang, Z., Jing, B., Deng, Y., Jin, Y., Li, Y., et al., 2019. Real-time artificial intelligence for detection of upper gastrointestinal cancer by endoscopy: a multicentre, case-control, diagnostic study. *Lancet Oncol.* 20, 1645–1654.
- [128] Maier-Hein, L., Wagner, M., Ross, T., Reinke, A., Bodenstedt, S., Full, P.M., Hempe, H., Mindroc-Filimon, D., Scholz, P., Tran, T.N., et al., 2021. Heidelberg colorectal data set for surgical data science in the sensor operating room. *Scientific data* 8, 101.
- [129] Mårtensson, G., Ferreira, D., Granberg, T., Cavallin, L., Oppedal, K., Padovani, A., Rektorova, I., Bonanni, L., Pardini, M., Kramberger, M.G., et al., 2020. The reliability of a deep learning model in clinical out-of-distribution mri data: a multicohort study. *Medical Image Analysis* 66, 101714.
- [130] Matta, S., Hassine, M.B., Lecat, C., Borderie, L., Le Guilcher, A., Massin, P., Cochener, B., Lamard, M., Quellec, G., 2023a. Federated learning for diabetic retinopathy detection in a multi-center fundus screening network, in: 2023 45th Annual International Conference of the IEEE Engineering in Medicine & Biology Society (EMBC), IEEE. pp. 1–4.
- [131] Matta, S., Lamard, M., Conze, P.H., Le Guilcher, A., Lecat, C., Carette, R., Basset, F., Massin, P., Rottier, J.B., Cochener, B., et al., 2023b. Towards population-independent, multi-disease detection in fundus photographs. *Scientific Reports* 13, 11493.
- [132] Meng, Q., Rueckert, D., Kainz, B., 2020. Unsupervised cross-domain image classification by distance metric guided feature alignment, in: Medical Ultrasound, and Preterm, Perinatal and Paediatric Image Analysis: First International Workshop, ASMUS 2020, and 5th International Workshop, PIPPI 2020, Held in Conjunction with MICCAI 2020, Lima, Peru, October 4–8, 2020, Proceedings 1, Springer. pp. 146–157.
- [133] Misra, I., Maaten, L.v.d., 2020. Self-supervised learning of pretext-invariant representations, in: Proceedings of the IEEE/CVF conference on computer vision and pattern recognition, pp. 6707–6717.
- [134] Miyato, T., Maeda, S.i., Koyama, M., Ishii, S., 2018. Virtual adversarial training: a regularization method for supervised and semi-supervised learning. *IEEE transactions on pattern analysis and machine intelligence* 41, 1979–1993.
- [135] Moreira, I.C., Amaral, I., Domingues, I., Cardoso, A., Cardoso, M.J., Cardoso, J.S., 2012. Inbreast: toward a full-field digital mammographic database. *Academic radiology* 19, 236–248.
- [136] Moreno-Torres, J.G., Raeder, T., Alaiz-Rodríguez, R., Chawla, N.V., Herrera, F., 2012. A unifying view on dataset shift in classification. *Pattern recognition* 45, 521–530.

- [137] Müller, S.G., Hutter, F., 2021. Trivialaugument: Tuning-free yet state-of-the-art data augmentation, in: Proceedings of the IEEE/CVF international conference on computer vision, pp. 774–782.
- [138] Niemeijer, M., Loog, M., Abramoff, M.D., Viergever, M.A., Prokop, M., van Ginneken, B., 2010. On combining computer-aided detection systems. *IEEE Transactions on Medical Imaging* 30, 215–223.
- [139] Northcutt, C., Jiang, L., Chuang, I., 2021. Confident learning: Estimating uncertainty in dataset labels. *Journal of Artificial Intelligence Research* 70, 1373–1411.
- [140] Nyúl, L.G., Udupa, J.K., Zhang, X., 2000. New variants of a method of mri scale standardization. *IEEE transactions on medical imaging* 19, 143–150.
- [141] Oord, A.v.d., Li, Y., Vinyals, O., 2018. Representation learning with contrastive predictive coding. *arXiv preprint arXiv:1807.03748*.
- [142] Patrini, G., Rozza, A., Krishna Menon, A., Nock, R., Qu, L., 2017. Making deep neural networks robust to label noise: A loss correction approach, in: Proceedings of the IEEE conference on computer vision and pattern recognition, pp. 1944–1952.
- [143] Paul, A., Shen, T.C., Lee, S., Balachandar, N., Peng, Y., Lu, Z., Summers, R.M., 2021. Generalized zero-shot chest x-ray diagnosis through trait-guided multi-view semantic embedding with self-training. *IEEE Transactions on Medical Imaging* 40, 2642–2655.
- [144] Pawlowski, N., Coelho de Castro, D., Glocker, B., 2020. Deep structural causal models for tractable counterfactual inference. *Advances in Neural Information Processing Systems* 33, 857–869.
- [145] Peng, T., Zhu, C., Luo, Y., Liu, J., Wang, Y., Jin, M., 2020. Noise robust learning with hard example aware for pathological image classification, in: 2020 IEEE 6th International Conference on Computer and Communications (ICCC), IEEE. pp. 1903–1907.
- [146] Philipp, M., Alperovich, A., Gutt-Will, M., Mathis, A., Saur, S., Raabe, A., Mathis-Ullrich, F., 2022. Dynamic cnns using uncertainty to overcome domain generalization for surgical instrument localization, in: Proceedings of the IEEE/CVF Winter Conference on Applications of Computer Vision, pp. 3612–3621.
- [147] Pooch, E.H., Ballester, P., Barros, R.C., 2020. Can we trust deep learning based diagnosis? the impact of domain shift in chest radiograph classification, in: Thoracic Image Analysis: Second International Workshop, TIA 2020, Held in Conjunction with MICCAI 2020, Lima, Peru, October 8, 2020, Proceedings 2, Springer. pp. 74–83.
- [148] Qiu, L., Zhao, L., Hou, R., Zhao, W., Zhang, S., Lin, Z., Teng, H., Zhao, J., 2023. Hierarchical multimodal fusion framework based on noisy label learning and attention mechanism for cancer classification with pathology and genomic features. *Computerized Medical Imaging and Graphics* 104, 102176.
- [149] Quellec, G., Lamard, M., Conze, P.H., Massin, P., Cochener, B., 2020. Automatic detection of rare pathologies in fundus photographs using few-shot learning. *Medical image analysis* 61, 101660.
- [150] Rahman, T., Khandakar, A., Qiblawey, Y., Tahir, A., Kiranyaz, S., Kashem, S.B.A., Islam, M.T., Al Maadeed, S., Zughhaier, S.M., Khan, M.S., et al., 2021. Exploring the effect of image enhancement techniques on covid-19 detection using chest x-ray images. *Computers in biology and medicine* 132, 104319.
- [151] Raipuria, G., Shrivastava, A., Singhal, N., 2022. Stain-aglr: Stain agnostic learning for computational histopathology using domain consistency and stain regeneration loss, in: MICCAI Workshop on Domain Adaptation and Representation Transfer, Springer. pp. 33–44.
- [152] Rame, A., Dancette, C., Cord, M., 2022. Fishr: Invariant gradient variances for out-of-distribution generalization, in: International Conference on Machine Learning, PMLR. pp. 18347–18377.
- [153] Rathod, S.R., Khanuja, H.K., 2021. Automatic segmentation of covid-19 pneumonia lesions and its classification from ct images: A survey, in: 2021 International Conference on Intelligent Technologies (CONIT), IEEE. pp. 1–8.
- [154] Ratner, A.J., De Sa, C.M., Wu, S., Selsam, D., Ré, C., 2016. Data programming: Creating large training sets, quickly. *Advances in neural information processing systems* 29.
- [155] Razavi, S., Dambandkhameneh, F., Androustos, D., Done, S., Khademi, A., 2021. Cascade r-cnn for midog challenge, in: International Conference on Medical Image Computing and Computer-Assisted Intervention, Springer. pp. 81–85.
- [156] Reinhard, E., Adhikhmin, M., Gooch, B., Shirley, P., 2001. Color transfer between images. *IEEE Computer graphics and applications* 21, 34–41.
- [157] Reiter, W., 2023. Domain generalization improves end-to-end object detection for real-time surgical tool detection. *International Journal of Computer Assisted Radiology and Surgery* 18, 939–944.
- [158] Ros, G., Stent, S., Alcantarilla, P.F., Watanabe, T., 2016. Training constrained deconvolutional networks for road scene semantic segmentation. *arXiv preprint arXiv:1604.01545*.
- [159] Ross, A.S., Hughes, M.C., Doshi-Velez, F., 2017. Right for the right reasons: Training differentiable models by constraining their explanations. *arXiv preprint arXiv:1703.03717*.
- [160] Sagawa, S., Koh, P.W., Hashimoto, T.B., Liang, P., 2019. Distributionally robust neural networks for group shifts: On the importance of regularization for worst-case generalization. *arXiv preprint arXiv:1911.08731*.
- [161] Saito, K., Kim, D., Sclaroff, S., Darrell, T., Saenko, K., 2019. Semi-supervised domain adaptation via minimax entropy, in: Proceedings of the IEEE/CVF international conference on computer vision, pp. 8050–8058.
- [162] Samala, R.K., Chan, H.P., Hadjiiski, L.M., Helvie, M.A., Richter, C.D., 2020. Generalization error analysis for deep convolutional neural network with transfer learning in breast cancer diagnosis. *Physics in Medicine & Biology* 65, 105002.
- [163] Scalbert, M., Vakalopoulou, M., Couzinié-Devy, F., 2022. Test-time image-to-image translation ensembling improves out-of-distribution generalization in histopathology, in: International Conference on Medical Image Computing and Computer-Assisted Intervention, Springer. pp. 120–129.
- [164] Schoeffmann, K., Husslein, H., Kletz, S., Petscharnig, S., Muenzer, B., Beecks, C., 2018a. Video retrieval in laparoscopic video recordings with dynamic content descriptors. *Multimedia Tools and Applications* 77, 16813–16832.
- [165] Schoeffmann, K., Taschwer, M., Sarny, S., Münzer, B., Primus, M.J., Putzgruber, D., 2018b. Cataract-101: video dataset of 101 cataract surgeries, in: Proceedings of the 9th ACM multimedia systems conference, pp. 421–425.
- [166] Seenivasan, L., Islam, M., Ng, C.F., Lim, C.M., Ren, H., 2022. Biomimetic incremental domain generalization with a graph network for surgical scene understanding. *Biomimetics* 7, 68.
- [167] Seenivasan, L., Islam, M., Xu, M., Lim, C.M., Ren, H., 2023. Task-aware asynchronous multi-task model with class incremental contrastive learning for surgical scene understanding. *International Journal of Computer Assisted Radiology and Surgery* , 1–8.
- [168] Seibold, C., Reiß, S., Sarfraz, M.S., Stiefelhagen, R., Kleesiek, J., 2022. Breaking with fixed set pathology recognition through report-guided contrastive training, in: International Conference on Medical Image Computing and Computer-Assisted Intervention, Springer. pp. 690–700.
- [169] Setio, A.A.A., Traverso, A., De Bel, T., Berens, M.S., Van Den Bogaard, C., Cerello, P., Chen, H., Dou, Q., Fantacci, M.E., Geurts, B., et al., 2017. Validation, comparison, and combination of algorithms for automatic detection of pulmonary nodules in computed tomography images: the luna16 challenge. *Medical image analysis* 42, 1–13.
- [170] Shankar, S., Piratla, V., Chakrabarti, S., Chaudhuri, S., Jyothi, P., Sarawagi, S., 2018. Generalizing across domains via cross-gradient training. *arXiv preprint arXiv:1804.10745*.
- [171] Shen, Y., Zhou, Y., Yu, L., 2022. Cd2-pfed: Cyclic distillation-guided channel decoupling for model personalization in federated learning, in: Proceedings of the IEEE/CVF Conference on Computer Vision and Pattern Recognition, pp. 10041–10050.
- [172] Shen, Z., Liu, J., He, Y., Zhang, X., Xu, R., Yu, H., Cui, P., 2021. Towards out-of-distribution generalization: A survey. *arXiv preprint arXiv:2108.13624*.

- [173] Sheth, P., Liu, H., 2023. Causal domain generalization, in: *Machine Learning for Causal Inference*. Springer, pp. 161–185.
- [174] Sheth, P., Moraffah, R., Candan, K.S., Raglin, A., Liu, H., 2022. Domain generalization—a causal perspective. *arXiv preprint arXiv:2209.15177*.
- [175] Shi, X., Su, H., Xing, F., Liang, Y., Qu, G., Yang, L., 2020. Graph temporal ensembling based semi-supervised convolutional neural network with noisy labels for histopathology image analysis. *Medical image analysis* 60, 101624.
- [176] Shi, Y., Seely, J., Torr, P.H., Siddharth, N., Hannun, A., Usunier, N., Synnaeve, G., 2021. Gradient matching for domain generalization. *arXiv preprint arXiv:2104.09937*.
- [177] Shu, Y., Cao, Z., Wang, C., Wang, J., Long, M., 2021. Open domain generalization with domain-augmented meta-learning, in: *Proceedings of the IEEE/CVF conference on computer vision and pattern recognition*, pp. 9624–9633.
- [178] Sikaroudi, M., Rahnamayan, S., Tizhoosh, H.R., 2022. Hospital-agnostic image representation learning in digital pathology, in: *2022 44th Annual International Conference of the IEEE Engineering in Medicine & Biology Society (EMBC)*, IEEE. pp. 3055–3058.
- [179] Silva-Rodríguez, J., Colomer, A., Sales, M.A., Molina, R., Naranjo, V., 2020. Going deeper through the gleason scoring scale: An automatic end-to-end system for histology prostate grading and cribriform pattern detection. *Computer methods and programs in biomedicine* 195, 105637.
- [180] Sim, J., Wright, C.C., 2005. The kappa statistic in reliability studies: use, interpretation, and sample size requirements. *Physical therapy* 85, 257–268.
- [181] Simpson, B., Dutil, F., Bengio, Y., Cohen, J.P., 2019. Grad-mask: Reduce overfitting by regularizing saliency. *arXiv preprint arXiv:1904.07478*.
- [182] Son, J., Kim, J., Kong, S.T., Jung, K.H., 2021. Leveraging the generalization ability of deep convolutional neural networks for improving classifiers for color fundus photographs. *Applied Sciences* 11, 591.
- [183] Stacke, K., Eilertsen, G., Unger, J., Lundström, C., 2019. A closer look at domain shift for deep learning in histopathology. *arXiv preprint arXiv:1909.11575* 10.
- [184] Stacke, K., Eilertsen, G., Unger, J., Lundström, C., 2020. Measuring domain shift for deep learning in histopathology. *IEEE journal of biomedical and health informatics* 25, 325–336.
- [185] Sudlow, C., Gallacher, J., Allen, N., Beral, V., Burton, P., Danesh, J., Downey, P., Elliott, P., Green, J., Landray, M., et al., 2015. Uk biobank: an open access resource for identifying the causes of a wide range of complex diseases of middle and old age. *PLoS medicine* 12, e1001779.
- [186] Sun, B., Saenko, K., 2016. Deep coral: Correlation alignment for deep domain adaptation, in: *Computer Vision—ECCV 2016 Workshops: Amsterdam, The Netherlands, October 8–10 and 15–16, 2016, Proceedings, Part III* 14, Springer. pp. 443–450.
- [187] Sun, W., Wu, D., Luo, Y., Liu, L., Zhang, H., Wu, S., Zhang, Y., Wang, C., Zheng, H., Shen, J., et al., 2022. A fully deep learning paradigm for pneumoconiosis staging on chest radiographs. *IEEE Journal of Biomedical and Health Informatics* 26, 5154–5164.
- [188] Team, N.L.S.T.R., 2011a. The national lung screening trial: overview and study design. *Radiology* 258, 243–253.
- [189] Team, N.L.S.T.R., 2011b. Reduced lung-cancer mortality with low-dose computed tomographic screening. *New England Journal of Medicine* 365, 395–409.
- [190] Terrail, J.O.d., Ayed, S.S., Cyffers, E., Grimberg, F., He, C., Loeb, R., Mangold, P., Marchand, T., Marfoq, O., Mushtaq, E., et al., 2022. Flamby: Datasets and benchmarks for cross-silo federated learning in realistic healthcare settings. *arXiv preprint arXiv:2210.04620*.
- [191] Thagaard, J., Hauberg, S., van der Vegt, B., Ebstrup, T., Hansen, J.D., Dahl, A.B., 2020. Can you trust predictive uncertainty under real dataset shifts in digital pathology?, in: *Medical Image Computing and Computer Assisted Intervention—MICCAI 2020: 23rd International Conference, Lima, Peru, October 4–8, 2020, Proceedings, Part I* 23, Springer. pp. 824–833.
- [192] Tian, Y., Sun, C., Poole, B., Krishnan, D., Schmid, C., Isola, P., 2020. What makes for good views for contrastive learning? *Advances in neural information processing systems* 33, 6827–6839.
- [193] Tschandl, P., Rosendahl, C., Kittler, H., 2018. The ham10000 dataset, a large collection of multi-source dermatoscopic images of common pigmented skin lesions. *Scientific data* 5, 1–9.
- [194] Vahadane, A., Peng, T., Albarqouni, S., Baust, M., Steiger, K., Schlitter, A.M., Sethi, A., Esposito, I., Navab, N., 2015. Structure-preserved color normalization for histological images, in: *2015 IEEE 12th international symposium on biomedical imaging (ISBI)*, IEEE. pp. 1012–1015.
- [195] Van Woudenberg, N., Jafari, M., Abolmaesumi, P., Tsang, T., 2022. Differential learning from sparse and noisy labels for robust detection of clinical landmarks in echo cine series, in: *Simplifying Medical Ultrasound: Third International Workshop, ASMUS 2022, Held in Conjunction with MICCAI 2022, Singapore, September 18, 2022, Proceedings*, Springer Nature. p. 44.
- [196] Veeling, B.S., Linmans, J., Winkens, J., Cohen, T., Welling, M., 2018. Rotation equivariant cnns for digital pathology, in: *Medical Image Computing and Computer Assisted Intervention—MICCAI 2018: 21st International Conference, Granada, Spain, September 16–20, 2018, Proceedings, Part II* 11, Springer. pp. 210–218.
- [197] Verenich, E., Velasquez, A., Khan, N., Hussain, F., 2020. Improving explainability of image classification in scenarios with class overlap: application to covid-19 and pneumonia, in: *2020 19th IEEE International Conference on Machine Learning and Applications (ICMLA)*, IEEE. pp. 1402–1409.
- [198] Vindas, Y., Guépié, B.K., Almar, M., Roux, E., Delachartre, P., 2022. Semi-automatic data annotation based on feature-space projection and local quality metrics: An application to cerebral emboli characterization. *Medical Image Analysis* 79, 102437.
- [199] Vinyals, O., Blundell, C., Lillicrap, T., Wierstra, D., et al., 2016. Matching networks for one shot learning. *Advances in neural information processing systems* 29.
- [200] Viviano, J.D., Simpson, B., Dutil, F., Bengio, Y., Cohen, J.P., 2019. Saliency is a possible red herring when diagnosing poor generalization. *arXiv preprint arXiv:1910.00199*.
- [201] Vlonizos, A., Rueckert, D., Kainz, B., 2022. A review of causality for learning algorithms in medical image analysis. *arXiv preprint arXiv:2206.05498*.
- [202] Vuong, T.T.L., Vu, Q.D., Jahanifar, M., Graham, S., Kwak, J.T., Rajpoot, N., 2022. Impash: A novel domain-shift resistant representation for colorectal cancer tissue classification, in: *European Conference on Computer Vision*, Springer. pp. 543–555.
- [203] Wang, H., Xia, Y., 2023. Domain-ensemble learning with cross-domain mixup for thoracic disease classification in unseen domains. *Biomedical Signal Processing and Control* 81, 104488.
- [204] Wang, J., Lan, C., Liu, C., Ouyang, Y., Qin, T., Lu, W., Chen, Y., Zeng, W., Yu, P., 2022a. Generalizing to unseen domains: A survey on domain generalization. *IEEE Transactions on Knowledge and Data Engineering*.
- [205] Wang, R., Chaudhari, P., Davatzikos, C., 2021. Harmonization with flow-based causal inference, in: *Medical Image Computing and Computer Assisted Intervention—MICCAI 2021: 24th International Conference, Strasbourg, France, September 27–October 1, 2021, Proceedings, Part III* 24, Springer. pp. 181–190.
- [206] Wang, R., Chaudhari, P., Davatzikos, C., 2022b. Embracing the disharmony in medical imaging: A simple and effective framework for domain adaptation. *Medical image analysis* 76, 102309.
- [207] Wang, X., Peng, Y., Lu, L., Lu, Z., Bagheri, M., Summers, R.M., 2017. Chestx-ray8: Hospital-scale chest x-ray database and benchmarks on weakly-supervised classification and localization of common thorax diseases, in: *Proceedings of the IEEE conference on computer vision and pattern recognition*, pp. 2097–2106.
- [208] Wilkinson, C.P., Ferris III, F.L., Klein, R.E., Lee, P.P., Agardh, C.D., Davis, M., Dills, D., Kampik, A., Pararajasegaram, R., Verdaguer, J.T., et al., 2003. Proposed international clinical diabetic retinopathy and diabetic macular edema disease severity scales. *Ophthalmology*

- 110, 1677–1682.
- [209] Wilm, F., Marzahl, C., Breininger, K., Aubreville, M., 2021. Domain adversarial retinanet as a reference algorithm for the mitosis domain generalization challenge, in: International Conference on Medical Image Computing and Computer-Assisted Intervention, Springer. pp. 5–13.
- [210] Xiang, J., Wang, X., Wang, X., Zhang, J., Yang, S., Yang, W., Han, X., Liu, Y., 2023. Automatic diagnosis and grading of prostate cancer with weakly supervised learning on whole slide images. *Computers in Biology and Medicine* 152, 106340.
- [211] Xie, M., Li, S., Yuan, L., Liu, C., Dai, Z., 2024. Evolving standardization for continual domain generalization over temporal drift. *Advances in Neural Information Processing Systems* 36.
- [212] Xiong, J., He, A.W., Fu, M., Hu, X., Zhang, Y., Liu, C., Zhao, X., Ge, Z., 2020. Improve unseen domain generalization via enhanced local color transformation, in: Medical Image Computing and Computer Assisted Intervention–MICCAI 2020: 23rd International Conference, Lima, Peru, October 4–8, 2020, Proceedings, Part II 23, Springer. pp. 433–443.
- [213] Xu, D., Chen, R., 2022. Meta-learning for decoding neural activity data with noisy labels. *Frontiers in Computational Neuroscience* 16, 913617.
- [214] Xu, M., Islam, M., Lim, C.M., Ren, H., 2021a. Class-incremental domain adaptation with smoothing and calibration for surgical report generation, in: Medical Image Computing and Computer Assisted Intervention–MICCAI 2021: 24th International Conference, Strasbourg, France, September 27–October 1, 2021, Proceedings, Part IV 24, Springer. pp. 269–278.
- [215] Xu, Q., Zhang, R., Zhang, Y., Wang, Y., Tian, Q., 2021b. A fourier-based framework for domain generalization, in: Proceedings of the IEEE/CVF Conference on Computer Vision and Pattern Recognition, pp. 14383–14392.
- [216] Xu, Z., Liu, D., Yang, J., Raffel, C., Niethammer, M., 2020. Robust and generalizable visual representation learning via random convolutions. *arXiv preprint arXiv:2007.13003*.
- [217] Xue, C., Yu, L., Chen, P., Dou, Q., Heng, P.A., 2022a. Robust medical image classification from noisy labeled data with global and local representation guided co-training. *IEEE Transactions on Medical Imaging* 41, 1371–1382.
- [218] Xue, Z., Angara, S., Guo, P., Rajaraman, S., Jeronimo, J., Rodriguez, A.C., Alfaro, K., Charoenkwan, K., Mungo, C., Domingue, J.F., et al., 2022b. Image quality classification for automated visual evaluation of cervical precancer, in: Medical Image Learning with Limited and Noisy Data: First International Workshop, MILanD 2022, Held in Conjunction with MICCAI 2022, Singapore, September 22, 2022, Proceedings, Springer. pp. 206–217.
- [219] Yamashita, R., Long, J., Banda, S., Shen, J., Rubin, D.L., 2021a. Learning domain-agnostic visual representation for computational pathology using medically-irrelevant style transfer augmentation. *IEEE Transactions on Medical Imaging* 40, 3945–3954.
- [220] Yamashita, R., Long, J., Longacre, T., Peng, L., Berry, G., Martin, B., Higgins, J., Rubin, D.L., Shen, J., 2021b. Deep learning model for the prediction of microsatellite instability in colorectal cancer: a diagnostic study. *The Lancet Oncology* 22, 132–141.
- [221] Yang, Y., Zhang, H., Katabi, D., Ghassemi, M., 2023. Change is hard: A closer look at subpopulation shift. *arXiv preprint arXiv:2302.12254*.
- [222] Yellapragada, S., Graikos, A., Prasanna, P., Kurc, T., Saltz, J., Samaras, D., 2024. Pathldm: Text conditioned latent diffusion model for histopathology, in: Proceedings of the IEEE/CVF Winter Conference on Applications of Computer Vision, pp. 5182–5191.
- [223] Yi, K., Wu, J., 2019. Probabilistic end-to-end noise correction for learning with noisy labels, in: Proceedings of the IEEE/CVF conference on computer vision and pattern recognition, pp. 7017–7025.
- [224] Yin, B., Sun, M., Zhang, J., Liu, W., Liu, C., Wang, Z., 2022. Afa: adversarial frequency alignment for domain generalized lung nodule detection. *Neural Computing and Applications* 34, 8039–8050.
- [225] Ying, X., Liu, H., Huang, R., 2023. Covid-19 chest x-ray image classification in the presence of noisy labels. *Displays* 77, 102370.
- [226] Yu, X., Feng, Z., Zhang, X., Wang, Y., Li, T., 2022. Space and level cooperation framework for pathological cancer grading, in: 2022 IEEE International Conference on Visual Communications and Image Processing (VCIP), IEEE. pp. 1–5.
- [227] Zech, J.R., Badgeley, M.A., Liu, M., Costa, A.B., Titano, J.J., Oermann, E.K., 2018. Variable generalization performance of a deep learning model to detect pneumonia in chest radiographs: a cross-sectional study. *PLoS medicine* 15, e1002683.
- [228] Zhang, H., Dullerud, N., Seyyed-Kalantari, L., Morris, Q., Joshi, S., Ghassemi, M., 2021. An empirical framework for domain generalization in clinical settings, in: Proceedings of the conference on health, inference, and learning, pp. 279–290.
- [229] Zhang, H., Gu, X., Zhang, M., Yu, W., Chen, L., Wang, Z., Yao, F., Gu, Y., Yang, G.Z., 2022a. Re-thinking and re-labeling lidc-idri for robust pulmonary cancer prediction, in: Medical Image Learning with Limited and Noisy Data: First International Workshop, MILanD 2022, Held in Conjunction with MICCAI 2022, Singapore, September 22, 2022, Proceedings, Springer. pp. 42–51.
- [230] Zhang, H., Gu, Y., Qin, Y., Yao, F., Yang, G.Z., 2020. Learning with sure data for nodule-level lung cancer prediction, in: Medical Image Computing and Computer Assisted Intervention–MICCAI 2020: 23rd International Conference, Lima, Peru, October 4–8, 2020, Proceedings, Part VI 23, Springer. pp. 570–578.
- [231] Zhang, R., Xu, Q., Huang, C., Zhang, Y., Wang, Y., 2022b. Semi-supervised domain generalization for medical image analysis, in: 2022 IEEE 19th International Symposium on Biomedical Imaging (ISBI), IEEE. pp. 1–5.
- [232] Zhang, Y., Li, M., Li, R., Jia, K., Zhang, L., 2022c. Exact feature distribution matching for arbitrary style transfer and domain generalization, in: Proceedings of the IEEE/CVF Conference on Computer Vision and Pattern Recognition, pp. 8035–8045.
- [233] Zhang, Z., Sabuncu, M., 2018. Generalized cross entropy loss for training deep neural networks with noisy labels. *Advances in neural information processing systems* 31.
- [234] Zheng, K., Wu, J., Yuan, Y., Liu, L., 2023. From single to multiple: Generalized detection of covid-19 under limited classes samples. *Computers in Biology and Medicine*, 107298.
- [235] Zhou, K., Liu, Z., Qiao, Y., Xiang, T., Loy, C.C., 2022. Domain generalization: A survey. *IEEE Transactions on Pattern Analysis and Machine Intelligence*.
- [236] Zhou, K., Yang, Y., Hospedales, T., Xiang, T., 2020. Deep domain-adversarial image generation for domain generalisation, in: Proceedings of the AAAI conference on artificial intelligence, pp. 13025–13032.
- [237] Zhou, K., Yang, Y., Qiao, Y., Xiang, T., 2021a. Domain generalization with mixstyle. *arXiv preprint arXiv:2104.02008*.
- [238] Zhou, S.K., Greenspan, H., Davatzikos, C., Duncan, J.S., Van Ginneken, B., Madabhushi, A., Prince, J.L., Rueckert, D., Summers, R.M., 2021b. A review of deep learning in medical imaging: Imaging traits, technology trends, case studies with progress highlights, and future promises. *Proceedings of the IEEE* 109, 820–838.
- [239] Zhou, Y., Chia, M.A., Wagner, S.K., Ayhan, M.S., Williamson, D.J., Struyven, R.R., Liu, T., Xu, M., Lozano, M.G., Woodward-Court, P., et al., 2023a. A foundation model for generalizable disease detection from retinal images. *Nature* 622, 156–163.
- [240] Zhou, Y., Huang, L., Zhou, T., Sun, H., 2023b. Combating medical noisy labels by disentangled distribution learning and consistency regularization. *Future Generation Computer Systems* 141, 567–576.
- [241] Zhu, C., Chen, W., Peng, T., Wang, Y., Jin, M., 2021. Hard sample aware noise robust learning for histopathology image classification. *IEEE transactions on medical imaging* 41, 881–894.
- [242] Zhu, M., Zhang, L., Wang, L., Li, D., Zhang, J., Yi, Z., 2023. Robust co-teaching learning with consistency-based noisy label correction for medical image classification. *International Journal of Computer Assisted Radiology and Surgery* 18, 675–683.